ELECTRODEPOSITION OF COMPOUND SEMICONDUCTOR THIN FILMS USING E-ALD PROCESSES

by

Peter W. Sisk

(Under the Direction of John Lewellen Stickney)

ABSTRACT

Using Electrochemical Atomic Layer Deposition (E-ALD) and its one-solution counterpart, Potential Pulse Atomic Layer Deposition (PP-ALD), programs were developed for the deposition of compound semiconductor thin films. Both E-ALD and PP-ALD utilize the property of underpotential deposition (UPD), but while E-ALD requires solution switching, PP-ALD is done from one solution bottle. The PP-ALD deposition requires careful alternation of cathodic and anodic pulses to limit the material deposited. This allows for PP-ALD to be a much faster deposition process, but it can be more challenging to design a deposition program as both solutions must be soluble in the same pH's and deposit and strip at similar electrochemical potentials. By choosing optimal parameters governed by the Nernst equation such as pH, potential, and precursor concentration as well as physical conditions such as duty time, light exposure, and supporting electrolyte concentration, optimal deposition conditions can be achieved using both processes. Use of cyclic voltammetry and current-time traces allow for the monitoring of the deposition process in-situ while a variety of characterization methods can be used on the thin films after the deposition process is complete. Morphology of the deposits was characterized using SEM while the structural composition was analyzed with EDX and EPMA. Structural characterization was done by XRD and Raman Spectroscopy.

Many different semiconductor compounds can be formed using E-ALD processes. In_2Se_3 and InSe are interesting as potential photoanodes or photocathodes in a photoelectrochemical cell but can also be combined with other binary compounds into the super-structure, Copper Indium Gallium Selenide (CIGS) as well for solar cell use. GeTe is often used in Phase Change Random Access Memory (PRAM) applications as a phase change material due to its stable amorphous and crystalline states as well as its fast switching speed. Lastly, when combined with Surface Limited Redox Replacement (SLRR), E-ALD allows for the conformal deposition of epitaxial layers of noble metals such as Cu and Au which can serve as capping layers to protect the underlying films from unwanted oxidation.

INDEX WORDS: Electrodeposition, Electrochemical Atomic Layer Deposition (E-ALD) Potential Pulse Atomic Layer Deposition (PP-ALD), Underpotential Deposition (UPD), Surface Limited Redox Replacement (SLRR), GeTe In2Se3, InSe, Au, CIGS, SEM, XRD, Raman Spectroscopy, PRAM, EPMA, EDX, Nernst Equation, Cyclic Voltammetry

ELECTRODEPOSITION OF COMPOUND SEMICONDUCTORS THIN FILMS USING E-ALD PROCESSES

by

PETER W. SISK

B.S., The University of Georgia, 2012

A Dissertation Submitted to the Graduate Faculty of The University of Georgia in Partial Fulfillment of the Requirements for the Degree

DOCTOR OF PHILOSOPHY

ATHENS, GEORGIA

2020

ELECTRODEPOSITION OF COMPOUND SEMICONDUCTORS THIN FILMS USING E-ALD PROCESSES

by

PETER W. SISK

Major Professor: John Luwellen Stickney

Committee: Jeffrey L. Urbauer

Jon I. Amster

Electronic Version Approved:

Ron Walcott

Interim Dean of the Graduate School

The University of Georgia

May 2020

DEDICATION

I would like to dedicate this work to my supporting family and friends who helped to keep me going when it got rough. Thanks to my parents for assistance in more ways than I can count; you truly helped to make this happen. To Joey and friends that I have known since undergrad or longer, thanks for being there as a get-away. To my grad school friends, the monthly outings were crucial, and I loved the holiday dinners we would have while we were away from family. A special dedication to Pauline Howell, the best lab partner one could want. I would also like to thank Dr. Stickney for his guidance in chemistry as well as general life advice.

ACKNOWLEDGEMENTS

I received fantastic training in the UGA chemistry department and have grown up a lot during my time here. This was all made possible by the support that was given to me by every member of the staff, faculty, janitorial staff, and students. I appreciate you all and hope that I was able to return the favor somewhat.

Previous Stickney group members were very helpful in training me and helping get on my feet. Nhi taught me the proper lab technique as well as helped me to be a confident teacher and grader. Other members were always there for advice or to talk through ideas. Without the support and partnership with Pauline Howell, this doctorate would not have been possible. When things got busy I could always count on you to help both in lab or with teaching; we made quite the duo, didn't we?

Dr. Amster and Dr. Urbauer were more than just teachers, but also served as mentors and committee members. Thank you for always being available despite your crazy schedules. A special thanks to Dr. Suggs. You had to deal with me in undergrad and graduate school and you were always kind. You taught me a ton about electronics and how to manage the teaching/researching balance.

Lastly, this would not have been possible without the help of Dr. John Stickney. You are a great motivator and teacher and I learned an immense amount. You afforded me every opportunity to succeed and then go share that success at conferences. I am also very thankful to the support that you gave me even when you had to change to Emeritus status. You stuck with us and worked hard to make sure we would succeed, even though it had to be draining.

TABLE OF CONTENTS

CHAPTER 1

Introduction and Literature Review

1.1 Photovoltaics (PV) For Solar Cell Use

Due to the environmental and sustainability concerns of current energy methods such as coal or oil, new avenues of research into renewable energy sources has increased since the 1970s. Solar energy is a viable alternative due to the 1.8×10^{11} MW of power from the sun reaching the earth every year. If this entire resource were harnessed, it would greatly surpass the worlds current energy usage.[1] However, there are challenges to capturing the full spectrum of energy as even the most efficient solar cells made in laboratory environments top out at 40.6% according to the NREL.[2] To combat this, new more efficient materials and ways of stacking semiconductor junctions are being explored.

The use of PV semiconductor materials allows for the harnessing of the incoming sunlight and converting it into a chemical energy to either be used or stored in methods such as batteries or water pumping.[3,4] The composition of these materials is very important as their individual bandgaps allow for the capturing of different wavelengths of the spectrum. A bandgap is the energy gap between the valence and conduction bands of the material. As energy is absorbed by the material an electron is promoted from the valence band to the conduction band, allowing the flow of current and generation of electrical energy. This is done by use of a PN junction which combines a P-type material with a charge carrier of holes (or lack of electrons) and an N-type material where the charge carrier is electrons. When these two materials are connected, they form a junction where no charge can pass unless acted on by

an external energy source.[5,6] In the case of PV solar cells, this energy is incident light allowing the electrons in the N-type material to be ejected and holes from the P-type are moved to the opposite direction. When attached to an external circuit, these holes and electrons can be recombined to allow current flow and energy for immediate use or storage purposes.

Because the bandgaps of these materials are so important, there has been a vast number of different combinations tried. Early work focused on silicon of varying crystallinities as well as amorphous silicon cells, but the efficiency was limited to around 20%.[1,2] Other classifications arose with the study of III-V semiconductors such as GaAs and chalcogenide-based semiconductors such as CdTe and Copper-Indium-Gallium-Selenide/Sulfide (CIGS). Due to the efficiency and ease of deposition, CdTe as a solar cell material became very popular.[1-6] However, the drawback is that Cd is relatively toxic and Te is a finite resource, so research into other materials remains ongoing. These low efficiencies for even the best materials were a challenge that has been somewhat overcome by putting multiple cells in series to form multi-junction cells. These multi-junction cells allow for the combination of different semiconductors that will absorb different wavelengths of light. By combining their energy harvesting properties together, more of the solar spectrum can be captured.

1.2 Photo-electrochemical Cells (PEC) for Use as Chemical Energy for Water Splitting Purposes

An alternative use for semiconducting PN junctions is to take incident energy from the sun and convert it to chemical energy for use of splitting an aqueous compound into its component gases. These gases are then used as a renewable fuel source.[5-9] This is typically done with water to generate H_2 and O_2 gases, but other compounds can be used. The choice of materials is particularly important for these applications due to the 1.2 V of photovoltage needed for the splitting of water to occur. In these cells, N-type photoanodes would generate O_2 and P-type photocathodes would generate H_2. Oftentimes, these

can be paired together in the same cell. One of the major challenges involved in PEC work is that there is a solid-liquid boundary instead of the solid-solid boundary for PV applications. This can often lead to corrosion at the semiconductor surface as it gets oxidized and may require a capping material for longer use.[9]

1.3 Electrochemical Atomic Layer Deposition (E-ALD)

E-ALD, developed in the Stickney labs 30 years ago, is an electrochemical analog of Atomic Layer Deposition (ALD) which is typically a gas phase process. Historically gas phase reactions such as Chemical Vapor Deposition (CVD) and Molecular Beam Epitaxy (MBE) are used when thin films with atomic layer control are desired. However, by utilizing the property of Underpotential Deposition (UPD), atomic control can be achieved in the solution phase.[10-22] UPD is the phenomenon where one precursor metal (M1) can be deposited onto a substrate at an electrochemical potential "under" or at a more positive potential than would be necessary to deposit the metal onto itself. This leads to a surface limited amount of material where up to one monolayer (ML) will be deposited, meaning that there will be no bulk deposition.[10-22] A monolayer will be defined as one surface atom deposited for every substrate atom available. Once the first UPD amount of metal has been deposited onto the substrate, a second metal (M2) can be deposited onto M1 using the same UPD process. As alternating layers of M1 and M2 are deposited, a thin film can be formed where the thickness can be determined by the number of alternations.

E-ALD was born from the desire to achieve atomic layer control without the need for expensive reactors that make use of vacuum or high temperatures that may damage the substrate or films, that are common in gas phase reactions.[23] In fact, E-ALD uses relatively cheap hardware and can be done at room temperature and standard pressure. This allows a flexibility with what precursor metals and

substrates that can be used as compared to vapor methods. A general schematic of the E-ALD set-up is available in Figure 1.1 In this standard E-ALD set-up, solution make-up is key because any unwanted side reactions or contaminants can damage the films and cause inhomogeneity and promote nucleation sites instead of the desired epitaxial growth. To combat this, solutions are comprised of only: the precursor metal at millimolar concentrations, electrolyte, a buffer, and 18 MΩ Nanopure water. By keeping the precursors at millimolar concentrations excess deposition can be curbed, promoting only the surface limited features. These ultrapure solutions are then purged of O_2 using N_2 gas. This process holds a dual purpose of avoiding O_2 bubbles which may keep solution from reaching the substrate surface as well as limiting the oxidation of the deposited films.[10-22] The solution is then pulled through a valve block and then into the flow cell where it will flow laminarly up across the substrate followed by being pumped out of the cell into a waste container. In theory, since such low concentrations of the metal precursor ion will be deposited, these solutions could be recycled for maximum sustainability, but it has yet to be put into practice. The E-ALD process requires the alternation of solutions of each precursor metal as well as a blank solution in between each precursor that will serve to wash out the previous solution to avoid any unwanted side reactions. The blank will be comprised of only the electrolyte, buffer, and Nanopure water. By carefully controlling the pH and potential that every solution is introduced at, the films can be tuned to the desired stoichiometry.

The electrochemical flow cell in Figure 1.2 contains a 3-electrode system with the polycrystalline Au substrate serving as the working electrode, an inlaid “S” shaped Au wire as the Auxiliary or “counter” electrode, and an Ag/AgCl reference electrode. As potential is applied to the working electrode, the resulting current is supplied by the auxiliary electrode and read by a potentiostat which feeds the information to the computer by way of an in-house program called SEQUENCER. By controlling the potentials sent to the working electrode and which solution is in the cell at a given time, a deposition sequence can be created to give the desired epitaxial thin films.[10-22] The main drawbacks to this method

are scalability, as the flow cell is only about 2.2cm^2 in area as well as time, due to the lengthy nature of solution switching.

1.4 Potential Pulse Atomic Layer Deposition (PP-ALD)

PP-ALD is another E-ALD process relying on the same principles of UPD and producing alternating surface limited reactions to achieve a thin film with atomic layer control. However, it is like traditional codeposition techniques in that all the precursor metals are in the same solution. This allows for a much quicker deposition process than traditional E-ALD because there is no longer any solution switching; the same solution is flowed the whole time and there is no need for a blank. Because both precursor ions must be in the same solution there are a whole other set of challenges that must be overcome which limit the number of viable compounds formed in this manner.[24-27] In PP-ALD, both precursors must both be soluble at the same pH's as well as not react with each other to form unwanted side reactions. Additionally, they must be able to deposit and strip in similar electrochemical potential ranges or bulk deposition of one of the metals may occur. Alternating pulsed cathodic deposition and anodic stripping potentials are used to control the amount of material of each precursor metal deposited. The anodic pulses can serve to strip off any excess material of either metal that may have deposited at a slight overpotential as well as provide a period of quiescence for the deposit before the next layer is applied. Typically, longer anodic potentials are used around 500 ms as opposed to the shorter 130 ms cathodic pulses. [24-27] This duty cycle can be variable depending on the desired compound. PP-ALD differs from other codeposition methods in that alternating cathodic and anodic potentials are used instead of a constant applied potential. In the case of CdTe, previous work done in this group by Zhang et al. showed that PP-ALD produced smoother, more epitaxial films that its

codeposition counterpart.[27] Additionally it was found that giving the film longer, or more times to rest is advantageous to the film quality.

1.5 Surface Limited Redox Reaction (SLRR)

SLRR is another variant of the E-ALD process and often both processes are used together. SLRR relies upon the principle that at Open Circuit Potential (OCP), where no potential is applied, and no current can flow, a more noble metal will replace a less noble metal.[28-30] Typically, this is done when the desired material won't deposit at a potential compatible with the substrate and pH or, the material is extremely unreactive as with the case of Au or Pt. In work done by Brankovic's group he has used this principle to do atomic layer stripping of bulk materials to yield fine controlled surfaces.[31-34] When SLRR is instead used in conjunction with E-ALD, first a monolayer of a sacrificial metal can be deposited using the traditional E-ALD method and then a more noble metal will replace the sacrificial layer. This leads to repeatable growth of the noble metal on top of the original substrate and can make thin epitaxial films without having nucleation sites. One of the drawbacks to this method is that time of exposure for the more noble metals must be carefully controlled. Upon too much exposure, the underneath substrate may be exchanged, damaging the integrity of the compound.[35-37] If the exposure is too short, not all the sacrificial layer will be exchanged, and the sacrificial layer will be buried, leading to accidental doping effects. This technique is useful if very fine noble metal deposition is needed with the side effect that often the photocatalytic effects are boosted.[35]

1.6 Cyclic Voltammetry and Coulometry

Cyclic Voltammetry (CV) is a useful tool for determining at what potentials different reactions of the deposited metal will occur onto the substrate. As the potential is scanned, the resulting current features can be read to determine what reaction is occurring as well as how much material was deposited.[36] In this dissertation, negative potentials will be on the left-hand side and positive potentials will be to the right. Negative current is indicative of a reduction reaction, which usually leads to material being deposited onto the substrate. In the case of chalcogenides, reductive stripping can also occur at sufficiently negative potentials, a property unique to them.[12,36] Positive currents result in oxidation of the metal and is almost always a sign of the metal stripping. While quantification of the reduction reactions is challenging, quantification of the oxidation features is quite simple and yields detailed information about how many ML of material was stripped. Oftentimes, in the early stages of cycle development, an amount of material will be deposited and then subsequently stripped to determine the stoichiometry of both components that were on the surface. By use of Coulometry, the area under the curve for the current can be determined and if the size of the cell, and number of electrons in the process are known, the ML of material can be calculated. This is especially useful for very thin films that cannot be imaged using Scanning Electron Microscopy (SEM) and likewise Electron Dispersive X-ray Spectroscopy (EDS). By monitoring the voltammetry as the deposition process occurs, in-situ characterization of the films can be achieved.

1.7 Thin Film Characterization

Understanding the morphology, stoichiometry of the components, and compound identification for thin films is very important. In the Stickney lab, SEM/EDS is used to look at surface morphology and elemental identification. By using the Everhard-Thornley Detector (ETD), surface morphology is obtained which gives an idea of the roughness of the sample and checks that growth is epitaxial and not nucleation site limited. Nucleation growth is usually evident in the form of circular balls on the surface that are concentrated of one metal whereas epitaxial layers are much more homogenous and more resemble the patterning of the underlying substrate. Use of the Circular Backscatter Detector (CBS) allows elemental detection but does not offer any information on the stoichiometry. This is useful for the elemental mapping of wide areas of film. This helps to ensure that the film is forming a compound and not just areas of 2 different metals. The attached EDS allows for quantification of the species and gives a good overview of the stoichiometry. By using different excitation energies, different amounts of the film can be penetrated. A lesser energy gives a look more at the surface, whereas a larger energy will look deeper and incorporate he substrate data. Electron Probe Micro-Analyzer (EPMA) can also be used for quantification as it is a more accurate technique but requires more time and was less available. X-ray Diffraction (XRD) is used to identify the compound by reading the pattern and comparing it to a known database. This is useful because many compounds can have the same stoichiometry but display different phases or crystallinities. One of the difficulties of using XRD on these thin films (10-40nm thick) is that traditional XRD assumes that a sample is infinitely thick, which doesn't work with this lab's deposits.[39] To get around this limitation glancing angle XRD is used. By using a Eularian Cradle, the X-ray source can be positioned at a glancing angle to help to combat the penetration depth of the X-rays as it now sees a

larger slice of the film. Another technique for compound identification is Raman Spectroscopy. In this method an excitation laser source is used to excite the molecules in the film. By comparing the shifts in energy made by the vibrations of those molecules, a spectrum can be formed which can be compared to a known database. For the thinner samples imaging can be difficult. One way this lab obtains spectra in this case is to make use of a Surface Enhanced Raman Spectroscopy (SERS) substrate. A roughened substrate is used and then the thin film is deposited on top. Due to the enhanced surface area of the roughened substrate the localized plasmon effect is increased, leading to detectable signals.[40] Films as thin as 1-2 ML were imaged in this way for germanene growth. Film thickness can be determined using Spectroscopic Ellipsometry, however, cross-sectional SEM is this lab's preferred method. Lastly, photoelectrochemical characterization can be performed by exposing the semiconductor films to dark environments and comparing them to the photovoltage generated by exposure to different wavelength light sources. This is done at OCP in an electrolyte solution and can help to identify whether the material is N-Type or P-Type.

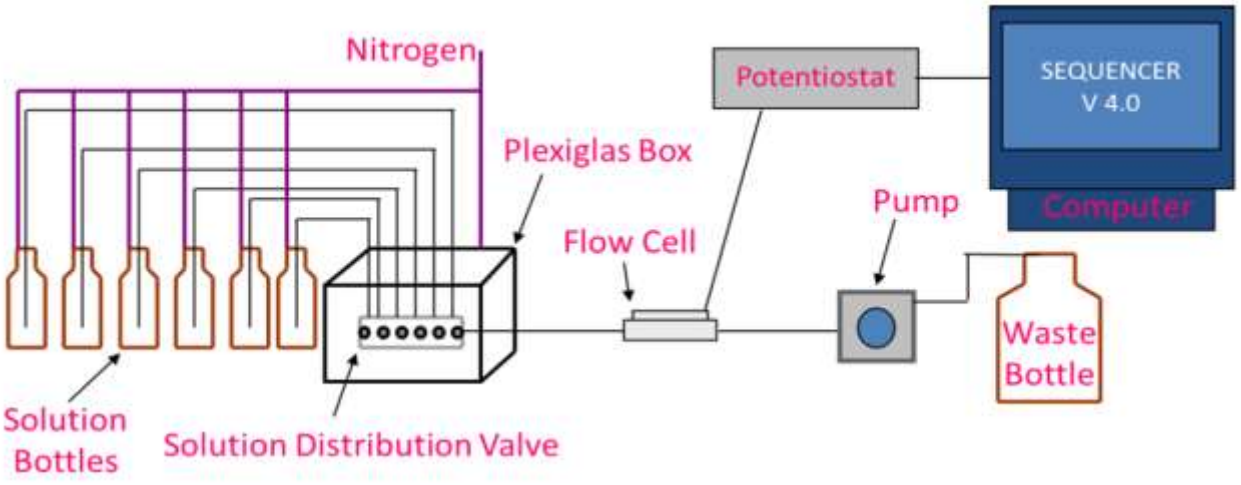

Figure 1.1- General schematic of the E-ALD process. Highly pure solutions enter the flow cell in a manner controlled by a valve distribution block. Once in the cell, 3 electrodes are used to control the potential while reading the resulting current. Once the ions in the solution have been deposited or stripped, the solution is pumped out to a waste container.

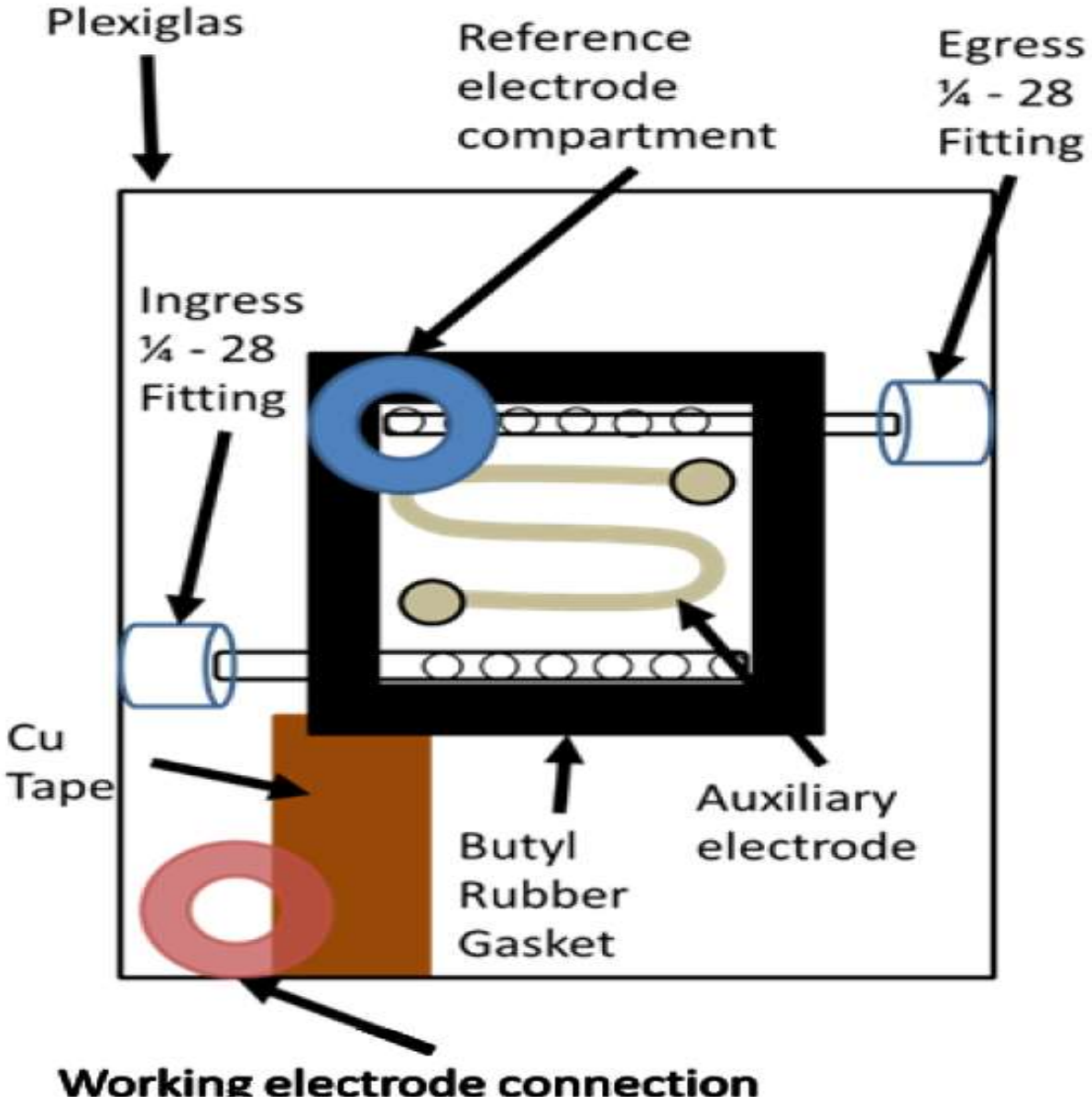

Figure 1.2- Schematic for the 3-electrode system in use in the electrochemical flow cell. Solution is directed in the ingress and flows laminarly up across the substrate surface where it is pumped out the egress. In this set-up the working electrode also serves as the Au substrate with the auxiliary electrode being an Au in-laid wire. The reference electrode in this set-up is a commercial Ag/AgCl electrode.

REFERENCES:

1. Parida, B.; Iniyan, S.; Goic, R. A review of solar photovoltaic technologies. *Renewable and Sustainable Energy Reviews* **2011**, 15, 1625–1636.

2. NREL.gov, Best Research-Cell Efficiencies. **2019**.

3. Blaabjerg, F.; Ma, K.; Yang, Y. Power Electronics for Renewable Energy Systems- Status and Trends. *CIPS* **2014**.

4. Sharma, S.; Jain, K.K.; Sharma, A. Solar Cells: In Research and Applications- A Review. *Materials Sciences and Applications* **2015**, 6, 1145-1155.

5. Li, J.; Wu, N. Semiconductor-based photocatalysts and photoelectrochemical cells for solar fuel generation: a review. *Catalysis Science and Technology* **2015**, 5, 1360-1384.

6. Fang, Z.; Wang, X.C.; Wu H.C.; Zhao, C.Z. Achievements and Challenges of CdS/CdTe Solar Cells. *International Journal of Photoenergy* **2011**, 1-9.

7. Joy, J.; Mathew, J.; George, S. Nanomaterials for photoelectrochemical water splitting- a review. *International Journal of Hydrogen Energy* **2018**, 43, 4804-4817.

8. Voloshin, R,A.; Kreslavski, V.D.; Zharmukhamedov, S,K.; Bedbenov, V.S.; Ramakrishna, S.; Allakhverdiev, S.I. Photoelectrochemical cells based on photosynthetic systems: a review. *Biofuel Research Journal* **2015**, 6, 227-235.

9. Manivannan, A.; Peterson, A.; Wilson, W.; Mukherjee, B.; Subramanian, V.R. Hydrogen Production and Photodegradation at TiO2/Metal/CdS Sandwich Using UV-Visible Light. *Semiconductor Materials for Solar Photovoltaic Cells* **2012**, 5, 141-167.

10. Gregory, B.W.; Stickney, J.L. Electrochemical Atomic Layer Epitaxy (Ecale). *Journal of Electroanalytical Chemistry* **1991**, 300, 543-561.

11. Suggs, D.W.; Stickney, J.L. Studies of the Surface-Structures Formed by the Alternated Electrodeposition of Cd and Te on the Low-Index Planes of Au Stm Studies. *Surface Science* **1993** 290, 375-387.

12. Lister, T.E.; Huang, B.M.; Herrick, R.D.; Stickney, J.L. Electrochemical Formation of Se Atomic Layers on Au (100). *Journal of Vacuum Science and Technology B* **1995**, 13, 1268-1273.

13. Lister, T.E.; Stickney, J.L. Atomic level studies of selenium electrodeposition on gold (111) and gold (110). *Journal of Physical Chemistry* **1996**, 100, 19568-19576.

14. Lister, T.E.; Stickney, J.L. Formation of the first monolayer of CdSe on Au (111) by electrochemical ALE. *Applied Surface Science* **1996**, 107, 153-160.

15. Stickney, J.L. Electrochemical atomic layer epitaxy. *Electroanalytical Chemistry* **1999** 21, 75-209.

16. Sorenson, T.A.; Lister, T.E.; Huang, B.M.; Stickney, J.L. A comparison of atomic layers formed by electrodeposition of selenium and tellurium- Scanning tunnel microscopy studies on Au (100) and Au (111). *Journal of the Electrochemical Society* **1999**, 146, 1019-1027.

17. Sorenson, T.A.; Suggs, D.W.; Nandhakumar, I.; Stickney, J.L. Phase transitions in the electrodeposition of tellurium atomic layers on Au (100). *Journal of Electroanalytical Chemistry* **1999**, 467, 270-281.

18. Vaidyanathan, R.; Stickney, J.L.; Cox, S.M.; Compton, S.P.; Happek, U. Formation of In2Se3 thin films and nanostructures using electrochemical atomic layer epitaxy. *Journal of Electroanalytical Chemistry* **2003**, 559, 55-61.

19. Venkatasamy, V.; Shao, I.; Huang, Q.; Stickney, J.L. ALD approach toward electrodeposition of Sb2Te3 for phase-change memory applications. *Journal of the Electrochemical Society* **2008**, 155, 693-698.

20. Liang, X.H.; Kim, Y.G.; Gebergziabiher, D.K.; Stickney J.L. Aqueous Electrodeposition of Ge Monolayers. *Langmuir* **2010**, 26, 2877-2884.

21. Banga, D.; Perdue, B.; Stickney, J.L. Formation of CuIn(1-x)GaxSe2 (CIGS) by Electrochemical Atomic Layer Deposition (ALD). *Journal of the Electrochemical Society* **2014**, 161, 141-146.

22. Bui, N.N.; Ledina, M.; Reber, T.J.; Jung, J.; Stickney, J.L. Electrochemical Scanning Tunneling Microscopic Study of the Potential Dependence of Germanene Growth on Au (111) at pH 9.0. *ACS Nano* **2017**, 11, 9481-9489.

23. Strevel, N.; Trippel, L.; Gloceckler, M. Performance characterization and superior energy yield of First Solar PV power plants in high-temperature conditions. *Photovoltaics International* **2012**, 17, 1-6.

24. Czerniawski, J.M.; Stickney, J.L. Electrodeposition of In2Se3 Using Potential Pulse Atomic Layer Deposition. *The Journal of Physical Chemistry C* **2016**, 120, 16162-16167.

25. Czerniawski, J.M.; Perdue, B.R.; Stickney, J.L. Potential Pulse Atomic Layer Deposition of Cu2Se. *Chemistry of Materials* **2016**, 28, 583-591.

26. Zhang, X.; Shen, S.; Howell, P.; Cheng, W.; Mubeen, S.; Stickney, J.L. Potential Pulse ALD for Room Temperature Fabrication of Stoichiometric CdTe Nanofilms. *Journal of the Electrochemical Society* **2019**, 166, 3249-3256.

27. Bui, N.; Cheng, W.; Mubeen, S.; Stickney, J.L. Potential Pulse Atomic Layer Deposition (PP-ALD): Electrodeposition of ZnS Nanofilms. To be submitted to ACS journal Chemistry of Materials.

28. Jayaraju, N.; Vairavapandian, D.; Kim, Y.G.; Banga, D.; Stickney, J.L. Electrochemical Atomic Layer Depostiong (E-ALD) of Pt Nanofilms Using SLRR Cycles. *Journal of the Electrochemical Society* **2012**, 159, 616-622.

29. Sheridan, L.B.; Czerniawski, J.; Jayaraju, N.; Gebregziabiher, D.K.; Stickney, J.L.; Robinson, D.B.; Soriaga, M.P. Electrochemical Atomic Layer Deposition (E-ALD) of Palladium Nanofilms by Surface Limited Redox Replacement (SLRR), with EDTA Complexation. *Electrocatalysis* **2012**, 3, 96-107.

30. Dimitrov, N. Recent Advances in the Growth of Metals, Alloys, and Multilayers by Surface Limited Redox Replacement (SLRR) Based Approaches. *Electrochimica Acta* **2016**, 1-47.

31. Gokcen, D.; Yuan, Q.; Brankovic, S.R. Nucleation of Pt Monolayers Deposited via Surface Limited Redox Replacement Reaction. *Journal of the Electrochemical Society* **2014**, 161, 3051-3056.

32. Gokcen, D.; Bae, S.E.; Brankovic, S.R. Reaction kinetics of metal deposition via surface limited red-ox replacement of underpotentially deposited metal monolayers. *Electrochimica Acta* **2011**, 56, 5545-5553.

33. Gokcen, D.; Bae, S.E.; Brankovic, S.R. Kinetics of Metal Deposition via Surface-limited Redox Replacement Reaction. *ECS Transactions* **2011** 35, 11-22.

34. Zhang, X.; Shen, S.; Stickney, J.L. Metal Thin Film Epitaxial Deposition by SLRR on Semiconductor Substrate. To be submitted to *Journal of the Electrochemical Society.*

35. Zhang, X.; Shen, S.; Stickney, J.L. Cu and Au Films Epitaxially Deposition by Surface Limited Redox Replacement (SLRR) on Metal Substrate. To be submitted to *Journal of the Electrochemical Society.*

36. Kamat, P. Manipulation of Charge Transfer Across Semiconductor Interface. A Criterion That Cannot Be Ignored in Photocatalyst Design. *J. Phys. Chem. Lett.* **2012**, 3, 663-672.

37. Kim, S.E.; Han, W.K.; Lee, J.H. Electrochemical characterization of CdSe and CdTe thin films using cyclic voltammetry. *Current Applied Physics* **2010**, 10, 481-483.

38. Lay, M.D.; Stickney, J.L. EC-STM Studies of Te and CdTe Atomic Layer Formation from a Basic Te Solution. *Journal of the Electrochemical Society* **2004**, 151, 431-435.

39. Baggetto, L.; Notten, P.H.L. Lithium-Ion (De)Insertion Reaction of Germanium Thin-Film Electrodes: An Electrochemical and In Situ XRD Study. *Journal of the Electrochemical Society* **2009**, 156, 169-175.

40. Jung, J.; Bui, N.N.; Shen, S.; Reber, T.J.; Brezner, J.M.; Mubeen, S.; Stickney, J.L. In Situ Surface-Enhanced Raman Spectroscopic Studies of Electrochemically Formed Germane. *J. Phys. Chem. C.* **2018**, 122, 15696-15705.

CHAPTER 2

ELECTROCHEMICAL ATOMIC LAYER DEPOSITION (E-ALD) OF GETE THIN FILMS

Sisk, P.; Howell, P.; Mubeen, S.; Stickney, J. To be submitted to ECS journal.

2.1 ABSTRACT

GeTe thin films were formed using E-ALD, a solution-based process. The same pH, buffer concentration, and supporting electrolyte were used in both precursor solutions as well as the blank, with only the concentration of the precursor ions differing. This allowed for the use of one blank to rinse the solutions out of the flow cell, so that material stability was maintained. The potentials chosen for deposition and stripping processes are paramount due to the overlapping of the Te stripping at potentials like where Ge normally deposits. This is largely due to the ability of Te to strip reductively as a stable Te^{2-} species, a unique property of the chalcogenide family. Another potential obstacle is the formation of germanene, the Ge analog of graphene, which forms sheets that self-limit and change the structure of the Ge layer. By depositing Ge at lesser potentials for longer hold times, the germanene structure can be avoided, leading to the formation of the desired GeTe compound. The stoichiometry was measured using coulometry from the stripping of the material and showed a linear 1:1 growth as a function of the number of cycles. Thicker deposits were characterized using SEM, EDS, and Raman Spectroscopy and proved that the 1:1 nature of the film is maintained without forming germanene in the process.

2.2 INTRODUCTION

Electrochemical Atomic Layer Deposition (E-ALD) was invented in the Stickney labs 30 years ago for the deposition of metal and compound semiconductor thin films. It relies on the principles of surface-limited reactions to form atomically thin layers of alternating metal materials. These surface-

limited reactions rely on a phenomenon called Underpotential Deposition (UPD) where one metal (M_1) can be deposited onto another metal (M_2) at an electrochemical potential less than would be needed to deposit M_1 onto itself. These reactions form fractions of a monolayer (ML) at a time, to build up a compound semiconductor without bulk deposits.[1-12] A monolayer will be defined as having one surface atom for each underlying substrate atom. These surface-limited deposits have traditionally been done in the gas phase, however, E-ALD allows for a cheaper, solution-based method for making these thin films. By keeping the solutions employed as pure as possible and without complexing agents, unwanted side reactions can be avoided that would damage the film. Because E-ALD can be done at room temperature and standard pressure, it is a much cheaper alternative to the expensive reactors used in Chemical Vapor Deposition (CVD) or Molecular Beam Epitaxy (MBE) which are prevalent in industry today.[1-12]

Phase change materials are those which have two different stable, solid phases; typically, one of these phases is amorphous and the other is crystalline. These different phases should have different properties such as large changes in resistivity and should be able to alternate between the phases rapidly and have very large lifetimes.[13-15,19-22] GeTe and the super compound GeSbTe (GST) became early attractive compounds due to the ideal properties and phase stability.[11-13,17] One of the issues with GST is that there is a relatively large amount of Ge vacancies, which is not present in the GeTe compound which has a tighter lattice.[13,15,19] The amorphous, low-temperature GeTe structure displays the *R*3*m* space group and when the correct temperature is input it will rearrange to the higher ordered *Fm*-3*m* structure.[15,17,20] Thin film of GeTe is desired due to the increase in recrystallization temperature as well as lower melting point when film thickness is decreased.[15] This is important because it will lead to better stability for each phase as well as allow GeTe to be used in more applications. GeTe has a recrystallization temperature of 185 °C, which is above the 150 °C necessary for PC and even some automotive applications.[16] This is greater than the 85-130 °C crystallinity temperature for GST,

suggesting that GeTe may be more optimal. GeTe can also be used in PEC applications for water splitting due to its ideal bandgap.[14]

Past work in the Stickney group on GeTe was done by Liang et al. and sought to combine the binary compounds GeTe and SbTe to form $Ge_xSb_yTe_z$ due to its properties as a PCM.[24] However, the deposits were characterized by being Ge rich. This is likely due to the unique property of chalcogenides, such as Te, to reductively strip as Te^{2-} due to the stability of the ion in solution. This reductive stripping of Te occurs at potentials where it is optimal for Ge deposition to occur. However, Figure 2.1 shows that there is a narrow region between -1000mV and -1200mV where it should be possible to get the desired 1:1 compound for the GeTe.[24] Another complicating factor in past studies is that these GeTe deposits were deposited on top of a 3.5 ML deposit of Ge, the maximum amount of Ge that was able to deposit on Au due to the self-limiting nature of Ge electrodeposition.[24,25] At the time, it wasn't understood that the 3.5 ML of Ge was not necessarily bulk Ge but instead was a different structure, germanene. Germanene is the 2D analog of graphene and consists of sheets of 6-membered rings of Ge. It has unique properties and is quite different than the bulk material for most metals. It is likely that this germanene substrate was not ideal for the continued growth of GeTe deposits due to how the germanene restructures itself. In another study, thicker Ge deposits were grown using the "bait and switch" method where Te was deposited as a sacrificial layer, allowing more Ge to be deposited on top of the Te.[26] Afterwards the Te was completely removed by going to sufficiently negative potentials to reductively strip it out. This further shows that not only can the bulk Te be stripped reductively, but so can the more tightly held surface-limited structures. Eventually, work by Bui, Ledina, and Jung were able to prove using Scanning Tunneling Microscopy (STM) and SERS Raman Spectroscopy that the "bulk" Ge deposits were sheets of germanene forming and changing the structure of the surface.[27-29] It is unknown what effect germanene would have on the lattice of GeTe so in this work, the formation of germanene was avoided as much as possible in deposition conditions. Another study by Liang et al. determined that

the optimal pH for the deposition of Ge and Te together was pH=9.3. The reasoning is two-fold. First, Ge growth is maximized at pH=9.3 with a coverage of 3.5 ML.[25] Second, the potential for Te reductive stripping and Ge deposition are closest at pH=9.3. At all other pH's, more Te would be stripped at Ge deposition potentials which will cause an even greater disparity in the relative coverages on the surface. Additionally, at more acidic pH's the Hydrogen Evolution Reaction (HER) occurs at increasingly positive potentials and interferes with the Ge deposition by forming bubbles on the surface leading to regions of inhomogeneity.

2.3 EXPERIMENTAL

All experiments were performed in an electrochemical flow cell (Electrochemical ALD L.C.) making use of a 3-electrode set-up. The auxiliary electrode was an inlaid Au wire and the reference electrode was Ag/AgCl in 3 M NaCl (Bioanalytical Systems, Inc.). The working electrode doubles as the polycrystalline Au substrate (Evaporated Metal Films) and was made from glass slides with a 5 nm Ti adhesion layer, topped with 100 nm of Au. The working electrode area was 2.2 cm^2. Solution flow was controlled by a valve block (Neptune Research & Development, Inc.) which was implemented by a potentiostat (Electrochemical ALD L.C.) and controlled by an in-house LabVIEW program named SEQUENCER. This set-up allowed for precise control over which solution was in the cell at any given time, as well as input potentials to the cell and read the resulting current generated.

Slide preparation was done by rinsing the Au substrate in 18 MΩ nanopure water (Millipore Advantage 10) and then washed with acetone (Fisher Chemical) and rinsed again in nanopure water. Next, the slides were exposed to concentrated HNO_3 (JT Baker) for 30 s and then rinsed again with nanopure water. The slides were immediately transferred into the flow cell and 0.1 M H_2SO_4 (Fisher Chemical) was flowed into the cell to limit air exposure time. The substrates were then

electrochemically cleaned by 4 alternating 5 s pulses of -200 mV and 1400 mV followed by 2 CV's at 20 mV/s from -200 mV to 1400 mV and back.

Solution bottles were cleaned with Nochromix (Godax Labratories) for at least an hour and then rinsed multiple times with nanopure water. Germanium precursor solution was pH=9.3, 5 mM GeO2 (Alfa Æsar 99.999% pure), 0.1 M $HClO_4$ (GFS Chemicals, Inc.), with a buffer of 50mM $Na_2B_4O_7 \cdot 10H_2O$ (Alfa Æsar 99+%), adjusted to the correct pH with NaOH pellets (Fisher Chemical) and then finished with nanopure water. Tellurium precursor solution was pH=9.3, 0.2 mM TeO_2 (Johnson Matthey Materials Company 99.9995% pure) and 0.1 M $HClO_4$, adjusted to the correct pH with NaOH. The blank solution was 0.1 M $HClO_4$, with a buffer of 50mM $Na_2B_4O_7 \cdot 10H_2O$, adjusted with NaOH to pH=9.3. Before the solutions were introduced to the cell, they were purged in N_2 gas (Airgas) for at least an hour to limit O_2 exposure. Solutions were quite stable, and able to survive for months before any precipitation occurred.

SEM (FE-SEM Thermo Fisher Teneo) was used to observe the morphology and elemental structure of the deposits using 5 keV and 10 keV accelerating voltages. The attached EDS detector (150mm Oxford $XMax^N$) was used for stoichiometry. Diffraction patterns from XRD (PANalytical X'PERT Pro) were obtained by use of an open Eulerian cradle to provide glancing angle data and the source was 1.54 Å Cu K_α radiation. Raman Spectroscopy (DXR Raman Microscope, Thermo Scientific) was used for structural identification with a 532 nm Laser source.

2.4 RESULTS AND DISCUSSION

2.4.1 CYCLIC VOLTAMMETRY OF PRECURSORS

Cyclic Voltammetry (CV) and Coulometry can be used to find the electrochemical potential regions where different structures of each Ge and Te will deposit on the surface and strip off. This is

important because deposition should be limited to only the surface limited features to promote crystallinity and lattice formation. If instead bulk material is deposited, then additional steps must be taken to strip off that excess material before the second metal can be deposited on top. Figure 2.2 gives an overview of the potentials where the various structures of Ge and Te deposit and strip. In this figure a white space indicates regions of OCP where nothing occurs, dark colored regions indicate deposition and lighter colored regions show regions of stripping of the material. A quick glance shows just how close these regions are, often overlapping, and highlights how important choosing the optimal potentials can be.

Figure 2.3 depicts voltammetry of the Te on Au substrate. By scanning to negative potentials and reading the resulting current, the regions of deposition for the Te can be identified for the reductive features. As the potential is scanned positively oxidative stripping can be seen with the more tightly held, surface limited features being stripped most positively. While quantification of reductive current is difficult in this situation, oxidative stripping current can easily be related to the number of monolayers (ML) that were stripped off the surface. This allows for in-situ characterization of surface coverage for very small amounts of material that wouldn't be observable in other available methods such as EDS or EPMA.

Starting at 0 mV and scanning negatively, the first reductive feature in the red box depicts the surface limited deposition of Te. As the potential is scanned into the purple region, bulk Te deposits and the current is greatly increased. Holding the potential in this region can generate a large amount of bulk material. Further negative scanning leads to the first reductive stripping feature. Here the bulk Te ions are stripped as the solution-stable Te^{2-} ion and flushed away. Further scanning negative leads to the region where even the surface limited Te is reductively stripped from the film. On the positive going scan there is no oxidation until -100 mV, where the stripping of bulk Te occurs. The most positive feature is the surface limited stripping. Peaks can be determined to be surface limited or bulk structures

based on how they grow with longer deposition times. The surface limited stripping of Te in Figure 2.4a shows a coverage of 0.37 ML of Te that will not grow larger. This coverage for Te is like those obtained by previous Stickney group members using EC-STM for UPD Te structures. As the potential approaches -1400 mV Figure 2.4b highlights just how fast the UPD Te layer is removed. However, as seen in the positive potential's region of Figure 2.5, when Te deposition is held longer in the bulk potential region, the peaks in the area between -100 mV and 50mV grow indefinitely on the subsequent stripping, confirming the bulk nature.

Figure 2.6 displays the voltammetry for the Ge on Au. Unlike the Te voltammetry, there is no reductive stripping at more negative potentials. Instead as the potential is scanned more negative the structure of the deposit changes and forms germanene sheets. By following the green scan, the surface limited Ge features can be identified in the green box. After -1050 mV a second reductive features starts, initiating the germanene transformation. The positive going scan is very different depending on what region the deposit was held at. In the green scan where only the surface limited structure was achieved, there are 3 stripping peaks. The -800 mV peak is a very weakly held surface limited structure that has been described as "pre-germanene" in previous Stickney group work. The STM showed that the Ge was starting to cover the surface but was not yet organized into sheets as full blown germanene would be. The feature at -400 mV shows that in this case, there was a small amount of germanene sheets starting to form. This sample was done at the edge of the boundary of germanene formation to maximize the amount of surface limited Ge structure deposited. The last oxidative feature at -150 mV is the most fundamental base surface limited Ge. This peak will always show up if there is Ge bound directly to Au. In the blue scan there are only 2 oxidative features. The first is a fronted peak which is indicative of the germanene sheets. The surface limited pre-germanene peak is no longer present and was likely incorporated into the more ordered sheets as the layers filled in. The most tightly held first layer of surface limited Ge remains even when germanene is present. When the voltammetry of the two

metals is put together, the challenges for depositing surface limited amounts of both together are evident.

2.4.2 SELECTION OF OPTIMAL DEPOSITION POTENTIALS FOR THE FIRST GETE LAYER

Because UPD Ge starts to strip oxidatively by -800mV, deposition of Te layers must occur at more negative potentials. This pushes the Te deposition potential out of the UPD Te region meaning that Te must be deposited at an overpotential which leads to bulk Te deposition. In the past work done on GeTe by the Stickney group, the Te was deposited in bulk conditions and subsequently stripped off in a further reductive stripping step. It is impossible to do an oxidative stripping step since all Ge will have also been oxidatively stripped at those potentials as highlighted in Figure 2.2. The previous method risked burying of Te as well as took significantly longer. These deposition sequences are already quite lengthy, so additional unneeded steps slow down growth significantly. Instead, in this study it has been discovered that if Te is deposited at potentials in the region where bulk Te is reductively stripped, only the surface limited coverage of 0.37 ML of Te is left as seen in Figure 2.4a. At -1200 mV the Te structure remains relatively unchanged, but at potentials past that large amount of stripping can be seen in Figure 2.4b. It was seen that deposition time for Te was quick in the reductive stripping region with deposition on Au completed by 5 s. Deposition conditions for the first layer were set at -1100 mV for 5 s. Light or dark growing environment did not seem to affect the speed or amount deposited for Te as has been observed for other chalcogenide materials.

From the Voltammetry in Figure 2.6, it seems that the deposition of the first layer of Ge at -1050 mV is enough for full UPD deposition. However, Figure 2.7 shows that Ge deposits at significantly more negative potentials when a Te layer is already present on the surface. In the black scan, Te is on the surface and the potential is scanned in a Ge solution to -1100 mV, a potential where Ge would easily

deposit on Au. On the subsequent positive scan, only the Te is present; there are no peaks for Ge. This suggests that a more negative potential is needed to deposit Ge when the surface resembles Te. In the red scan, a much more negative scan of potential of -1400 mV is used, sufficient to form germanene. The positive scan shows that these conditions were a little excessive, as now only Ge remains on the surface. However, the study highlights that Ge doesn't really start to deposit on Te until -1150 mV and then quickly gets into a regime where germanene is formed. This suggests that the region where Ge UPD fills out is relatively small. In fact, previous GeTe films ended up Ge rich with underlying Te being relatively stripped out. However, in this study it has been discovered that the Ge deposition is very time crucial. This was very important as it became apparent that when more gentle, lesser potentials were used for longer times, samples with the desired coverages could still be achieved. As shown in Figure 2.8, the structure of the Ge deposited varied quite differently as a function of time. By 5 s most of the first layer of Ge had deposited and by 10 s the second UPD feature started to fill in. However, as the second feature filled in, a little bit of germanene deposition was impossible to avoid. Various combinations of times and potentials were tested to try to optimize the first Ge deposition with -1075 mV for 20 s selected. Figure 2.9 gives a sample Current Time Trace for a typical GeTe sequence. Immediately upon the deposition pulse, there is a first feature in the current corresponding to the first UPD structure being filled out. As the potential is further held, the second UPD structure fills out with just the beginning of germanene formation. Further holding of the potential would result in much more germanene formation without gaining any further UPD Ge.

2.4.3 CREATING A DEPOSITION CYCLE FOR SUBSEQUENT GETE LAYERS

Early deposition sequences where the potentials for each element were used the entire sequence, led to deposits where one metal was in great excess. To combat this, the first layer of GeTe

was treated as its own film and then used as the substrate for future deposition cycles. As suggested in Figure 2.7, the Ge required a more negative deposition potential for shorter times once the electrode more resembled GeTe instead of Au. In Figure 2.10 a stripping curve of Te deposited on a Ge surface is shown in blue. The Te shows a slightly greater affinity for depositing on Ge with a coverage of 0.44 ML deposited as opposed to only the 0.37 ML that was achieved on Au in black. This resulted in the Te deposition region for the UPD Te being shifted to more positive potentials. The results of optimization suggested that for the second layer GeTe, a more negative Ge deposition potential of -1175 mV held for a shorter period of 9 s obtained optimal Ge coverage without stripping out the underlying Te. Unlike with the Ge which moved to more negative deposition potentials, reductive stripping of bulk Te happened at earlier potentials on GeTe. Because of this, a more positive deposition potential was needed for the Te than on Au or Ge. Second layer Te deposition was found to be optimal at -900 mV for 15 s.

The potential at which blanks were introduced became an important parameter for the sequence as the deposits got thicker. This is likely caused by the fact that Ge and Te stripped at slightly more negative potentials in blank solution instead of a precursor solution due to Le Chatlier's Principle. The precursor ions being present granted a slight deposit stability. If the blanks were introduced at too positive a potential the Ge stripped oxidatively. A potential of -900 was chosen because it allowed for maximum stability of the Ge on the surface. If -1000mV was used after Te deposition for the second layer, the Te films would be reductively stripped before Ge could be deposited on top to stabilize it. A sample Current Time Trace shows this occurence in Figure 2.11. The reduction feature when the blank is first introduced is attributed to this further reductive stripping of the UPD Te layer before it can be stabilized. Subsequent depositions where blank was introduced at -900 mV solved the problem and allowed further growth to occur.

The presence of the metals was very important for the growth of the other; Ge or Te could not grow without the other. If layers of Ge deposition were skipped, the surface would still be Te rich and Te growth would stall as the growth conditions would not allow bulk Te deposition. If layers of Te were skipped the Ge would eventually form germanene and the growth would be self-terminated after 3.5 ML. This suggests that a GeTe compound is being formed as the layers are dependent on each other. Other proof of a GeTe compound became evident as the mechanism for GeTe growth was better understood.

2.4.4 MECHANISM FOR GETE INTEGRATION

The first layer of GeTe involved Ge deposition followed by Te deposition. This was chosen as Ge starting films tended to be more linear in terms of stoichiometry per deposition cycle. The first Ge deposition covers 0.45 ML of the substrate. Following the Ge on Au, the Te is introduced and it is believed that the mechanism involves lifting the Ge structure off the substrate surface and depositing under it. This allows a slightly larger amount of Te to be deposited of 0.44 ML, as it is interacting with the Ge layer above it in addition to sitting on the Au surface. The Ge now is bound to the Te creating the GeTe compound instead of displaying the more disordered surface it had on the Au. This is evidenced in the stripping curves in Figure 2.10 by the blue scan. The Te oxidative stripping position is still similar with just a slight increase in charge. The real justification comes from the change in shape and location of the Ge component. The 3 Ge on Au structures in red are completely gone and merged into the one peak which has the same area of charge as all 3 previous structures combined. This suggests that the Ge isn't stripped when it is lifted from the Au, but is rather converted to the GeTe structure. The peak shape and position are also very different from that of germanene. In both the red and green scans, the germanene peak is irregularly shaped with a marked fronting of the peak and centered much closer to -350 mV.

Evidence that the new structure is now bound on top of the Te is suggested by the lack of a fundamental UPD Ge on Au peak at -150 mV. If the Ge is present on the Au surface, that peak would remain. Once this first layer of GeTe is formed future depositions of Ge and Te will alternate and help to stabilize each other.

2.4.5 QUANTIFICATION AND STOICHIOMETRY OF GETE FILMS

Quantification of the individual components was done using the in-situ coulometry until 30 deposition cycles. Past this point the charges started to get sufficiently large and the FWHM of the peaks started to converge on each other making quantification difficult. By examining the trend, it can be showed that as the films progressed in terms of number of cycles, the ratio of Ge to Te stayed very close to 1:1 as seen in Figure 2.12 where they grew almost linearly. By 30 cycles of GeTe growth, the Ge and Te measured at 2.75 ML of coverage. According to theoretical STM calculations made by Deringer et al., this suggested that the 30 cycle films were roughly 1nm thick.[30] It was determined that thicker films should be created and tested using SEM/EDS to confirm that the technique works as the films continue to grow. Films were made of 100 and 250 cycles to test the scalability of the deposits. While the films were barely visible to the naked eye, at a microscopic level, the films clearly had a coating of GeTe material which had the ideal 1:1 stoichiometry as confirmed by EDS as shown in Figure 2.13. EDS was taken at spots at the intlet, middle and outlet of the films and there was little stoichiometric variation with Te average at 49.4% and Ge at 50.6%

Due to how thin the films were, sideways SEM wasn't available to determine thickness of the samples. We know that they are still relatively thin, and the length of the process is quite time consuming. 250 cycles translated to roughly 7.5 hr of deposition time. To shorten the cycle there is only so much that can be done, due to the need of properly rinsing out each solution before the next one

enters the flow cell. A more likely avenue would be to stagger the Ge deposition potential a little more negative after a certain amount of cycle repetitions. The process is likely slowing down due to the limited amount of Ge depositing on thicker GeTe samples. Due to the dependence of the Ge growth on the stability of the Te layer, it is crucial that ample Ge is deposited each cycle or growth will stagnate.

2.4.6 IDENTIFICATION USING RAMAN SPECTROSCOPY

One of the challenges with Raman Spectroscopy on GeTe films is that the 780 nm laser source has been proven to promote germanene growth. To avoid this, a 532 nm laser source is used. It has been shown that the 532 nm laser cannot promote germanene growth, but it can however detect when the germanene sheets are present. Figure 2.14 shows the Raman spectrum for the center of the 250-cycle deposit. The resulting shifts are indicative of a GeTe film from the literature. More importantly, there is not a 295 wavenumber peak that is indicative of germanene formation.

2.5 CONCLUSION

GeTe thin films show promise as phase change materials in PRAM applications due to their stable crystalline and amorphous phases. Previous work on the E-ALD of GeTe reported films very Ge rich due to Te stripping out during the deposition cycles. By working in a very narrow potential region with controlled deposition times, the 1:1 stoichiometry can be achieved. This was done by manipulation of Ge deposition times at lesser potentials, allowing more Te to remain on the surface. Additionally, treating the first GeTe layer as its own compound and subsequent substrate for future deposition programs allowed for the stoichiometry to stay 1:1 throughout the whole process. For all following cycles, the Ge was deposited at a more negative potential and Te was deposited more positively. The

presence of the GeTe compound was proved using stripping coulometry. Peaks indicative of Ge on Au or germanene on Au were not present when GeTe was formed. Stoichiometry was measured for very thin samples using the in-situ coulometry and the thicker deposited films were investigated using SEM and EDS which revealed that the desired ratio was present as films grew thicker. Raman Spectroscopy was also used to investigate the properties of the film and confirmed that while GeTe was deposited, germanene was not being formed.

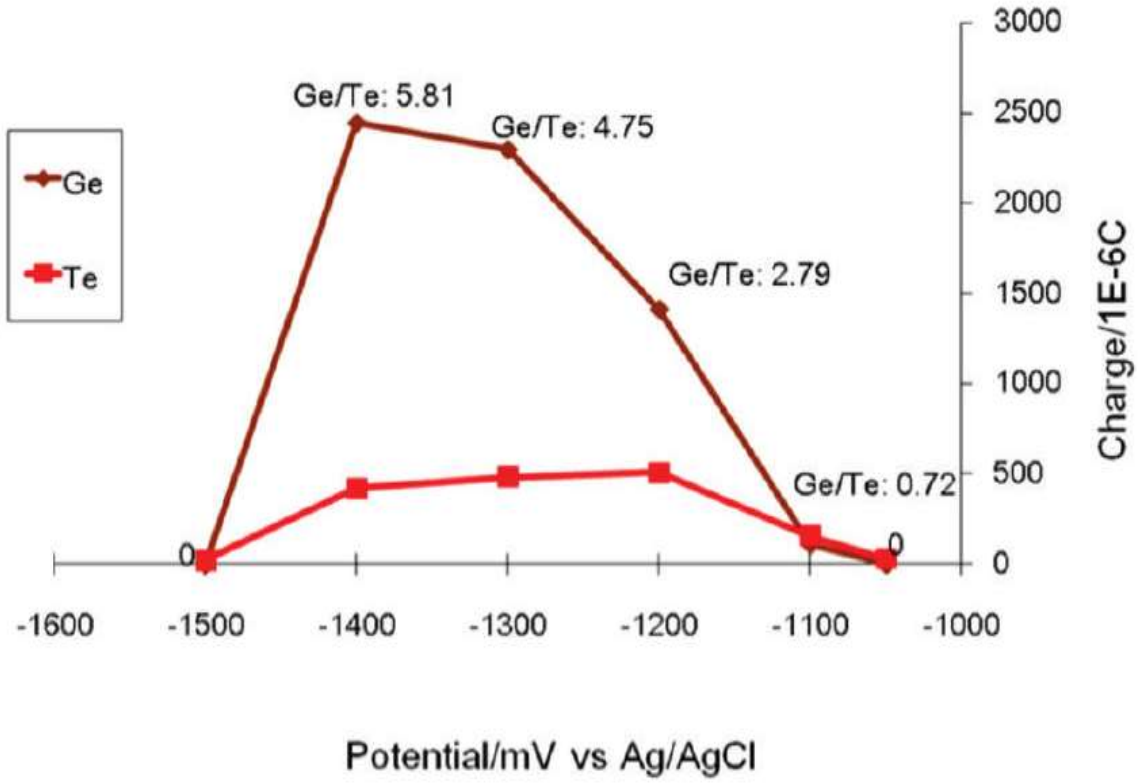

Figure 2.1- Ratios of Ge/Te in films using varying Ge deposition potentials. A trend towards Ge rich films is shown. This work appears in reference 24.

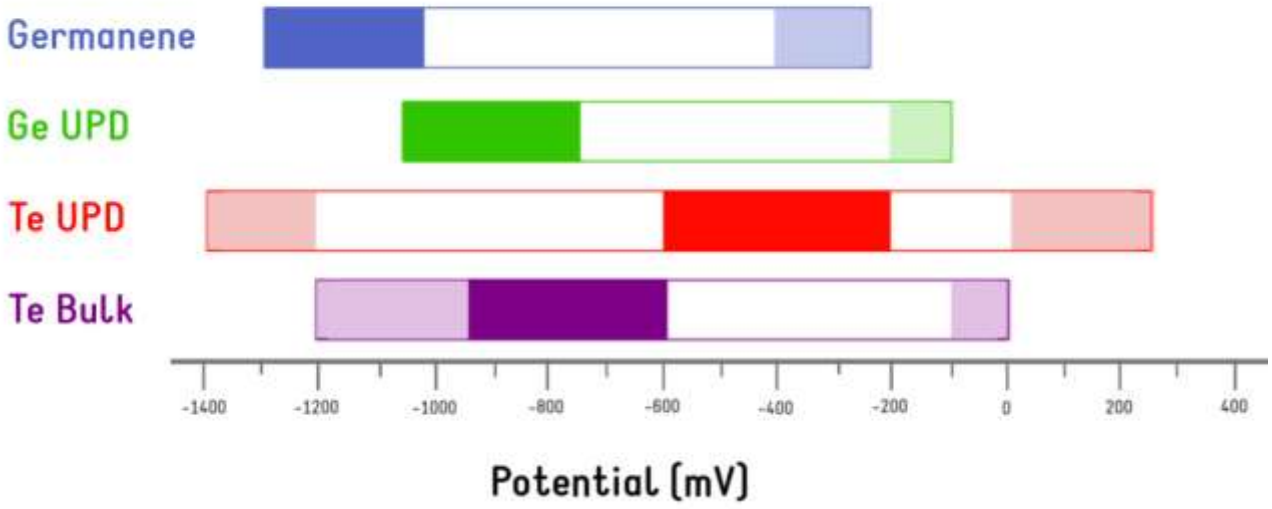

Figure 2.2- Overview of the deposition and stripping potentials of the UPD and bulk features of Ge and Te. Dark regions represent deposition with lighter regions being stripping. Any area in white designates that no reaction occurs in that region.

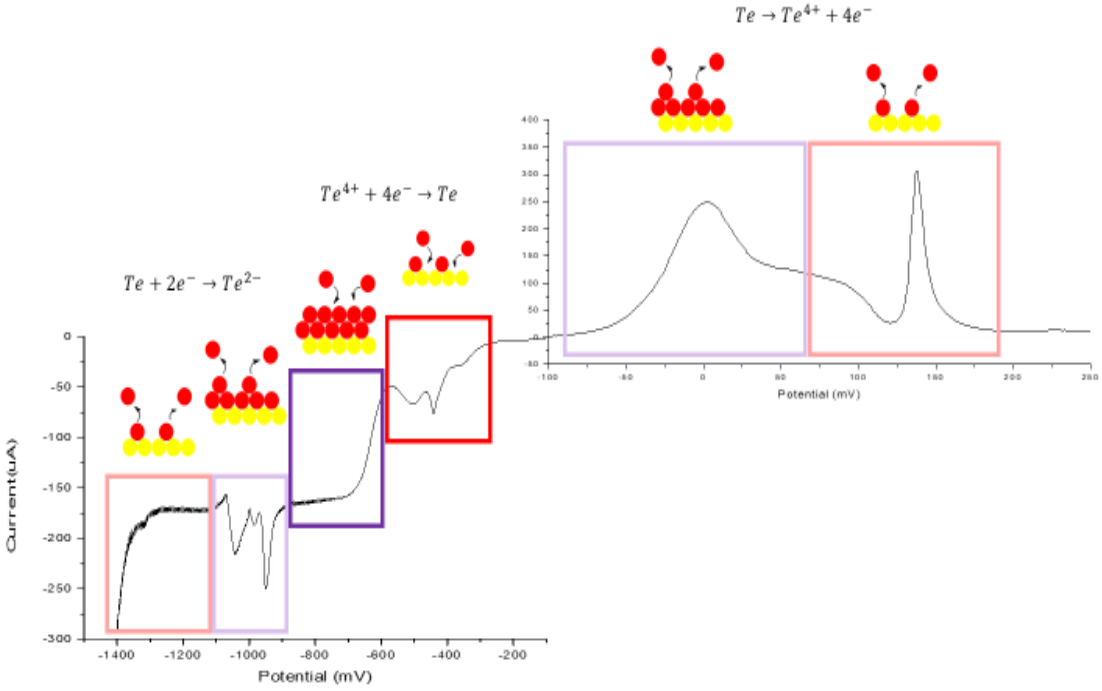

Figure 2.3- Voltammetry of Te precursor solution on Au substrate at pH=9.3 Due to the complicated nature of the Te ion, there are two regions of Te stripping, oxidative and reductive.

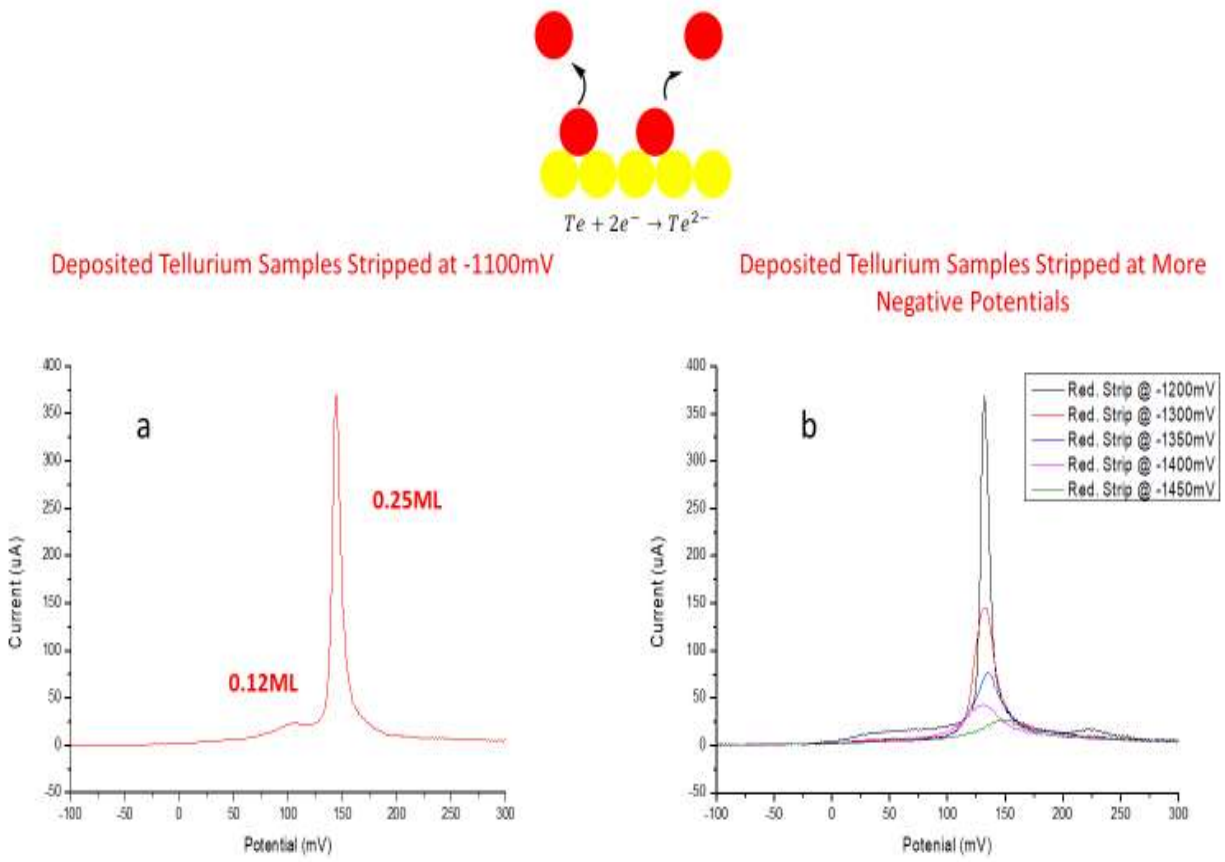

Figure 2.4- Part a depicts the stripping voltammetry of a UPD Te layer. There are two surface limited features that make up this structure. Part b shows the stripping voltammetry of Te that has been deposited at more negative potentials. As Te is deposited at more negative potentials, less UPD Te remains.

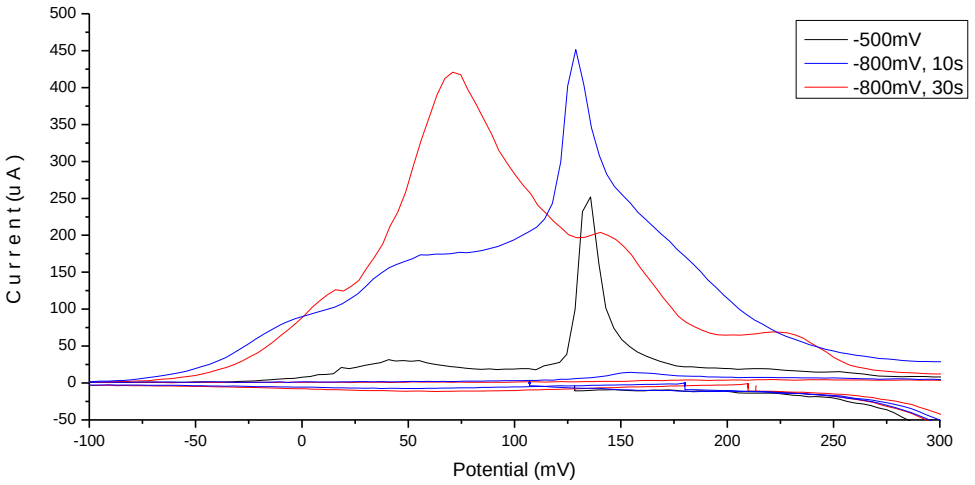

Figure 2.5- Te deposited at various potentials and then stripped. The black line shows a surface limited deposit for 30 s. In the blue scan, Te is deposited at a bulk region for 10 s and then stripped. Bulk formation is evident. In the red scan, Te is deposited in the bulk region for 30 s revealing much more bulk deposit.

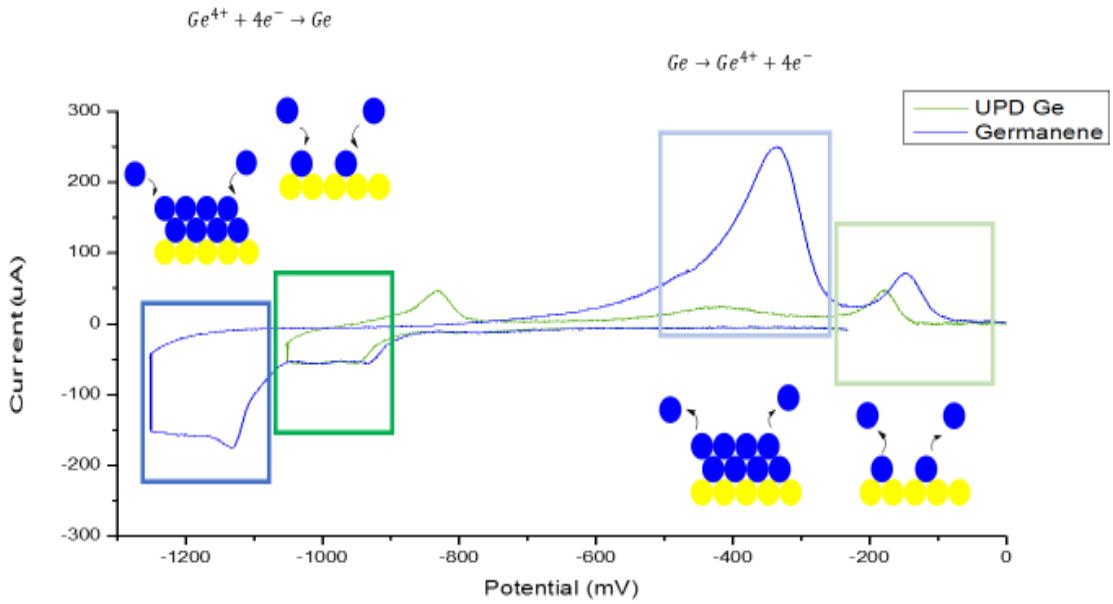

Figure 2.6- Voltammetry for Ge. Instead of having a normal bulk phase like most materials, Ge forms germanene at sufficiently negative potentials. This is indicated by a large transformation in stripping voltammetry.

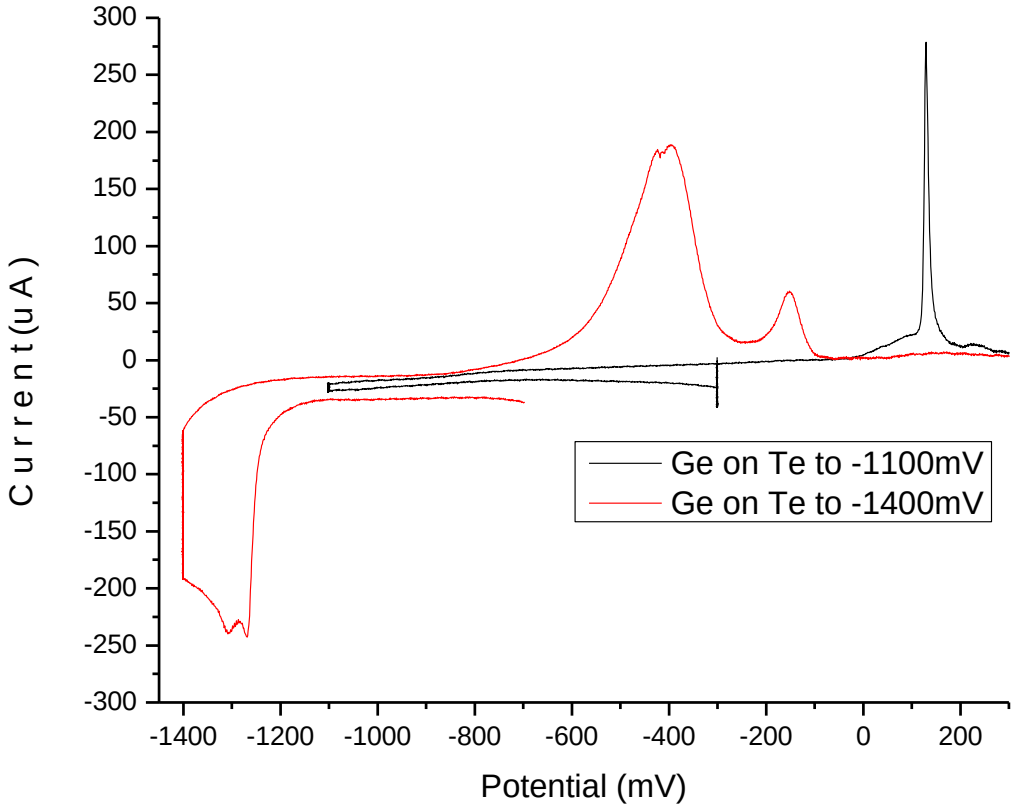

Figure 2.7- Deposition of Ge on a Te Substrate Surface. In the black scan, the potential is stopped at potentials where Ge would normally deposit on Au. In the red scan, the potential is scanned much more negatively until germanene formation is fully achieved.

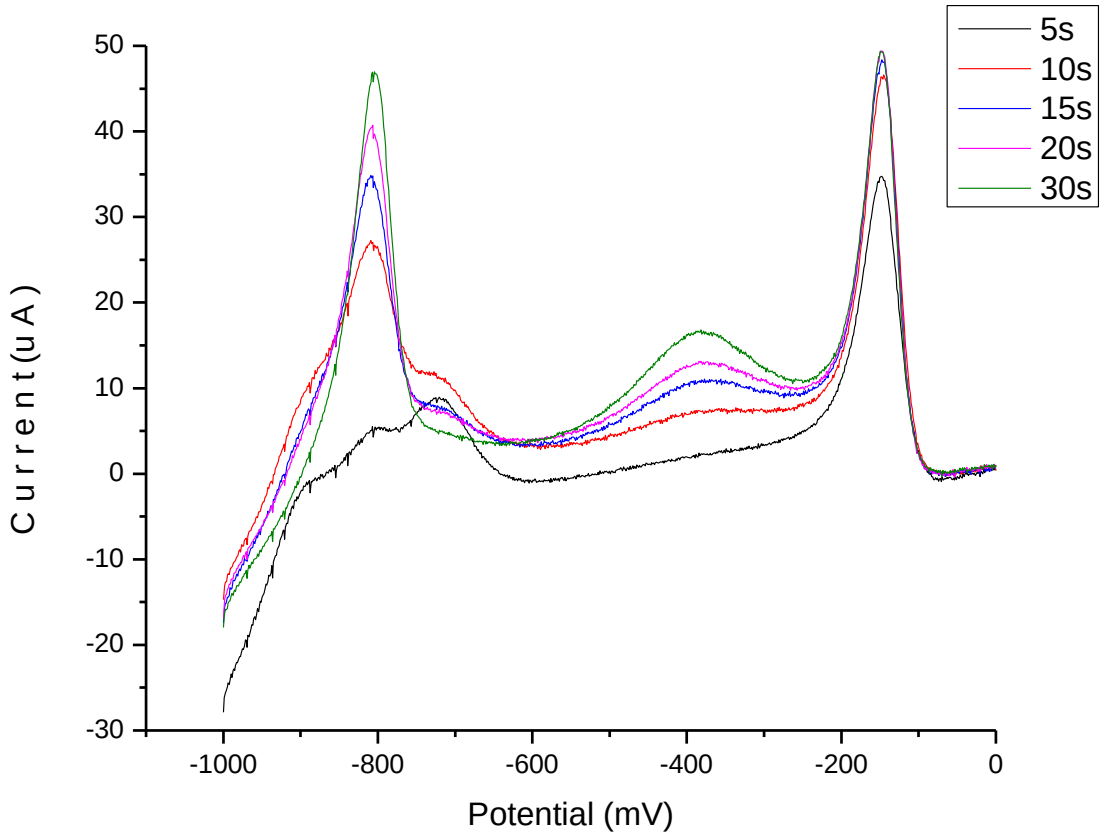

Figure 2.8- Ge was deposited on Au at -1075 mV. At this potential only UPD Ge should be able to form. As the potential is held for longer periods more of the Ge UPD layer fills in. Once the UPD layer is fully achieved, a bit of germanene deposition starts to occur.

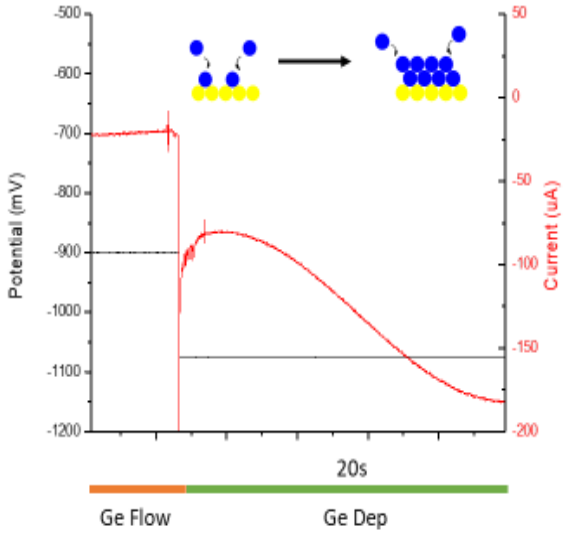

Figure 2.9- A typical deposition sequence for Ge on Au. Ge solution is flowed into the cell and then when the cell is filled, the potential is pulsed negatively to -1075mV for 20s. The resulting current can is indicative of how the deposition occurs. There are 2 different peaks in the current suggesting that two different steps occur when the pulse occurs as time increases.

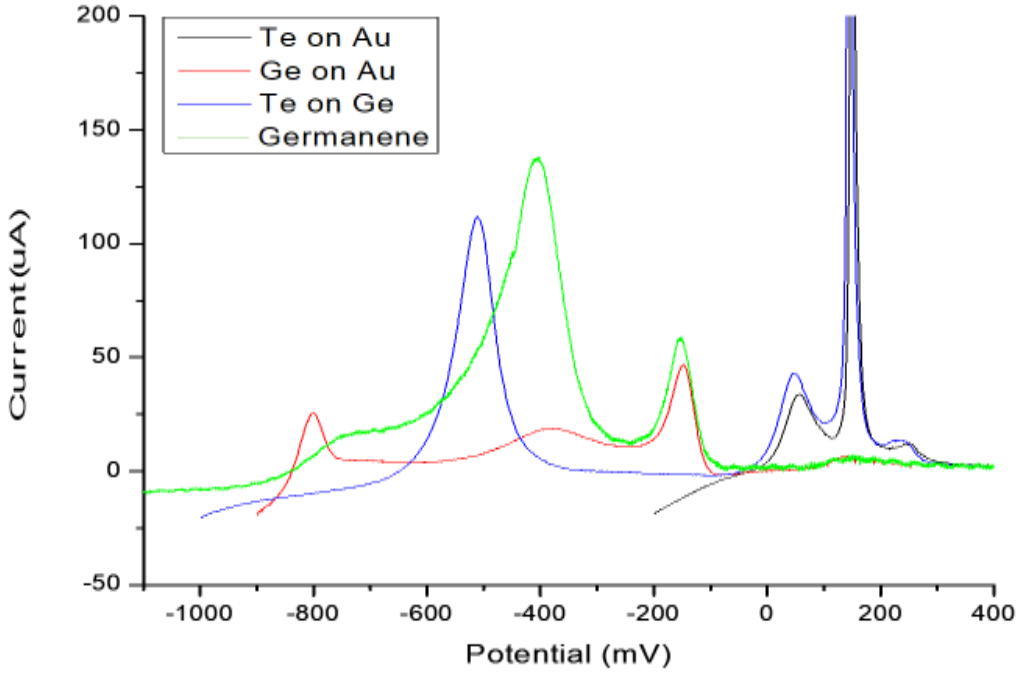

Figure 2.10- This figure depicts the stripping voltammetry of the first layer of GeTe formation. In black, stripping of Te on Au is shown. Red shows UPD Ge stripping on Au. Green depicts the unique peak for germanene formation as a form of comparison. In Blue, Ge is deposited onto the Au surface and then Te is deposited second. This leads to the Ge restructuring on top of the Te.

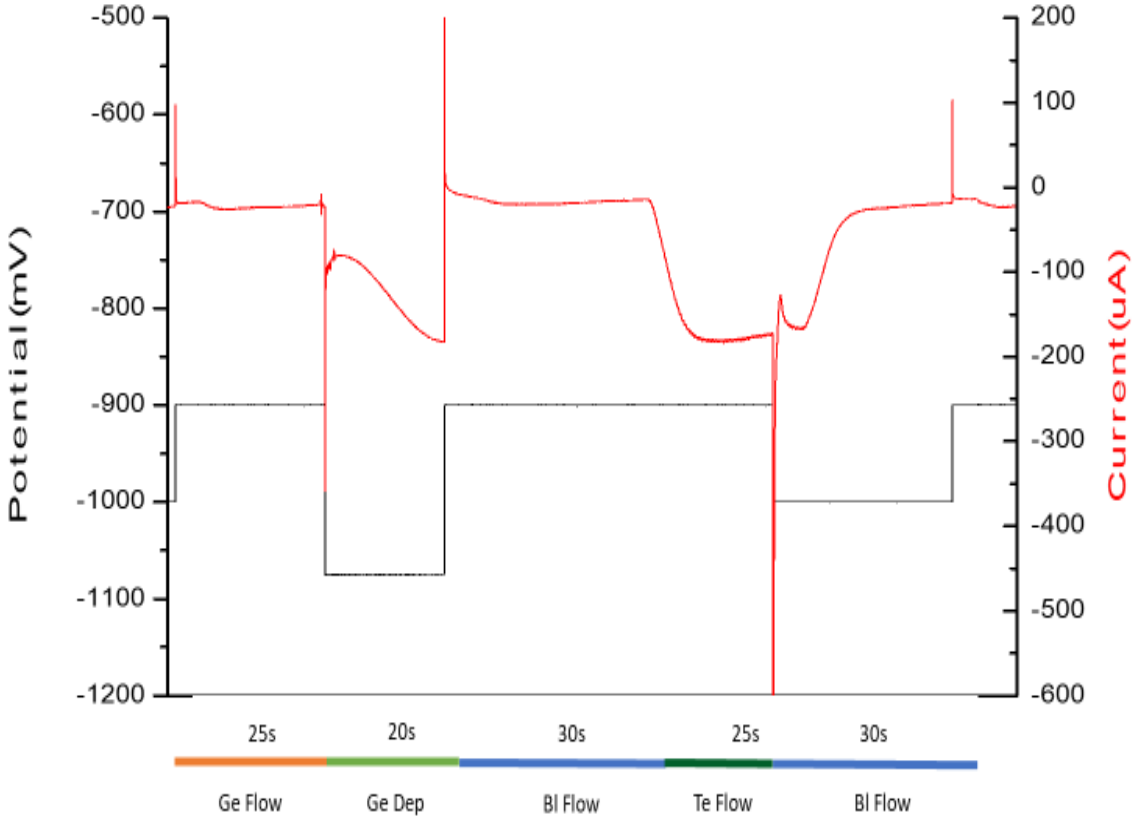

Figure 2.11- Sample deposition cycle for the 2nd layer of GeTe. When the blank is introduced after Te deposition, there is an initial reduction feature indicative of unintended Te UPD stripping.

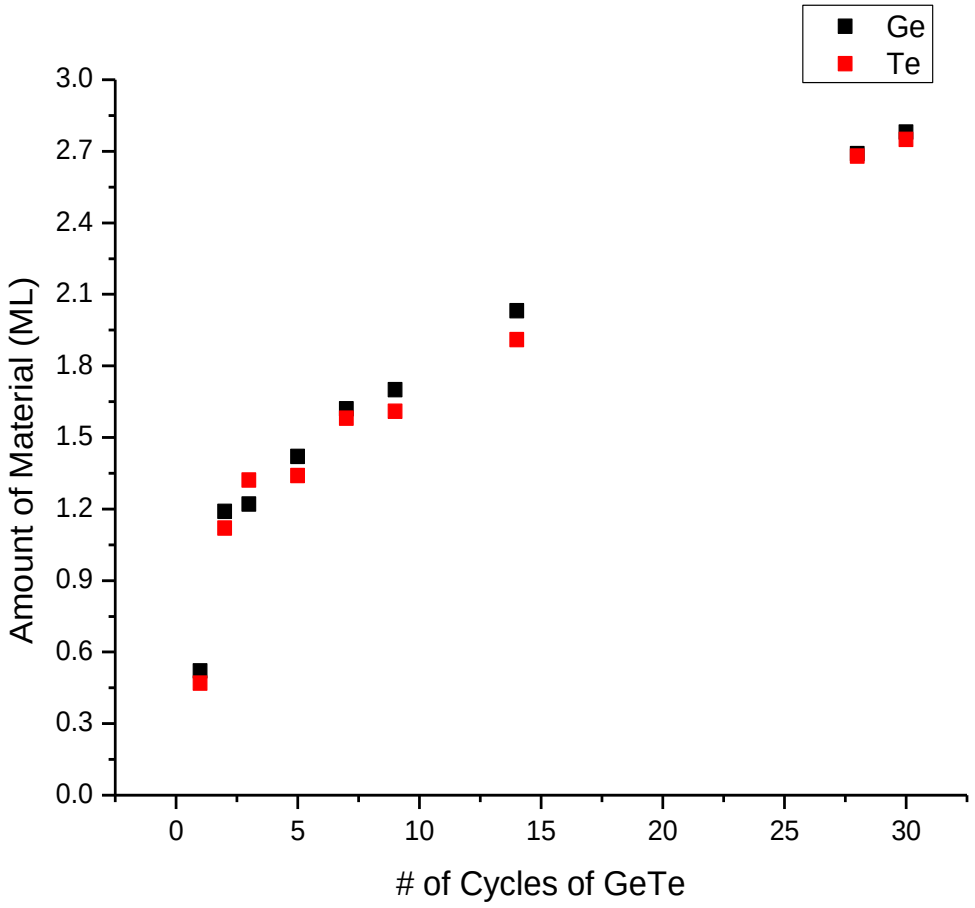

Figure 2.12- Amount of Ge and Te deposited as the number of cycles is increased. After the initial layer, the deposition is relatively linear in growth with both coverages staying very similar.

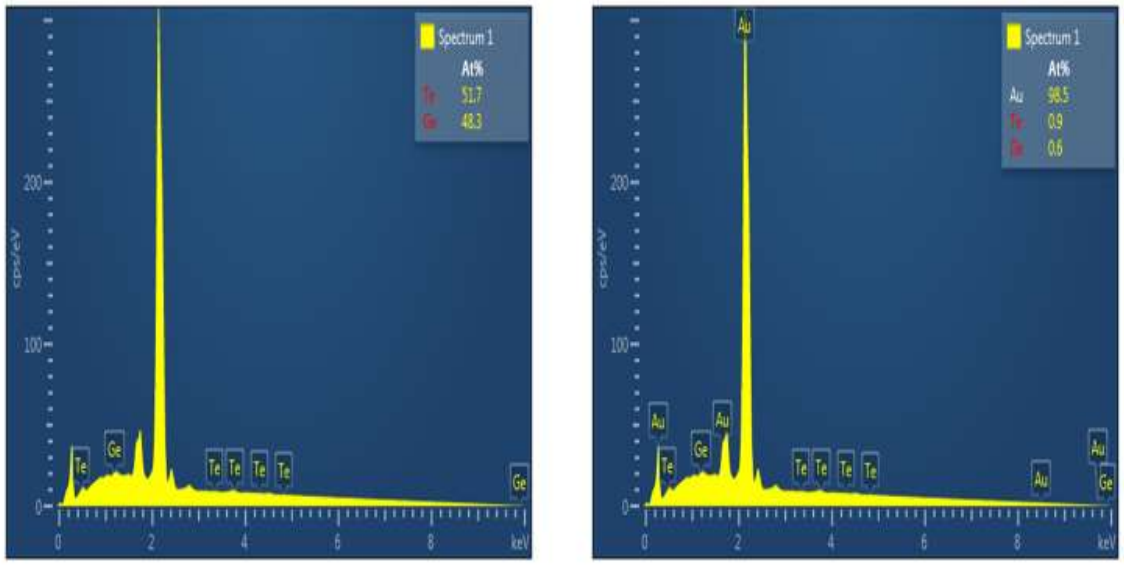

a b

Figure 2.13- EDS data for the 250 cycle GeTe films. Part a gives the ratio of Te to Ge on the film. Part b includes the input from the underlying Au substrate.

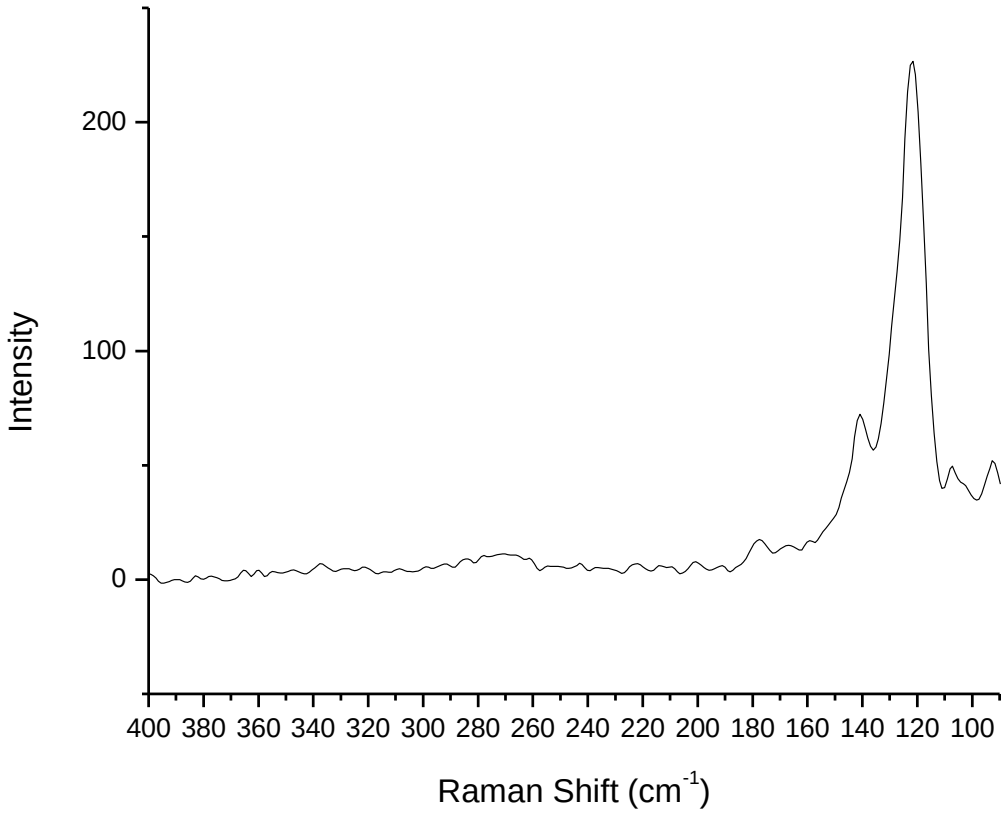

Figure 2.14- The spectrum for the thicker GeTe deposits compared well with literature data for GeTe and more importantly did not show the 295 peak which is indicative of germanene growth.

REFERENCES

1. Gregory, B.W.; Stickney, J.L. Electrochemical Atomic Layer Epitaxy (Ecale). *Journal of Electroanalytical Chemistry* **1991**, 300, 543-561.

2. Suggs, D.W.; Stickney, J.L. Studies of the Surface-Structures Formed by the Alternated Electrodeposition of Cd and Te on the Low-Index Planes of Au Stm Studies. *Surface Science* **1993** 290, 375-387.

3. Lister, T.E.; Huang, B.M.; Herrick, R.D.; Stickney, J.L. Electrochemical Formation of Se Atomic Layers on Au (100). *Journal of Vacuum Science and Technology B* **1995**, 13, 1268-1273.

4. Lister, T.E.; Stickney, J.L. Atomic level studies of selenium electrodeposition on gold (111) and gold (110). *Journal of Physical Chemistry* **1996**, 100, 19568-19576.

5. Lister, T.E.; Stickney, J.L. Formation of the first monolayer of CdSe on Au (111) by electrochemical ALE. *Applied Surface Science* **1996**, 107, 153-160.

6. Stickney, J.L. Electrochemical atomic layer epitaxy. *Electroanalytical Chemistry* **1999** 21, 75-209.

7. Sorenson, T.A.; Lister, T.E.; Huang, B.M.; Stickney, J.L. A comparison of atomic layers formed by electrodeposition of selenium and tellurium- Scanning tunnel microscopy studies on Au (100) and Au (111). *Journal of the Electrochemical Society* **1999**, 146, 1019-1027.

8. Sorenson, T.A.; Suggs, D.W.; Nandhakumar, I.; Stickney, J.L. Phase transitions in the electrodeposition of tellurium atomic layers on Au (100). *Journal of Electroanalytical Chemistry* **1999**, 467, 270-281.

9. Vaidyanathan, R.; Stickney, J.L.; Cox, S.M.; Compton, S.P.; Happek, U. Formation of In2Se3 thin films and nanostructures using electrochemical atomic layer epitaxy. *Journal of Electroanalytical Chemistry* **2003**, 559, 55-61.

10. Venkatasamy, V.; Shao, I.; Huang, Q.; Stickney, J.L. ALD approach toward electrodeposition of Sb2Te3 for phase-change memory applications. *Journal of the Electrochemical Society* **2008**, 155, 693-698.

11. Liang, X.H.; Kim, Y.G.; Gebergziabiher, D.K.; Stickney J.L. Aqueous Electrodeposition of Ge Monolayers. *Langmuir* **2010**, 26, 2877-2884.

12. Banga, D.; Perdue, B.; Stickney, J.L. Formation of CuIn(1-x)GaxSe2 (CIGS) by Electrochemical Atomic Layer Deposition (ALD). *Journal of the Electrochemical Society* **2014**, 161, 141-146.

13. Sosso, G.C.; Miceli, G.; Caravati, S.; Behler, J.; Bernasconi, M. Neural network interatomic potential for the phase change material GeTe. *Physical Review B* **2012**, 85, 174103-174113.

14. Akola, J.; Jones, R.O. Structural phase transitions on the nanoscale: The crucial pattern in the phase-change materials Ge2Sb2Te5 and GeTe. *Physical Review B* **2007**, 76, 235201-235210.

15. Lencer, D.; Salinga, M.; Grabowski, B.; Hickel, T.; Neugebauer, J.; Wuttig, M. A map for phase-change materials. *Nature Materials* **2008**, 7, 972-977.

16. Qiao, M.; Chen, Y.; Wang, Y.; Li, Yafei. The germanium telluride monolayer: a two dimensional semiconductor with high carrier mobility for photocatalytic water splitting. *J. Mater. Chem. A.* **2008**, 6, 4119-4125.

17. Sarnet, T.; Pore, V.; Hatanpaa, T.; Ritala, M.; Leskela, M.; Schrott, A.; Zhu, Y.; Raoux, S.; Cheng, H.Y. Atomic Layer Deposition and Characterization of GeTe Thin Films. *Journal of The Electrochemical Society* **2011**, 158, 694-697.

18. Peng, C.; Wu, L.; Rao, F.; Song, Z.; Zhou, X.; Zhu, M.; Liu, B.; Yao, D.; Feng, S.; Yang, P.; Chu, J. Nitrogen incorporated GeTe phase change thin film for high-temperature data retention and low-power application. *Scripta Materialia* **2011**, 65, 327-330.

19. Abrutis, A.; Plausinaitiene, V.; Skapas, M.; Wiemer, C.; Gawelda, W.; Siegel, J.; Rushworth, S. Hot-wire chemical vapor growth and characterization of crystalline GeTe films. *Journal of Crystal Growth* **2009**, 311, 362-367.

20. Giussani, A.; Perumal, K.; Hanke, M.; Rodenbach, P.; Riechert, H.; Calarco, R. On the epitaxy of germanium telluride thin films on silicon substrates. *Phys. Status Solidi B* **2012**, 10, 1939-1944.

21. Navarro, G.; Sousa, V.; Persico, A.; Pashkov, N.; Toffoli, A.; Bastien, J.C.; Perniola, L.; Maitrejean, S.; Roule, A.; Zuliani, P.; Annunziata, R.; De Salvo, B. Material engineering of GexTe100-x compounds to improve phase-change memory performances. *Solid-State Electronics* **2013** 89, 93-100.

22. Lee, H.S.; Kim, B.S.; Cho, C.W.; Oh, M.W.; Min, B.K.; Park, S.D.; Lee, H.W. Herringbone structure in GeTe-based thermoelectric materials. *Acta Materialia* **2015**, 91, 83-90.

23. Zhang, L.; Miao, N.; Zhou, J.; Mi, J.; Sun, Z. Insight into the role of W in amorphous GeTe for phase-change memory. *Journal of Alloys and Compounds* **2018**, 738, 270-276.

24. Liang, X.; Jayaraju, N.; Thambidurai, C.; Zhang, Q.; Stickney, J.L. Controlled Electrochemical Formation of GexSbyTez using Atomic Layer Deposition (ALD). *Chem. Mater.* **2011**, 23, 1742-1752.

25. Liang, X.; Kim, Y.G.; Gebergziabiher, D.K.; Stickney, J.L. Aqueous Electrodeposition of Ge Monolayers. *Langmuir* **2009**, 26, 2877-2884.

26. Liang, X.; Zhang, Q.; Lay, M.D.; Stickney, J.L. Growth of Ge Nanofilms Using Electrochemical Atomic Layer Deposition, with a “Bait and Switch” Surface-Limited Reaction. *Journal of The American Chemical Society* **2011**, 133, 8199-8204.

27. Bui, N.N.; Ledina, M.; Reber, T.J.; Jung, J.; Stickney, J.L. Electrochemical Scanning Tunneling Microscopic Study of the Potential Dependence of Germanene Growth on Au (111) at pH 9.0 *ACS Nano* **2017**, 11, 9481-9489.

28. Ledina, M.A.; Bui, N.; Liang, X.; Kim, Y.G.; Jung, J.; Perdue, B.; Tsang, C.; Drnec, J.; Carla, F.; Reber, T.J.; Stickney, J.L. Electrochemical Formation of Germanene: pH 4.5. *Journal of The Electrochemical Society* **2017**, 164, 469-477.

29. Jung, J.; Bui, N.N.; Shen, S.; Reber, T.J.; Brezner, J.M.; Mubeen, S.; Stickney, J.L. In Situ Surface-Enhanced Raman Spectroscopic Studies of Electrochemically Formed Germanene. *J. Phys. Chem. C.* **2018**, 122, 15696-15705.

30. Deringer, V.L.; Lumerij, M.; Dronskowski, R. Ab Inition Modeling of a-GeTe (111) Surface. *J. Phys. Chem. C* **2012**, 116, 15801-15811.

CHAPTER 3

POTENTIAL PULSE ATOMIC LAYER DEPOSITION (PP-ALD) OF INSE AND IN_2SE_3

Sisk, P.; Howell, P.; Mubeen, S.; Stickney, J. To be submitted to ECS journal.

3.1 ABSTRACT

Using Electrochemical Atomic Layer Deposition (E-ALD) and it's one-solution counterpart, Potential Pulse Atomic Layer Deposition (PP-ALD), programs were developed for the deposition of In_2Se_3 and InSe thin films. Both E-ALD and PP-ALD utilize the property of underpotential deposition, but while E-ALD requires solution switching, PP-ALD is done from one solution bottle and requires careful alternation of cathodic and anodic pulses to limit the material deposited. This allows for PP-ALD to be a much faster deposition process, but it can be more challenging to design a deposition program as both solutions must be soluble in the same pH's and deposit and strip at similar electrochemical potentials. By choosing optimal parameters governed by the Nernst equation such as pH, potential, and precursor concentration as well as physical conditions such as duty time, light exposure, and supporting electrolyte concentration, optimal deposition conditions can be achieved. Use of cyclic voltammetry and current-time traces allow for the monitoring of the deposition process in-situ while a variety of characterization methods can be used on the thin films after the deposition process is complete. Morphology of the deposits was characterized using SEM while the structural composition was analyzed with EDX and EPMA. Structural characterization was done by XRD and Raman Spectroscopy. On their own In_2Se_3 and InSe are interesting as potential photoanodes or photocathodes in a photoelectrochemical cell but can also be combined with other binary compounds into the super-structure, Copper Indium Gallium Selenide (CIGS) as well for solar cell use.

3.2 INTRODUCTION

In_2Se_3 is an N-Type semiconductor with a bandgap varying between 1.4-2.2 eV depending on what polytype of the structure was displayed.[1-5] There are 5 main polytypes of In_2Se_3 discovered, each having their own slight variations in bandgap and deposition technique: α, β,γ, δ, and κ phases.[2-5] It is not uncommon for films to display multiple polytypes, leading to poly-crystalline deposits. Due to the N-Type nature of these deposits and adequate bandgaps, these materials are optimal for use in Photoelectrochemical Cells (PEC) as photoanodes. Due to the bandgap of these materials exceeding the 1.2 V of photovoltage needed for the splitting of water, O_2 gas can be formed at these photoanodes, turning a cheap, widely available resource into a valuable fuel source.[6-10] Another stoichiometry of the compound, InSe is also stable and can be a P-Type semiconductor which is suitable for use as a photocathode in the PEC. At the photocathode, water is reduced into H_2 gas, another more expensive fuel source. Additionally, In_xSe_y can be used as one of the binary precursors to the super-compound Copper Indium Gallium Selenide/Sulfide (CIGS). CIGS is a very tunable compound that has found use in many different PV solar cell applications.[11-13] In addition to being used for its photovoltaic properties, In_xSe_y is finding use as a phase change material between the α and β phases.[2-5] Both the In_2Se_3 and InSe compounds have been shown to have the capability to be 2D materials, or compounds that exist in a single layer, often in ribbon form.[2] These layers can also be stacked on top of each other by Van der Waal's attraction and then subsequently exfoliated.[4,5]

Electrochemical Atomic Layer Deposition (E-ALD) was invented in the Stickney labs 30 years ago for the deposition of metal and compound semiconductor thin films. It relies on the principles of surface-limited reactions to form atomically thin layers of alternating metal materials.[14-25] These surface-

limited reactions rely on a phenomenon called Underpotential Deposition (UPD) where one metal (M_1) can be deposited onto another metal (M_2) at an electrochemical potential less than would be needed to deposit M_1 onto itself. These reactions form fractions of a monolayer (ML) at a time, to build up a compound semiconductor without bulk deposits. A monolayer will be defined as having one surface atom for each underlying substrate atom. These surface-limited deposits have traditionally been done in the gas phase, however, E-ALD allows for a cheaper, solution-based method for making these thin films. By keeping the solutions employed as pure as possible and without complexing agents, unwanted side reactions can be avoided that would damage the film.[14-25] Because E-ALD can be done at room temperature and standard pressure, it is a much cheaper alternative to the expensive reactors used in Chemical Vapor Deposition (CVD) or Molecular Beam Epitaxy (MBE) which are prevalent in industry today.

Potential-Pulse Atomic Layer Deposition (PP-ALD) is a one-solution variant of E-ALD. PP-ALD relies on the same principles of using UPD potentials to deposit a ML at a time of each material, however, now both metal precursors must co-exist in the same solution. PP-ALD is a combination of several electrochemical techniques such as Codeposition, Sequential Monolayer Deposition (SMD), Pulse Potential Electrodeposition, and E-ALD.[26-29] Codeposition in electrochemistry requires both precursors to be in the same solution and involves depositing a material at a constant deposition potential. This method is common in the industrial plating industries. In SMD, a single solution precursor is used, and the potential is scanned reductively and oxidatively to deposit film and then subsequently strip off any excess material. By combining an E-ALD cycle with a codeposition bath, pulsed alternations of deposition potential and a resting stripping step can be used to form epitaxial films. These films are deposited much quicker than their E-ALD counterparts and allow a high level of control based on the duty time and potentials of the pulses. There are some challenges to using PP-ALD technique. Both precursor ions must be stable in a solution of the same pH, as well as not interact with each other in the

solution at Open Circuit Potential (OCP). Additionally, they must be able to deposit and strip at similar potentials. This technique has been applied to thin film semiconductors such as ZnS, In_2Se_3, CdTe, and Cu_2Se.[26-29]

In previous In_2Se_3 work done in this lab using PP-ALD, the films were characterized by inhomogeneity caused by H_2 bubbles due to the Hydrogen Evolution Reaction (HER) as seen in Figure 3.1a.[26,27] The bubbles would form on the surface of the substrate and block further deposition in these areas. This would cause the film to have valleys and areas where it was much thicker, leading to a poorer film. While these bubbles can be disrupted by knocking on the flow cell with a hammer, it is difficult to clear the cell adequately due to the speed with which the bubbles form on the substrate surface. An easier way to combat the HER is outlined in this chapter where the pH of the solution is changed. The HER occurs at the same potentials as the In_2Se_3 deposition process as shown in Figure 3.2. The HER is characterized by a rapid exponential increase in current generated at a sufficiently negative potential. The opposite occurs as the Oxygen Evolution Reaction (OER) occurs at sufficiently positive potentials as shown on a clean scan of Au in blank solution in Figure 3.3. By using a slightly more basic pH such as pH=2.0, the In_2Se_3 deposition potential can be moved to slightly more positive potentials as governed by the Nernst Equation in Equation 1. At the same time, the Nernst equation can be manipulated to show that HER will be moved to a slightly more negative potential as shown in Equation 2. By separating the potentials for the two different reactions, In_2Se_3 can be deposited onto the substrate without having to worry about bubble formation. This will yield more homogenous films. Further testing of In_2Se_3 PP-ALD methods at pH=3.0 was conducted by previous group members. The films deposited were very inhomogeneous and failed to adhere well to the substrate. This is likely due to the stability of the precursor solutions as the solutions were found to precipitate likely causing unwanted side reactions.

3.3 EXPERIMENTAL

All experiments were performed in an electrochemical flow cell (Electrochemical ALD L.C.) making use of a 3-electrode set-up. The auxiliary electrode was an inlaid Au wire and the reference electrode was Ag/AgCl in 3 M NaCl (Bioanalytical Systems, Inc.). The working electrode doubles as the polycrystalline Au substrate (Evaporated Metal Films) and was made from glass slides with a 5 nm Ti adhesion layer, topped with 100 nm of Au. The working electrode area was 2.2 cm^2. Solution flow was controlled by a valve block (Neptune Research & Development, Inc.) which was implemented by a potentiostat (Electrochemical ALD L.C.) and controlled by an in-house LabVIEW program named SEQUENCER. This set-up allowed for precise control over which solution was in the cell at any given time, as well as input potentials to the cell and read the resulting current generated.

Slide preparation was done by rinsing the Au substrate in 18 MΩ nanopure water (Millipore Advantage 10) and then washed with acetone (Fisher Chemical) and rinsed again in nanopure water. Next, the slides were exposed to concentrated HNO_3 (JT Baker) for 30 s and then rinsed again with nanopure water. The slides were immediately transferred into the flow cell and 0.1 M H_2SO_4 (Fisher Chemical) was flowed into the cell to limit air exposure time. The substrates were then electrochemically cleaned by 4 alternating 5 s pulses of -200 mV and 1400 mV followed by 2 CV's at 20 mV/s from -200 mV to 1400 mV and back.

Solution bottles were cleaned with Nochromix (Godax Labratories) for at least an hour and then rinsed multiple times with nanopure water. Indium precursor solution was pH=2.0, 1.5 mM $In(ClO_4)_3$ (Sigma-Aldrich) and 0.5 M $HClO_4$ (GFS Chemicals, Inc.) and adjusted to the correct pH with NaOH pellets (Fisher Chemical) and then finished with nanopure water. Selenium precursor solution was pH=2.0, 0.1

mM SeO_2 (Alfa Æsar 99.999% pure) and 0.5 M $HClO_4$, adjusted to the correct pH with NaOH. The Indium Selenide solution was pH=2.0, 1.5 mM $In(ClO_4)_3$ and 0.1 mM SeO_2 with 0.5M $HClO_4$ and adjusted with NaOH. The blank solution was 0.5 M $HClO_4$ adjusted with NaOH to pH=2.0. Before the solutions were introduced to the cell, they were purged in N_2 gas (Airgas) for at least an hour to limit O_2 exposure. Solutions were quite stable, and able to survive for months before any precipitation occurred.

SEM (FE-SEM Thermo Fisher Teneo) was used to observe the morphology and elemental structure of the deposits using 5 keV and 10 keV accelerating voltages. The attached EDS detector (150mm Oxford $XMax^N$) was used for stoichiometry. This stoichiometry was further confirmed using EPMA (JEOL 8600 Superprobe) with 10 keV accelerating voltage. Diffraction patterns from XRD (PANalytical X'PERT Pro) were obtained by use of an open Eulerian cradle to provide glancing angle data and the source was 1.54 Å Cu K_α radiation. Raman Spectroscopy (DXR Raman Microscope, Thermo Scientific) was used for structural identification with a 532 nm Laser source.

3.4 RESULTS AND DISCUSSION

3.4.1 SELECTION OF A SUITABLE pH FOR PP-ALD

Due to the competition with the HER, In_2Se_3 deposits made at pH=1.0 were inhomogeneous, shown in Figure 3.1. By manipulating the Nernst Equation, a shift to more basic pH leads to a separation of the deposition potentials between the In_2Se_3 and HER, allowing for a larger, more stable region for In_2Se_3 films to deposit without the inhomogeneity. Figure 3.2 shows the difference between the cyclic voltammetry of In_2Se_3 solution at pHs 1.0 and 2.0 on a clean Au surface. There is a marked difference between the voltammetry in the region between -600 mV to -1000 mV. In pH=1.0, the HER occurs negative of -750 mV while the In_2Se_3 reaction starts to occur around -650 mV. Due to the very short pulse times of 130 ms, a slight overpotential of -750 mV in past pH=1.0 studies was used for the cathodic

pulse potential, which is at the start of HER. This led to the inhomogeneity shown in Figure 1.1a. Shifting the solution to pH=2.0 yields the voltammetry in Figure 3.2b. In_2Se_3 deposition starts at -600 mV and there is a 2nd deposition feature presented at -800 mV. After the peak at -800 mV, HER starts to occur around -900 mV. Identification of these peaks will be addressed in section 3.4.2. Since more basic potentials seem desirable, pH=3.0 solution was tested previously by Stickney members. These experiments were repeated in this study and confirmed that films did not adhere to the substrate and had spotty coverage. Additionally, solution precipitation in these pH=3.0 solutions was evident after only a few hours of creation. This was likely the In precursor ions precipitating as suggested by the Pourbaix diagrams. It is also possible that In and Se precursor ions were reacting at the more basic pH, creating side reactions before even being introduced to the substrate. It is unlikely that Se ion itself was precipitating because Se solutions as basic as pH=9.3 have been created in this lab where solution stability has not been an issue.

3.4.2 WINDOW OPENINGS AND IDENTIFICATION OF STRUCTURES IN VOLTAMMETRY

Figure 3.3 displays the voltammogram of a blank solution on clean Au. OER starts to occur at 1000 mV after the oxidation of the Au features. Au reduction occurs at 350 mV and then HER doesn't start until -1000 mV. This long region of OCP between OER and HER is valuable because it allows for a large window of thin film deposition without bubble interference.

The individual precursor solutions give a general relative idea of where deposition potentials occur, however, they are greatly shifted when introduced to the codeposition solution. For this reason, in this study the focus is on the voltammetry of the codeposition solution in Figure 3.2b. OCP for the solution occurs in the region between 400 mV and 700 mV. As the potential is scanned negatively, the first reduction feature is seen at 300 mV and is indicative of the first Se UPD structure. Se is known to

have relatively slow kinetics at this pH, so it is likely that this UPD peak extends until the second reduction feature seen at -200 mV. The peak at -200 is the first In UPD feature with the second one starting at -600 mV. The second In feature fills out the UPD In as well as begins the bulk In deposition. After -800 mV the current reveals the beginning of another peak which is indicative of Se reductive stripping, until HER starts to take over at -900 mV. On the positive going scan, bulk In stripping occurs at -550 mV in a relatively sharp peak. There is not much evidence of anything occurring until -200 mV where the beginning of In UPD stripping starts. By 200 mV all the In has been stripped from the surface and now only a Se deposit remains. Stripping of the Se occurs at 800 mV at this pH.

3.4.3 SELECTION OF DEPOSITION AND STRIPPING POTENTIALS FOR PULSES

Based on the voltammetry there are a few considerations needed for selecting pulse potentials. The In stripping is much more volatile than that of Se as evidenced by the much more negative anodic stripping. By 200 mV all of the In is removed from the surface, whereas Se is stable until 800 mV. The spread-out nature of the In stripping peak suggests that it will be optimal to fine tuning the amount of In in the films by stripping certain amounts off at certain potentials. This suggests that the upper limit for the stripping potential is 200 mV. At the negative potentials, In does not have a stable way to reductively strip so going to more negative potentials will only increase the overpotential for bulk In deposition. Due to the ability of the Se to reductively strip to Se^{2-}, as the potentials get more negative at some point even the most tightly held UPD Se will strip and the film will be completely In.

To determine the optimal cathodic deposition pulse potential, a series of samples were made where the cathodic potential was varied, and the anodic potential was held constant at -200 mV. The resulting films were characterized by EDS to determine the stoichiometry and ratio of Se to In in the film. Figure 3.4 shows the change in stoichiometry as a function of the cathodic potential. For the In_2Se_3

compound the ratio between Se/In should be 1.5. As expected, at potentials greater than -650 mV In is unable to adhere to the surface and the films are very Se rich. However, as the voltammetry in Figure 2.2b shows, In deposition starts to occur fully by -700 mV and this is reflected in the stoichiometric ratio. Between -700 mV and -800 mV there is a plateau region in both the voltammetry and the stoichiometry. This suggests that this is a stable region to deposit the In_2Se_3 compound. At -900 mV, it is observed that a 1:1 ratio is obtainable suggesting the InSe compound. This is made possible due to the change to pH=2 shifting the HER sufficiently negative. This feature in the voltammetry is right at -900 mV as well. Here the excess Se is being reductively stripped leaving only the structure that binds tightest to the In. The effects of this are clear as well in the sample current time trace for the deposition cycle provided in Figure 3.5. When the sample is deposited at -750 mV in Figure 3.5a, there is a single reduction feature as the In and Se deposit together and the In_2Se_3 structure is grown. However, in Figure 3.5b, there are 2 clear reduction features upon the cathodic pulse. In the first feature, the In_2Se_3 compound is grown and then the extra Se is further stripped in the second feature.

A similar experiment was performed where the cathodic potential was held constant at -750 mV while the anodic potential was varied. The results shown in Figure 3.6 suggest that the stoichiometry is less dependent on anodic potential than it was with cathodic. There was a very steady plateau region between -600 mV and 0 mV where samples close to the optimal In_2Se_3 stoichiometry was achieved. Initially, a stripping potential of -200 mV was chosen as its ratio was exactly 1.5 Se/In. If a potential greater than 100 mV was selected, the deposits became very Se rich as all of the In was stripped out which makes sense based on the potentials from the voltammetry. Additionally, if the stripping potential was negative of -650 mV, the bulk In could not be stripped and the films became very In rich. The results were similar when a constant cathodic potential of -950 mV was used; The InSe ratio was relatively unchanged unless drastic potentials were used.

One issue with the 1:1 stoichiometry film is that the deposition potential chosen of -950 mV overlapped with the HER. As shown in Figure 3.7 the films suffered from some H_2 bubble formation which caused inhomogeneity and pitting on the surface. This likely could have been combatted by using a less negative deposition potential at the edge of the second Se deposition feature in Figure 3a. By having a slightly longer cathodic deposition time with a more positive potential, a deposit might have yielded the same stoichiometry without approaching the HER conditions. The effect of the duty cycle of the potentials for the cathodic or anodic pulses were not determined. Instead a cathodic pulse of 130 ms was selected and an anodic stripping/resting step was 500 ms long.

For the In_2Se_3 compound, the optimal stoichiometry led to a rather rough surface structure as shown in Figure 3.8a with balls of In littering the surface uniformly. It was found that by increasing the In concentration to a ratio of 1.33:1 Se/In instead of 1.5:1 that the film was incorporated better and was much smoother as shown in Figure 3.8b. Despite the change in the surface morphology, the Raman Spectroscopy signals were nearly identical in Figure 3.9. The lower signal of the 1.3 samples suggests a smoother, more crystalline deposit, but could easily be due to minute changes in the thickness of the films. However, the spectra didn't match the cards of known polymorphs of the In_2Se_3. Instead they were more consistent with a polycrystalline deposit. This is not wholly surprising given the polycrystalline nature of the underlying Au substrate. Future work on a single crystalline Au substrate might yield films displaying only one of the polymorphs. Another way that films could be improved would be thermal annealing which would allow for the films to be heated so that they could move around and settle into the most thermodynamically stable polymorph as they were cooled.

It was found that for all the stoichiometries of In_xSe_y that were made, that they scaled well with longer deposition sequences. As the deposition sequence time for the film was increased, the samples got thicker as indicated by the increased atomic percentages obtained by EDS of the precursor metals in the resulting film. As the samples got thicker, the substrate became less evident and the deposited film

became more prevalent. Additionally, as the thickness was increased, the stoichiometries were constant, which is desirable for making sure the film is homogenous throughout.

3.4.4 PHOTO EFFECTS ON DEPOSITION POTENTIAL

The amount of light present during the deposition process isn't governed by the Nernst Equation. However, it has a profound effect on the stoichiometry and morphology of the films depending on which atmosphere is present. In a typical PP-ALD experiment the lighting in the room is ambient light. The flow cell, shown in Figure 3.10 is held at ~45° angle which leads to the top of the flow cell being relatively less exposed to the light source than the bottom is. Additionally, the flow cell has the auxiliary electrode in an S shape set into the front half of the flow cell. This obstructs the light exposure slightly, leading to maximum light exposure in the bottom 1/3rd of the sample. In the areas most exposed to light during deposition, the Se had higher incorporation into the films. The atomic % of the In stayed constant in films grown in or out of light. This suggests that the light affected the deposition of the chalcogenide, Se. The difference between the areas deposited in mostly light conditions or mostly dark conditions when the lights are on, is shown in Figure 3.11. The EDS results and SEM images show how different the regions are in stoichiometry and morphology. This is mostly pronounced in the InSe samples where you can clearly see the difference in the film on a macroscopic level. In the bottom 1/3rd section of the film where the light is on the film during deposition, the Se% is much greater and the morphology is changed due to the Se's tendency to form 8-membered rings for higher coverage structures. When InSe films were grown in a completely dark environment, the results were much more uniform and had lesser Se incorporation in Figure 3.12. The same trends are seen in the In_2Se_3 samples but in a much less drastic way. Figure 3.13 shows the differences in morphology and

stoichometry and reveals that the morphology and smoothness of the samples seems unchanged. However, the ratio decreases from 1.33 in the light to 1.24 in the dark.

This difference in InSe surface structure is also noticed in the Raman Spectra in Figure 3.14 which show a greater proportion of amorphous Se and less InSe structure in the bottom 1/3 of the deposits. In the darker region the film has a more expected stoichiometry and a more pronounced InSe spectra according to the spectra. When the entire sample is deposited in a dark environment the sample is much more uniformly 1:1 Se/In without a Se-rich region. The spectra for the In_2Se_3 samples were unchanged no matter if the film was grown in dark or light.

3.4.5 P-N DETERMINATION OF DEPOSITED THIN FILMS

The effect of light during deposition had a great effect on stoichiometry and morphology. Once the films were deposited, the effects of the light or dark environment continued to affect the properties of the films. In this study deposited films were kept in the flow cell with a blank solution at OCP. Figure 3.15a shows the effect of the 1:1 sample being exposed to dark conditions with ambient light being the control. The photovoltage decayed ~-90 mV in the dark environment suggesting a P-type material suitable for photocathode use in PEC. This was further confirmed when there was a rise in photovoltage when a red and green laser were shone on the window of the flow cell. When the same experiment was done on the 1.3:1 sample in Figure 3.15b, the photovoltage increased by ~270 mV when exposed to the dark. This suggests that the films are N-Type as would be expected. This suggests that it might be possible to make a completely In_xSe_y compound structure PEC structure with multiple junctions which would be able to allow H_2O splitting to its precursor gasses when exposed to the sun. This type of baggy reactor has been suggested by Dr. Mubeen of University of Iowa and is shown in Figure 3.16. This

reactor could be left out in the sun with a H_2O solution and the 2 semiconductor junctions. During solar radiation, the solution would be split into commercially usable fuel gasses.

3.4.6 RAMAN SPECTROSCOPY and XRD CHARACTERIZATION

Raman Spectroscopy was useful for film polymorph identification as well as identifying when Se 8-membered rings were starting for form as amorphous Se. While neither the 1.3:1 Se/In ratio or 1:1 structure were indicative of a single crystalline, one polymorph structure, they were different from each other. This suggested that while both samples were polycrystalline, they were indeed different compounds as suggested by their stoichiometries. This polycrystallinity is expected due to the polycrystallinity of the underlying Au substrate.

XRD patterns are shown in Figure 3.17a and 3.17b. The major peaks at 38 and 45 degrees are indicative of the Au substate. These peaks are dominant due to the limitations of the glancing angle technique to focus only on the as deposited film. Instead, the X-Rays penetrate deep into the substate and that is why the resulting pattern is so highly indicative of an Au surface. However, the In_2Se_3 and InSe films have their own distinct features at the lower angles. They are different enough to that the two stoichiometries produce different compounds but not to help identify exactly which polymorph is present.

3.5 CONCLUSION

By using a solution pH=2 instead of pH=1, In2Se3 and InSe were able to be formed without interference from HER. Due to manipulations of the parameters in the Nernst Equation, pH=2 allows for a wider deposition potential range and introduces a second deposition feature where reductive

stripping of Se to Se^{2-} occurs. By use of the reductive stripping the InSe is shown to grow. Using cyclic voltammetry, optimal pulse potentials were determined for both the 130 ns cathodic deposition pulse as well as the 500 ms anodic stripping step. This allowed for the development of a PP-ALD sequence which produced In_2Se_3 and InSe films up to ~60nm. These films displayed the desired stoichiometry even as thicker films were created. One interesting effect was the observed change in stoichiometry and morphology when samples were grown in the light vs in a dark environment. Particularly in the InSe films, films grown in the light had deformed regions where amorphous Se 8-membered rings would form. The rest of the film grown in a darker environment showed the desired stoichiometry and was homogenous. This was mimicked to a lesser degree in the In_2Se_3 films where overall in the samples grown in the dark, the Se concentration was lessened. Raman Spectroscopy and XRD revealed that the In_2Se_3 and InSe films were both polycrystalline films which is likely due to the polycrystallinity of the underlying Au substrate. When PEC experiments were performed, the In_2Se_3 films were shown to be N-Type semiconductor materials, whereas the InSe films were P-Type. This suggests that these materials might be potential materials for photoanodes and photocathodes respectively in a PEC water splitting device.

$$E = E^0 - \frac{RT}{nF} ln \frac{[Red]}{[Ox]}$$

Equation 1- Nernst Equation

$$E^0 = E - 0.0591\text{mV}^* \text{ pH}$$

Equation 2- Nernst Equation effect of HER E^0 as a function of pH

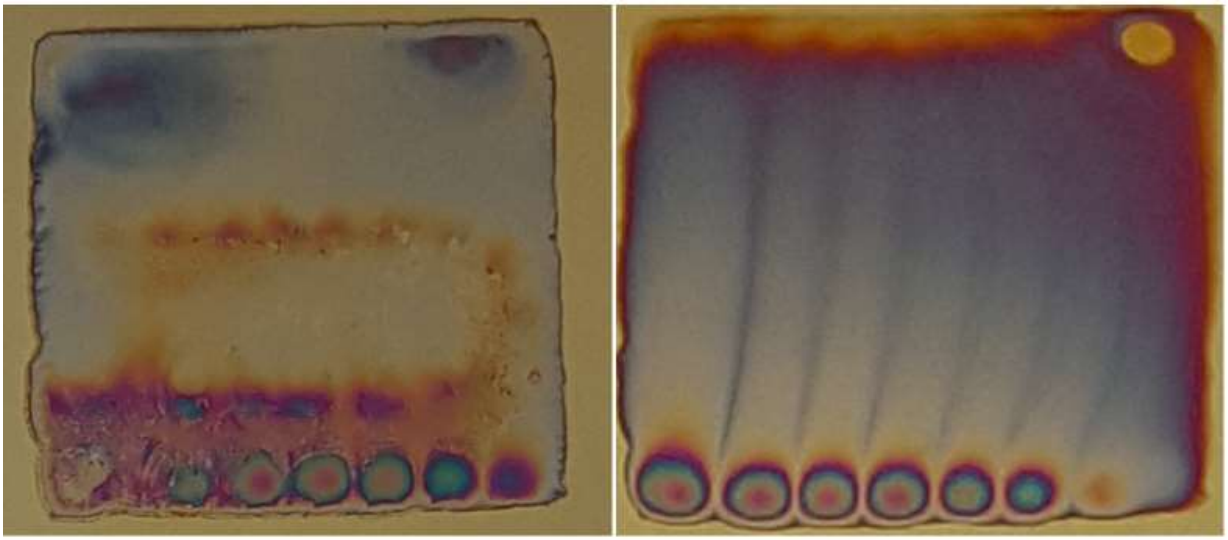

Figure 3.1- Part a shows the morphology of the In_2Se_3 films deposited at pH=1.0 which are characterized by regions of inhomogeneity. In part b, done at pH=2.0, the films are much smoother and homogenous.

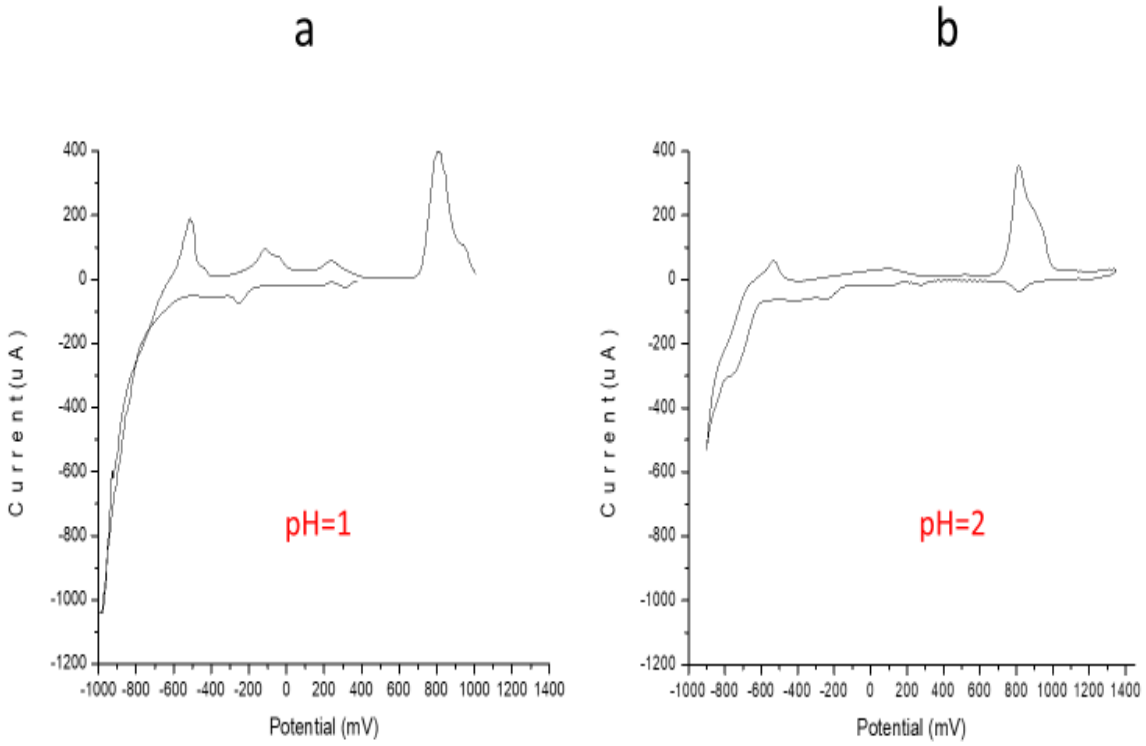

Figure 3.2- This figure shows the differences in the voltammetry for InSe solution at different pHs. In part a, pH=1.0 is used and the HER interferes with the InSe deposition reaction. In part b which is done at pH=2.0, the HER onset is pushed further negative and the voltammetry for InSe opens up revealing another deposition feature.

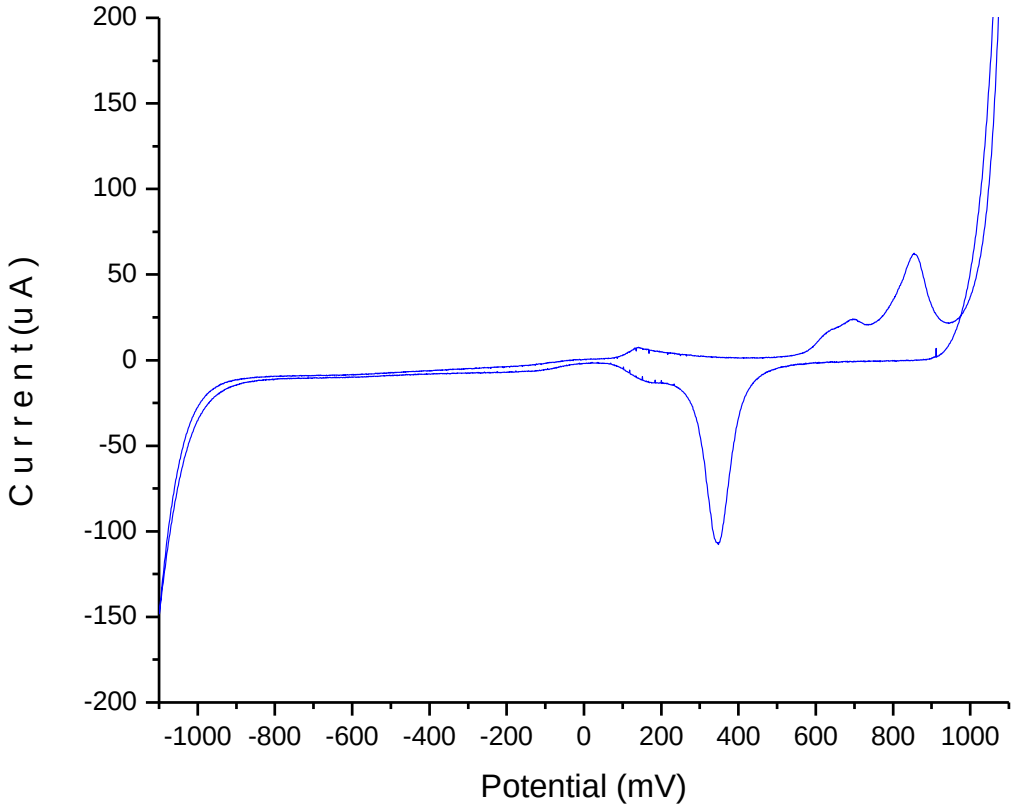

Figure 3.3- CV of the blank solution on Au substrate. At the higher potentials the current can be seen to go off scale indicative of O_2 formation. At the more negative potentials H_2 forms due to the HER.

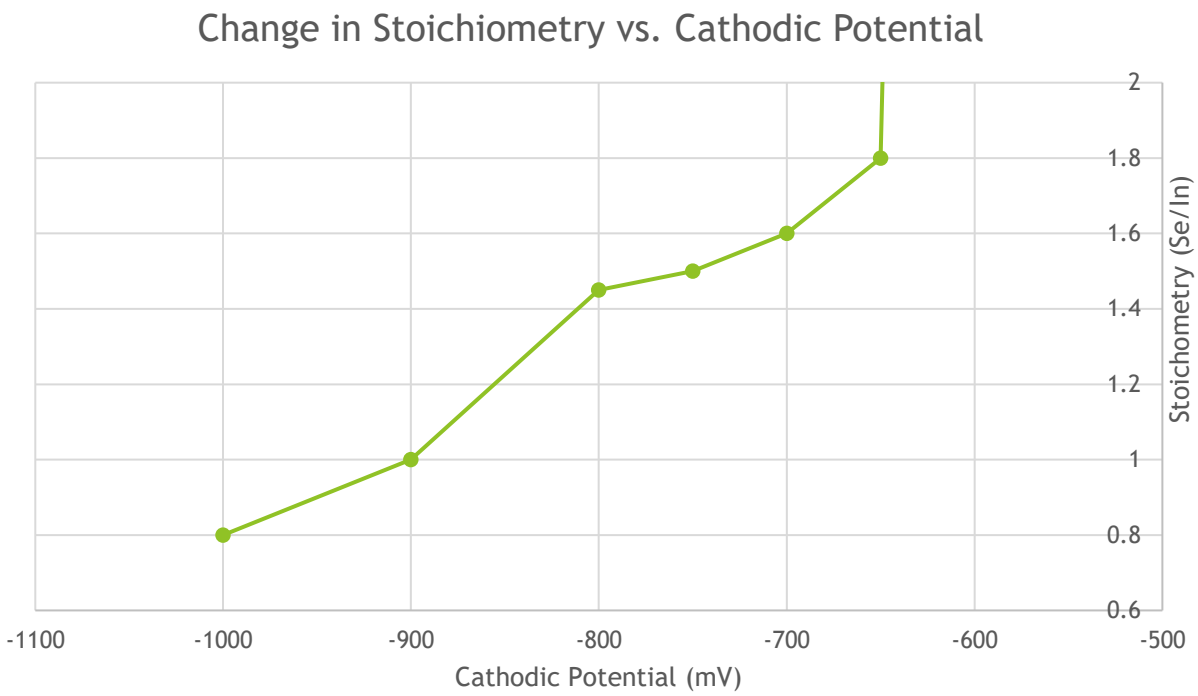

Figure 3.4- The stoichiometry of the resulting films is greatly dependent on the deposition pulse potential. At potentials greater than -650 mV, films were very Se rich, but more negative than -1000 mV promoted excess In.

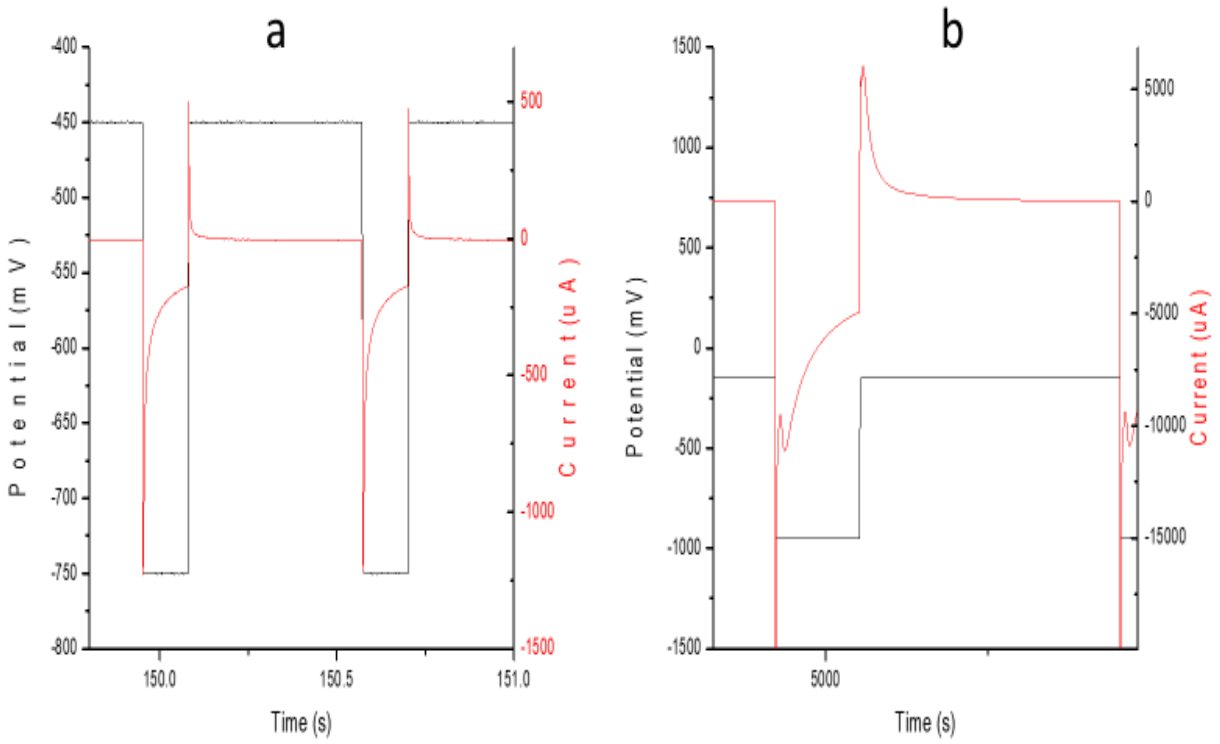

Figure 3.5- Current Time Traces give the potential and current simultaneously as a function of time. They are perfect to follow along with a deposition sequence in real time. In Figure a, an In_2Se_3 deposition sequence is shown, and Figure b shows a sequence for InSe.

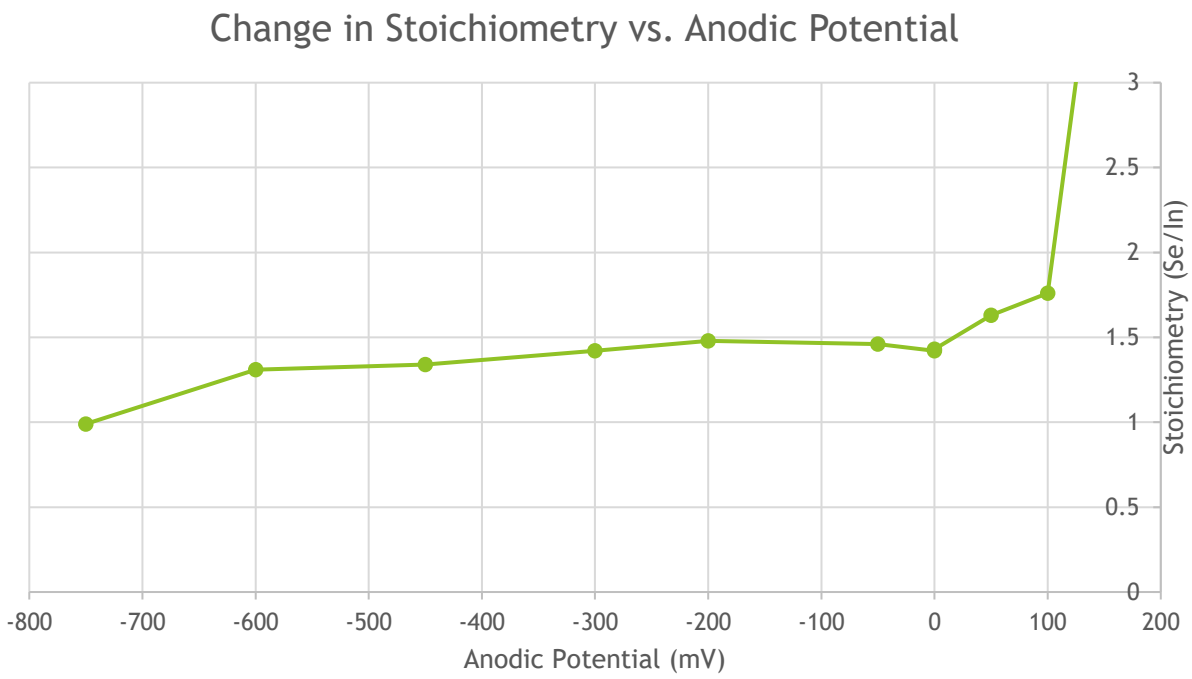

Figure 3.6- The stoichiometry is relatively unchanged based on stripping potential unless extreme potentials are used. Greater than 100 mV yields films that are entirely Se, with films negative of -900 mV consisting of mostly In.

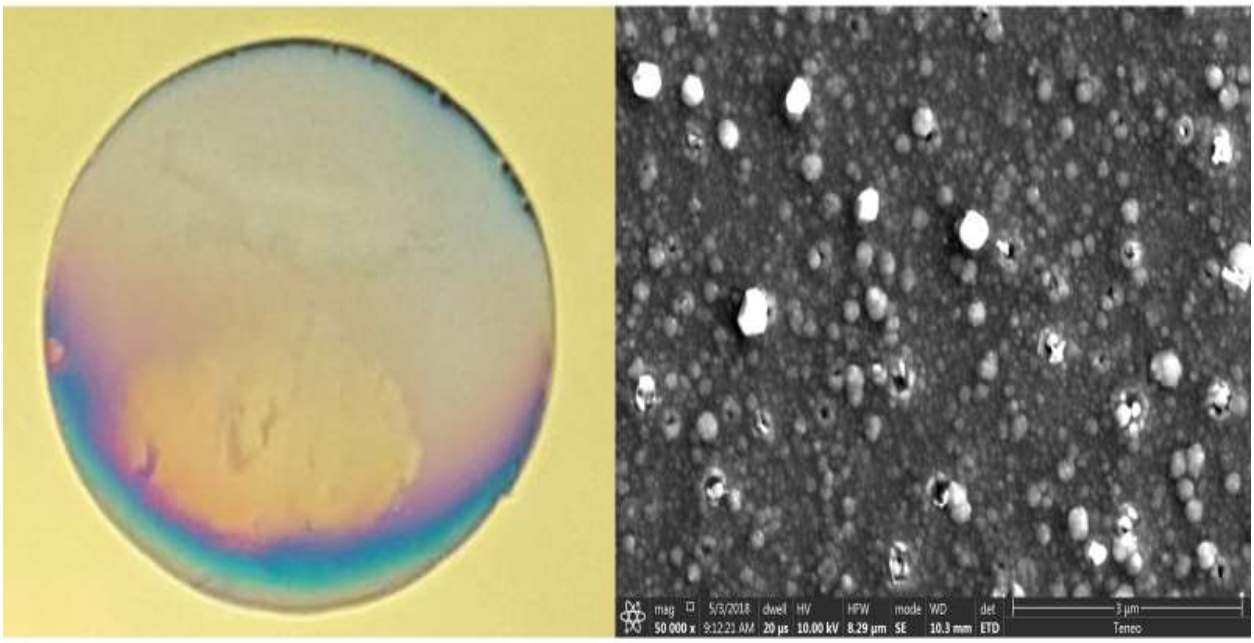

Figure 3.7- The left figure shows a macroscopic view of the InSe deposits made at -950 mV. At the top of the film the area is visibly rougher due to the H_2 bubbles collecting over top. The effects of those bubbles is observed on the surface by the pitting in the 50,000x SEM image.

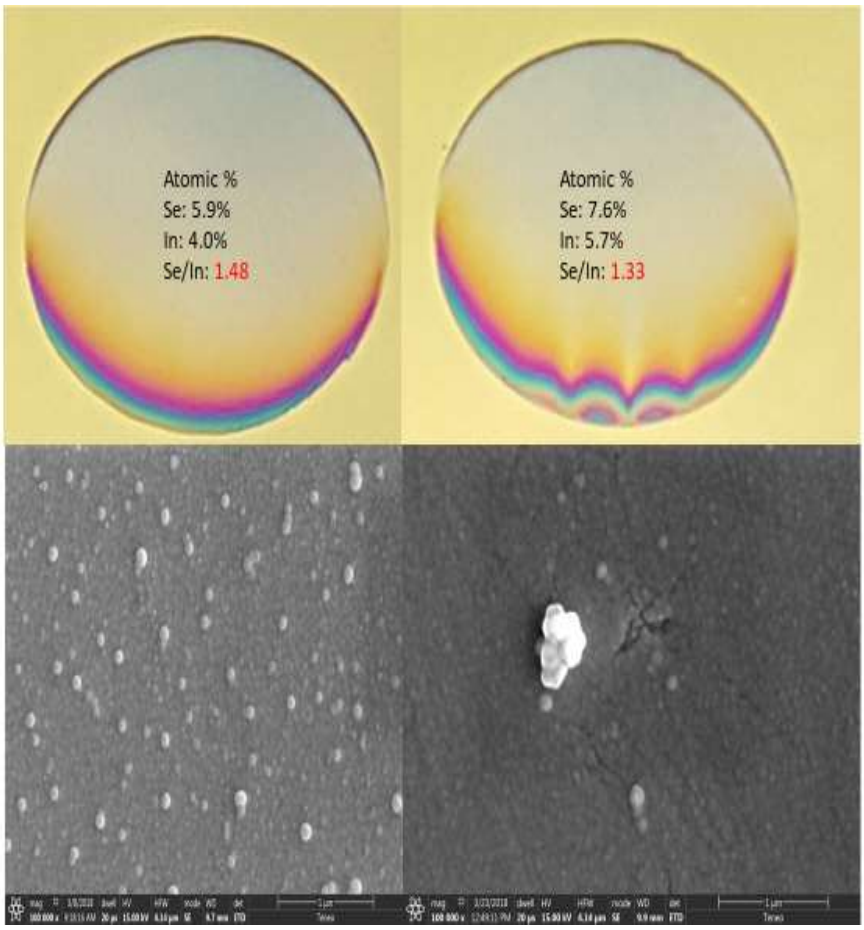

Figure 3.8- In_2Se_3 samples with the ideal 1.5 Se/In ratio were found to be decorated uniformly with In balls on the surface. If the amount of In in the films is increased as in the films made at the 1.33 ratio, the surface is much smoother.

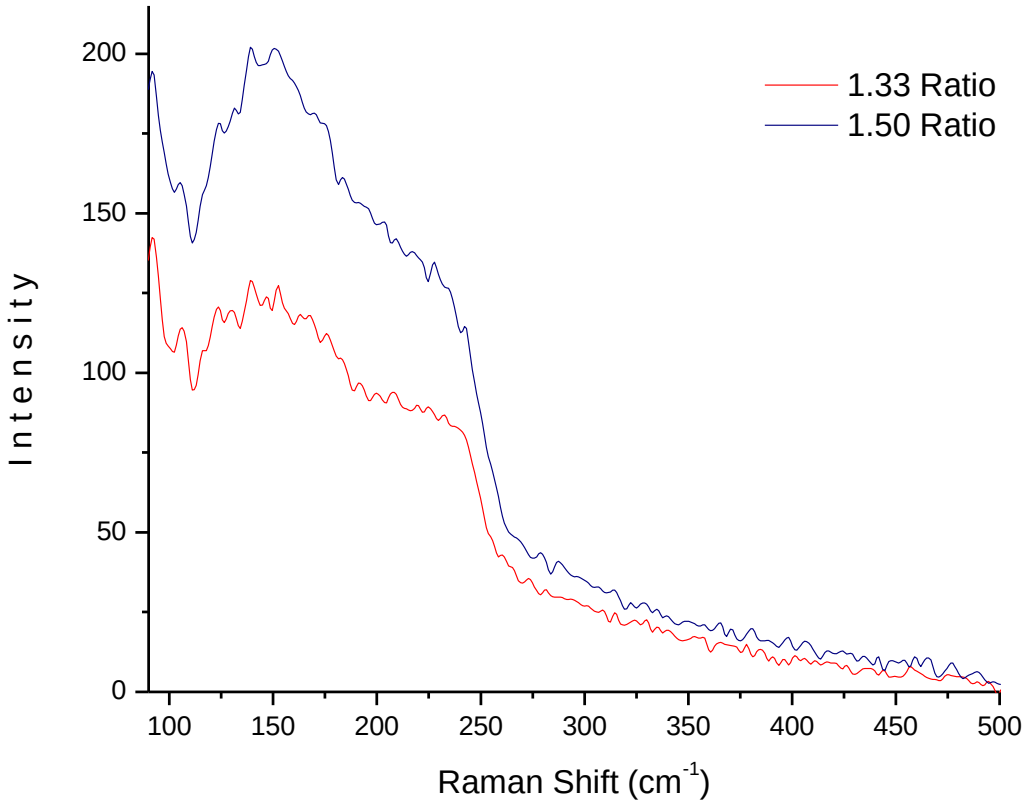

Figure 3.9- Raman Spectroscopy confirmed that the same In_2Se_3 compound was formed even though the ratio of Se/In was changed from 1.5 to 1.33. The shape and location of all the peaks is identical with only the intensity changing. This change in intensity could have been due to slight changes of the thickness or smoothness of the sample.

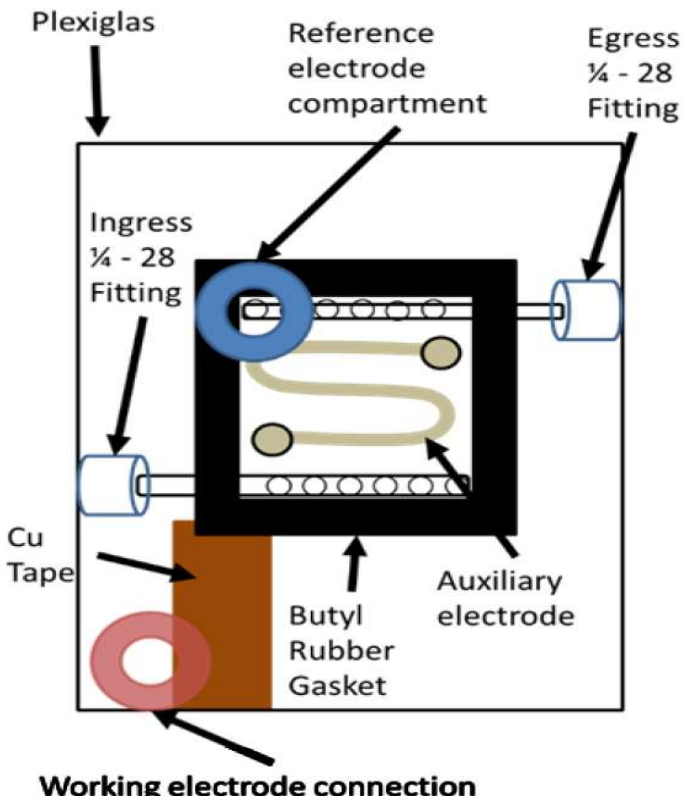

Figure 3.10- Schematic of the flow cell used for PP-ALD experiments. The auxiliary electrode is inlaid into the top half of the flow cell. This causes light to be blocked to the substrate surface. Because the flow cell sits at a 45 ° angle only the bottom 1/3 of the flow cell is washed in ambient light.

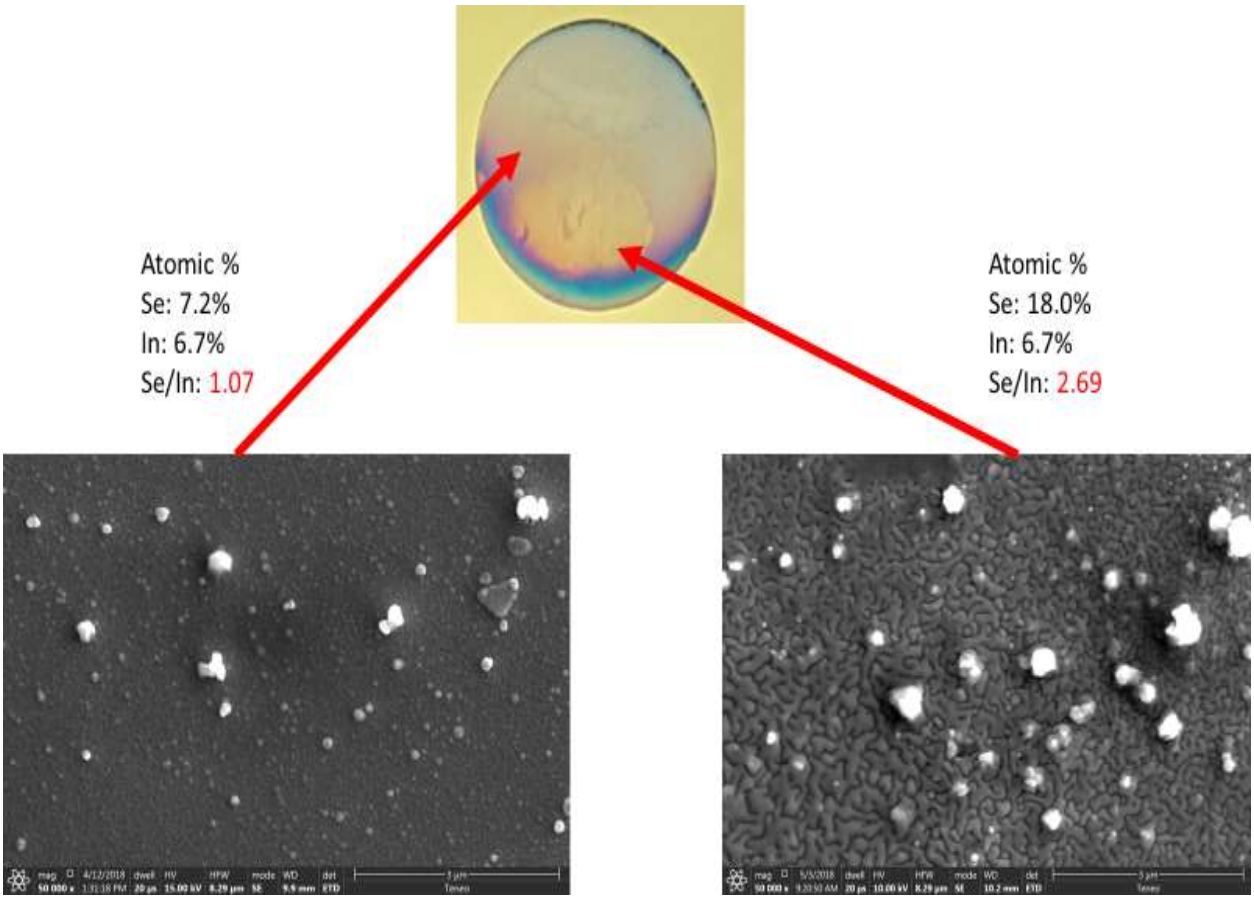

Figure 3.11- Macroscopically it is visible that the lower 1/3 of the InSe deposit has a different morphology than the rest. By looking at the SEM images of the surfaces, the change in morphology is confirmed. EDS suggests that the lighted regions have a structure more resembling amorphous Se than InSe.

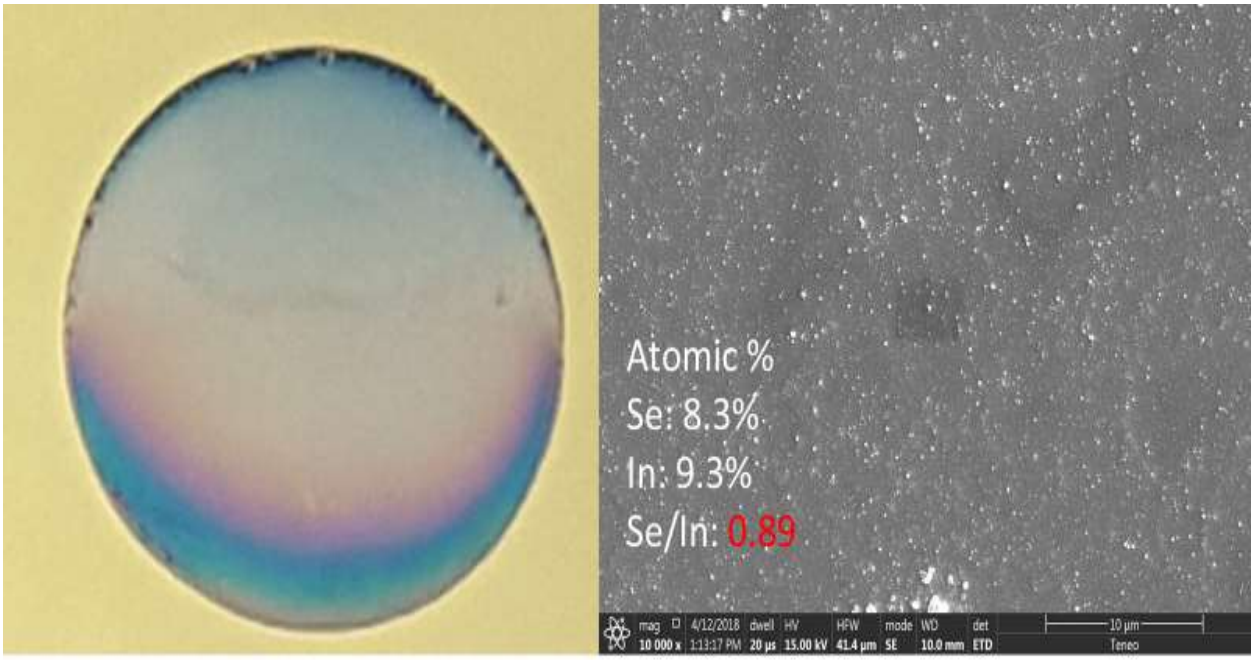

Figure 3.12- When InSe films are grown in a dark environment the result is a more uniform surface and a lesser Se incorporation into the films.

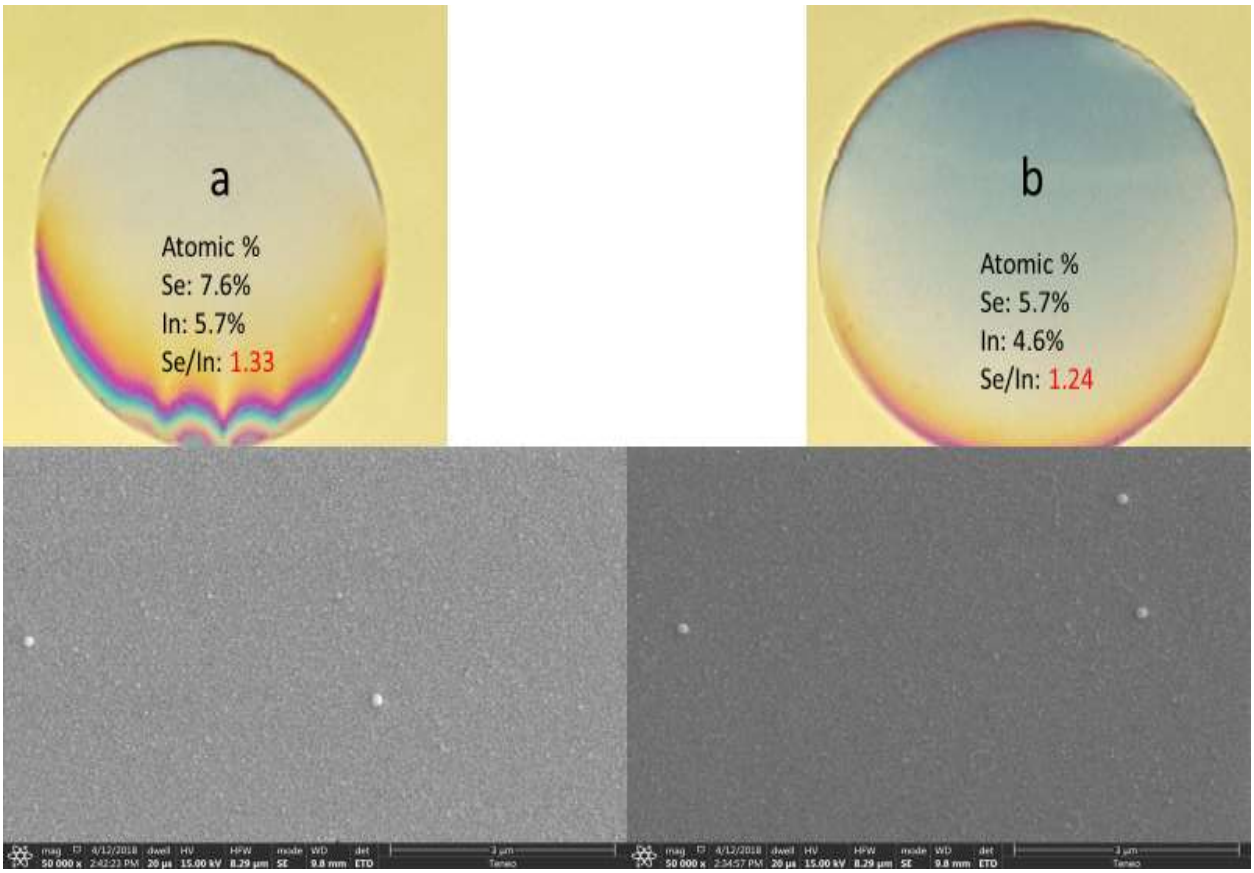

Figure 3.13- In Figure a, the sample is grown in ambient light, however, in Figure b the sample is grown completely in the dark. The dark grown sample has a lower amount of Se but is just as smooth and looks similar morphologically.

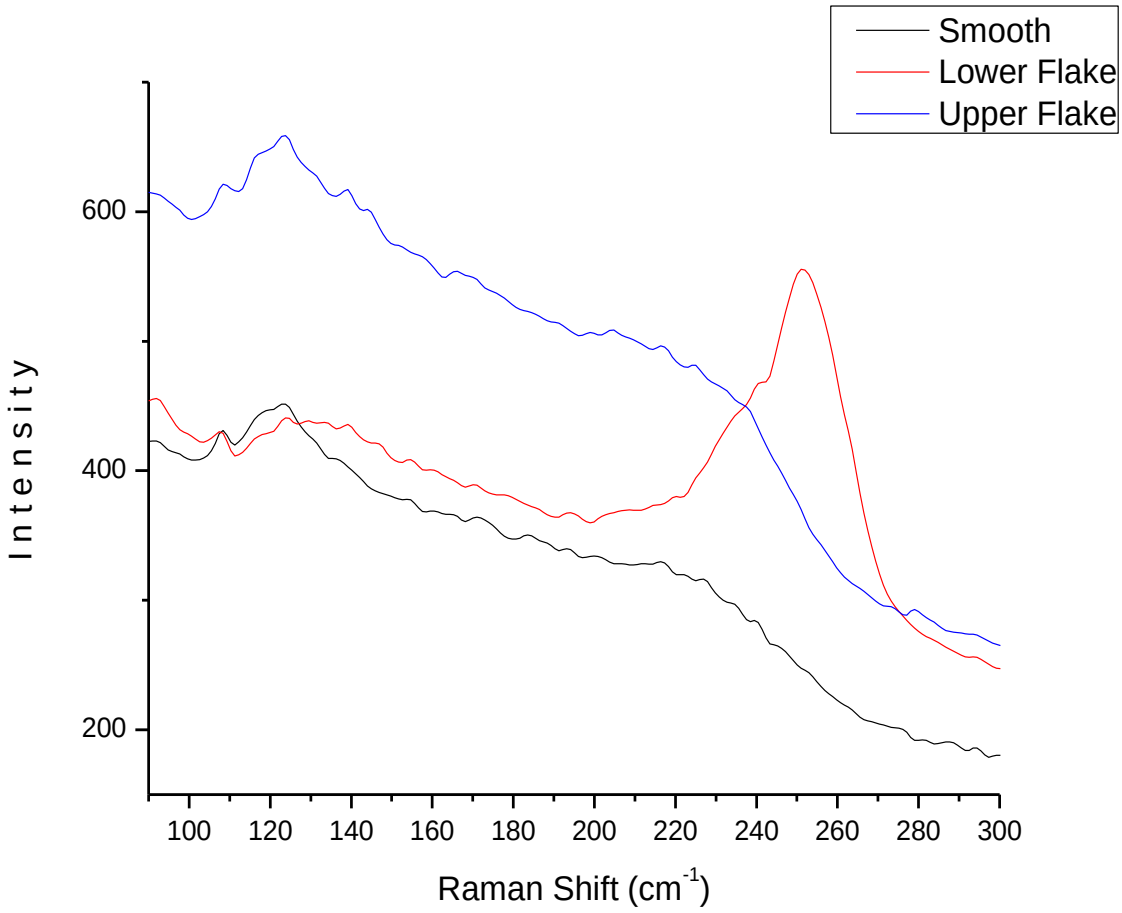

Figure 3.14- Raman Spectroscopy characterization of different areas of an InSe deposit. In the regions where light exposure does not occur the spectra are very similar in peak shape. However, when the areas that were illuminated are tested, there is a clear amorphous Se peak present.

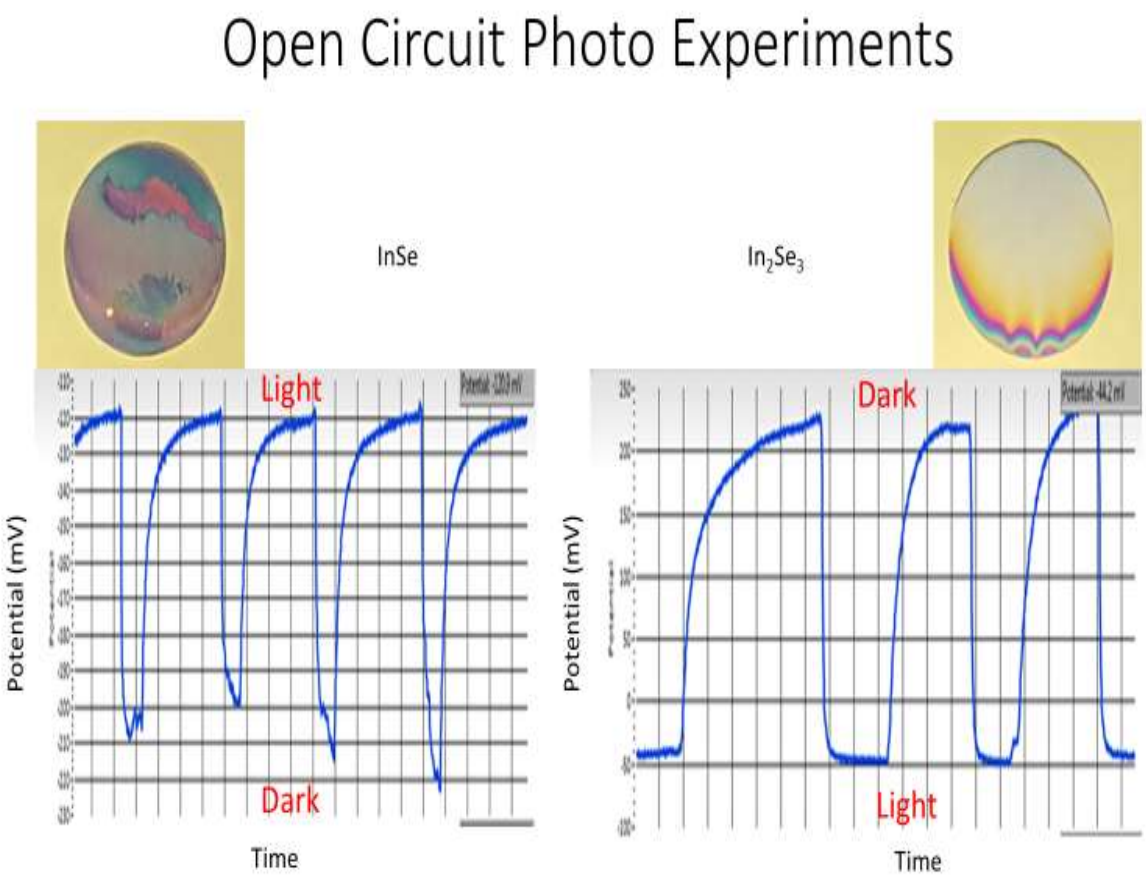

Figure 3.15- Photovoltage response of InSe films is seen in Figure a where the voltage decays when put in a dark environment. In Figure b, when In_2Se_3 is exposed to the dark, the photovoltage increases drastically.

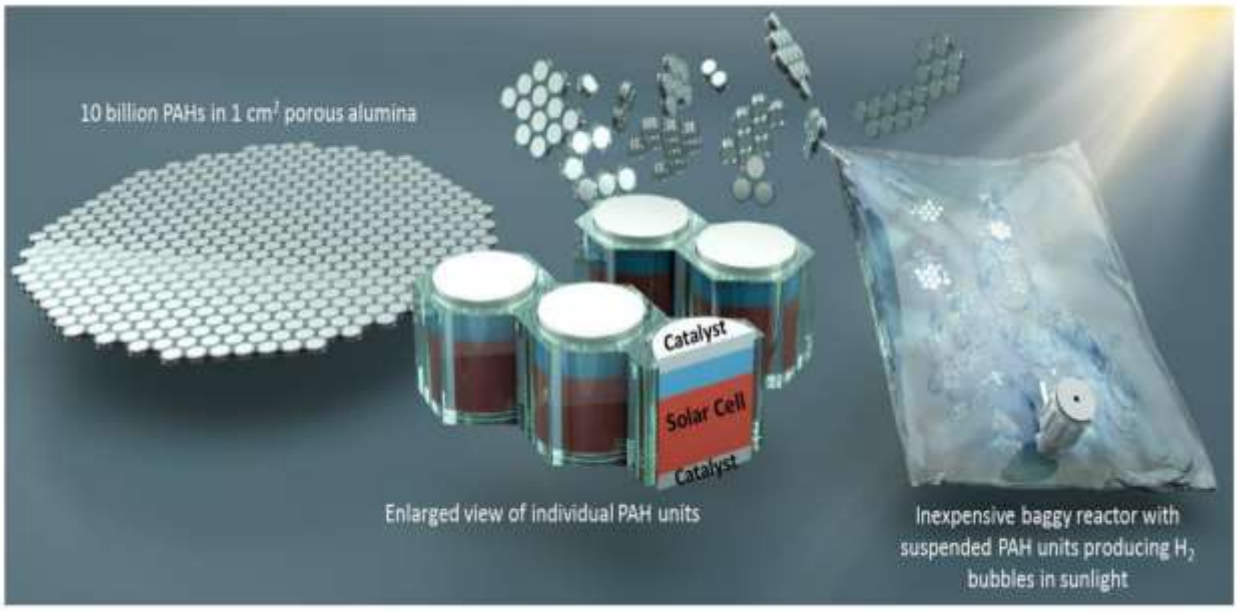

Figure 3.16- Schematic of a reusable type baggy reactor suggested by Dr. Mubeen. Photoanodes and photocathodes would be combined in H_2O to slowly turn the H_2O into H_2 and O_2 gases for future fuel use.

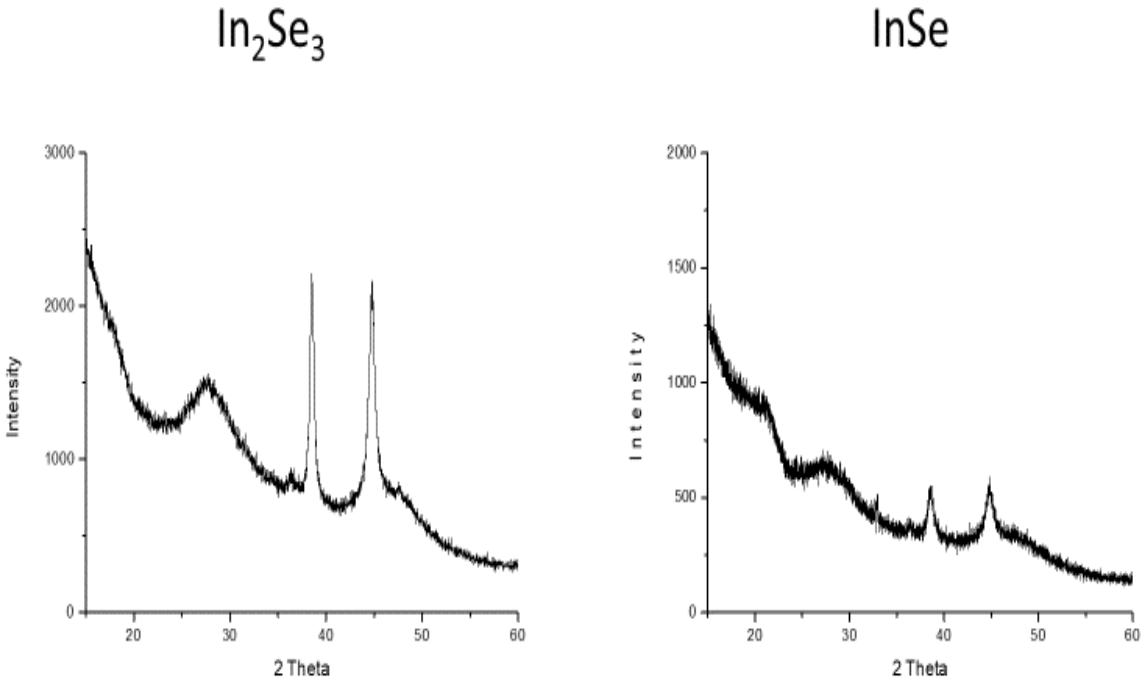

Figure 3.17- Figure a shows the XRD pattern for In_2Se_3 and Figure b shows the pattern for InSe

REFERENCES

1. Segura, A.; Pomer, F.; Cantarero, A.; Krause, W.; Chevy, A. Electron scattering mechanisms in n-type indium selenide. *Physical Review B* **1984** 29, 5708-5717.

2. Debbichi, L.; Eriksson, O.; Lebegue, S. Two-Dimensional Indium Selenides Compounds: An Ab Initio Study. *J. Phys. Chem. Lett.* **2015**, 6, 3098-3103.

3. Massaccesi, S.; Sanchez, S.; Vedel J. Electrodeposition of indium selenide In_2Se_3. *Journal of Electroanalytical Chemistry* **1996**, 412, 95-101.

4. Yudasaka, M.; Matsuoka, T.; Nakanishi, K. Indium Selenide Film Formation By the Double-Source Evaporation of Indium and Selenium. *Thin Solid Films* **1987**, 146, 65-73.

5. Han, G.; Chen, Z.G.; Drennan, J.; Zou, J. Indium Selenides: Structural Characteristics, Synthesis and Their Thermoelectric Performances. *Small* **2014**, 10, 2747-2765.

6. Li, J.; Wu, N. Semiconductor-based photocatalysts and photoelectrochemical cells for solar fuel generation: a review. *Catalysis Science and Technology* **2015**, 5, 1360-1384.

7. Fang, Z.; Wang, X.C.; Wu H.C.; Zhao, C.Z. Achievements and Challenges of CdS/CdTe Solar Cells. *International Journal of Photoenergy* **2011**, 1-9.

8. Joy, J.; Mathew, J.; George, S. Nanomaterials for photoelectrochemical water splitting- a review. *International Journal of Hydrogen Energy* **2018**, 43, 4804-4817.

9. Voloshin, R,A.; Kreslavski, V.D.; Zharmukhamedov, S,K.; Bedbenov, V.S.; Ramakrishna, S.; Allakhverdiev, S.I. Photoelectrochemical cells based on photosynthetic systems: a review. *Biofuel Research Journal* **2015**, 6, 227-235.

10. Manivannan, A.; Peterson, A.; Wilson, W.; Mukherjee, B.; Subramanian, V.R. Hydrogen Production and Photodegradation at TiO2/Metal/CdS Sandwich Using UV-Visible Light. *Semiconductor Materials for Solar Photovoltaic Cells* **2012**, 5, 141-167.

11. Bouttemy, M.; Tran-Van, P.; Gerard, I.; Hildebrandt, T.; Causier, A.; Pelouard, J.L.; Dagher, G.; Jehl, Z.; Naghavi, N.; Voorwinden, G.; Dimmler, B.; Powalla, M.; Guilllemoles, J.F.; Lincot, D.; Etcheberry, A.Thinning of CIGS solar cells: Part I: Chemical processing in acidic bromine solutions. *Thin Solid Films* **2011**, 519, 7207-7211.

12. Jehl, Z.; Erfurth, F.; Naghavi, N.; Lombez, L.; Gerard, I.; Bouttemy, M.; Tran-Van, P.; Etcheberry, A.; Voorwinden, G.; Dimmler, B.; Wischmann, W.; Powalla, M.; Guillemoles, J.F.; Lincot, D. Thinning of CIGS solar cells: Part II: Cell characterizations. *Thin Solid Films* **2011**, 519, 7212-7215.

13. Bailie, C.D.; Christoforo, M.G.; Mailoa, J.P.; Bowring, A.R.; Unger, E.L.; Nguyen, W.H.; Burschka, J.; Pellet, N.; Lee, J.Z.; Gratzel, M.; Noufi, R.; Buonassisi, T.; Salleo, A.; McGehee, M.D. Semi-transparent perovskite solar cells for tandems with silicon and CIGS. *Energy and Environmental Science* **2015**, 8, 956-963.

14. Gregory, B.W.; Stickney, J.L. Electrochemical Atomic Layer Epitaxy (ECALE). *Journal of Electroanalytical Chemistry* **1991**, 300, 543-561.

15. Suggs, D.W.; Stickney, J.L. Studies of the Surface-Structures Formed by the Alternated Electrodeposition of Cd and Te on the Low-Index Planes of Au STM Studies. *Surface Science* **1993** 290, 375-387.

16. Lister, T.E.; Huang, B.M.; Herrick, R.D.; Stickney, J.L. Electrochemical Formation of Se Atomic Layers on Au (100). *Journal of Vacuum Science and Technology B* **1995**, 13, 1268-1273.

17. Lister, T.E.; Stickney, J.L. Atomic level studies of selenium electrodeposition on gold (111) and gold (110). *Journal of Physical Chemistry* **1996**, 100, 19568-19576.

18. Lister, T.E.; Stickney, J.L. Formation of the first monolayer of CdSe on Au (111) by electrochemical ALE. *Applied Surface Science* **1996**, 107, 153-160.

19. Stickney, J.L. Electrochemical atomic layer epitaxy. *Electroanalytical Chemistry* **1999** 21, 75-209.

20. Sorenson, T.A.; Lister, T.E.; Huang, B.M.; Stickney, J.L. A comparison of atomic layers formed by electrodeposition of selenium and tellurium- Scanning tunnel microscopy studies on Au (100) and Au (111). *Journal of the Electrochemical Society* **1999**, 146, 1019-1027.

21. Sorenson, T.A.; Suggs, D.W.; Nandhakumar, I.; Stickney, J.L. Phase transitions in the electrodeposition of tellurium atomic layers on Au (100). *Journal of Electroanalytical Chemistry* **1999**, 467, 270-281.

22. Vaidyanathan, R.; Stickney, J.L.; Cox, S.M.; Compton, S.P.; Happek, U. Formation of In2Se3 thin films and nanostructures using electrochemical atomic layer epitaxy. *Journal of Electroanalytical Chemistry* **2003**, 559, 55-61.

23. Venkatasamy, V.; Shao, I.; Huang, Q.; Stickney, J.L. ALD approach toward electrodeposition of Sb2Te3 for phase-change memory applications. *Journal of the Electrochemical Society* **2008**, 155, 693-698.

24. Liang, X.H.; Kim, Y.G.; Gebergziabiher, D.K.; Stickney J.L. Aqueous Electrodeposition of Ge Monolayers. *Langmuir* **2010**, 26, 2877-2884.

25. Banga, D.; Perdue, B.; Stickney, J.L. Formation of CuIn(1-x)GaxSe2 (CIGS) by Electrochemical Atomic Layer Deposition (ALD). *Journal of the Electrochemical Society* **2014**, 161, 141-146.

26. Bui, N.N.; Ledina, M.; Reber, T.J.; Jung, J.; Stickney, J.L. Electrochemical Scanning Tunneling Microscopic Study of the Potential Dependence of Germanene Growth on Au (111) at pH 9.0. *ACS Nano* **2017**, 11, 9481-9489.

27. Czerniawski, J.M.; Stickney, J.L. Electrodeposition of In2Se3 Using Potential Pulse Atomic Layer Deposition. *The Journal of Physical Chemistry C* **2016**, 120, 16162-16167.

28. Czerniawski, J.M.; Perdue, B.R.; Stickney, J.L. Potential Pulse Atomic Layer Deposition of Cu2Se. *Chemistry of Materials* **2016**, 28, 583-591.

29. Zhang, X.; Shen, S.; Howell, P.; Cheng, W.; Mubeen, S.; Stickney, J.L. Potential Pulse ALD for Room Temperature Fabrication of Stoichiometric CdTe Nanofilms. *Journal of the Electrochemical Society* **2019**, 166, 3249-3256.

30. Bui, N.; Cheng, W.; Mubeen, S.; Stickney, J.L. Potential Pulse Atomic Layer Deposition (PP-ALD): Electrodeposition of ZnS Nanofilms. To be submitted to ACS journal Chemistry of Materials.

CHAPTER 4

SURFACE LIMITED REDOX REPLACEMENT (SLRR) OF AU ON CDSE NANORODS

Sisk, P.; Howell, P.; Zhang, X.; Mubeen, S.; Stickney, J. To be submitted to ECS journal.

4.1 ABSTRACT

Epitaxial, smooth Au layers were deposited on top of CdSe nanotubes to act as a Schottky junction and to serve as a capping layer to protect the films from oxidation. This was done using a combination of E-ALD and Surface Limited Redox Replacement (SLRR) methods. This process is used due to the difficulty of electrodepositing Au epitaxially. Instead epitaxial UPD methods are used to deposit sacrificial layers of materials that are then replaced using the electroless SLRR process. SLRR relies upon the principle where a more noble metal will exchange with a less noble one. In these experiments, first a sacrificial layer of surface limited Cd is deposited onto the CdSe surface. Then Cu solution is flowed into the cell for a time sufficient to make the exchange with the surface layer without penetrating into the CdSe film. Once the Cu exchange is complete, Au solution is introduced, and the exchange takes place until there is finally a thin layer of epitaxial Au on top of the CdSe nanotubes. Due to the stripping potentials of CdSe, Cd, and Cu it was not possible to use in-situ methods for checking if the exchange had occurred. Instead, SEM was used to view the morphology and EDS was used to check the composition of the new Au layer as well as to check the composition of the underlying film to make sure that Cd from the CdSe was not removed or that Cu was not buried.

4.2 INTRODUCTION

The deposition of smooth, epitaxial layers of Cu and Au is desirable for interconnects in electrical devices or photovoltaic capping layers. Cu deposition is often used in plating of trenches in electrical connects due to its very low resistivity.[1-5] The way that the Cu forms and its resulting density

have a large effect on the electronic properties of the film. The first atomic seed layer is especially important for determining how uniform the subsequent bulk Cu deposition will be. It is important in such applications that the layers be defect free as grain boundaries can lead to large drops in conductivity.[1,6] As Moore's Law calls for transistors to become smaller up to a point, so must the Cu interconnects while still maintaining their connectivity. To achieve this, usually deposition methods are done at elevated temperatures to allow the Cu layers to settle thermodynamically. However, these high temperatures can damage the underlying substrate.[3,6]

In PV and Photoelectrochemical (PEC) use, thin transparent layers of Au can be used as capping layers or boundary layers between PN junctions in a multijunction solar cell.[7-9] Boundary layers in the cells allow for efficient integration of layers that have lattice mismatch issues. They need to be very thin and transparent. The semiconductors exposed to the air or liquid barrier in PV or PEC devices are often subject to oxidation which decreases the efficiency and lifetime of the devices. By coating a thin layer of Au on exposed parts of the material, the lifetime of the device is increased without a decrease in cell efficiency because the Au layer is transparent. Also, due to the morphology of the thin Au layers, there can be an enhancement in electron transport due to the surface plasmon effect.[8,9] This only occurs if the layer is epitaxial and doesn't promote nucleation.

Electrochemical Atomic Layer Deposition (E-ALD) was invented in the Stickney labs 30 years ago for the deposition of metal and compound semiconductor thin films. It relies on the principles of surface-limited reactions to form atomically thin layers of alternating metal materials. These surface-limited reactions rely on a phenomenon called Underpotential Deposition (UPD) where one metal (M_1) can be deposited onto another metal (M_2) at an electrochemical potential less than would be needed to deposit M_1 onto itself.[10-22] These reactions form fractions of a monolayer (ML) at a time, to build up a compound semiconductor without bulk deposits. A monolayer will be defined as having one surface atom for each underlying substrate atom. These surface-limited deposits have traditionally been done in

the gas phase, however, E-ALD allows for a cheaper, solution-based method for making these thin films. By keeping the solutions employed as pure as possible and without complexing agents, unwanted side reactions can be avoided that would damage the film.[10-22] Because E-ALD can be done at room temperature and standard pressure, it is a much cheaper alternative to the expensive reactors used in Chemical Vapor Deposition (CVD) or Molecular Beam Epitaxy (MBE) which are prevalent in industry today. However, E-ALD is not as viable for bulk deposition processes. Instead, it can provide a first atomic layer that can later be sacrificed using SLRR.

SLRR is an electroless electrochemical technique which relies upon the general principle that a more noble metal will replace a less noble metal on the surface at open circuit potential (OCP), where no current can flow. This process occurs when the electrochemical redox potentials of the two metals is sufficiently different. SLRR has been used in many different applications for exchange and very precise surface stripping.[23-30] When combined with E-ALD methods, it can lead to the growth of very epitaxial noble films such as Pt or Au. These noble metals are difficult to deposit using traditional E-ALD methods due to the slow deposition kinetics. Also, it may not be possible to electrochemically deposit the metal at potentials where the underlying substrate isn't oxidized.[23-30] Additionally, these films of noble metals are often indicative of nucleation and growth technique instead of producing smooth, epitaxial films. By using E-ALD, a sacrificial single atomic layer of metal can be deposited and then SLRR can be used to replace it. This will yield epitaxial layer by layer growth of these noble films at room temperature.

Past work done by Zhang et al. in the Stickney group demonstrated that Cu or Au could be deposited using a Cd sacrificial layer that was deposited using E-ALD. Then a precursor solution of Cu or Au was flown in and replaced the Cd using SLRR. This was done on both a metal substrate of Au as well as on CdTe semiconductor substrate. It was found that a Cu SLRR process was very effective at building up a smooth Cu layer with Cu growth being linear per cycle done. This was tested by electrochemical anodic stripping of the deposits. As seen in Figure 4.1 stripping of Cd occurs at -100 mV, so the presence

of a peak in that region would indicate that Cd was remaining, buried under the Cu.[29,30] The presence of surface limited Cu would be stripped at 200 mV, with successive layers filling out the peak. Excess Cd was not found to be buried inside of the Cu layer meaning that the exchange occurred fully. Additionally, it wasn't found that excess Cd was stripped from the CdTe substrate during the Cu exchange. This confirms that the exchange is surface limited and isn't damaging the underlying substrate. Au SLRR could also be performed but required that Cu be the sacrificial metal for exchange, requiring a double SLRR process. This was because Au oxidized too far into the underlying CdTe, lowering the Cd ratio. By first putting down a few cycles of Cu by SLRR, the Au could then be exchanged without damaging the underlying substrate if exposure time was limited. It was found that there was a sweet spot where all the Cu could be exchanged to Au. Past that point the underlying substrate would be damaged. It was found that the resulting Cu films done by E-ALD and SLRR method were more conformal and lacked nucleation sites compared to Cu films grown using only traditional electrodeposition.[29,30]

4.3 EXPERIMENTAL

All experiments were performed in an electrochemical flow cell (Electrochemical ALD L.C.) making use of a 3-electrode set-up. The auxiliary electrode was an inlaid Au wire and the reference electrode was Ag/AgCl in 3 M NaCl (Bioanalytical Systems, Inc.). The working electrode doubles as the polycrystalline Au substrate (Evaporated Metal Films), and was made out of glass slides with a 5 nm Ti adhesion layer, topped with 100 nm of Au. The working electrode area was 2.2 cm^2. When experiments were performed on CdSe nanorods (Mubeen Research Laboratory, University of Iowa), the substrate was a stainless-steel substrate with CdSe films deposited on top. The working electrode area in these cases was 0.78cm^2. Solution flow was controlled by a valve block (Neptune Research & Development,

Inc.) which was implemented by a potentiostat (Electrochemical ALD L.C.) and controlled by an in-house LabVIEW program named SEQUENCER. This set-up allowed for precise control over which solution was in the cell at any given time, as well as input potentials to the cell and read the resulting current generated.

Slide preparation was done by rinsing the Au substrate in 18 MΩ nanopure water (Millipore Advantage 10) and then washed with acetone (Fisher Chemical) and rinsed again in nanopure water. Next, the slides were exposed to concentrated HNO_3 (JT Baker) for 30 s and then rinsed again with nanopure water. The slides were immediately transferred into the flow cell and 0.1 M H_2SO_4 (Fisher Chemical) was flowed into the cell to limit air exposure time. The substrates were then electrochemically cleaned by 4 alternating 5 s pulses of -200 mV and 1400 mV followed by 2 CV's at 20 mV/s from -200 mV to 1400 mV and back. In the case of the CdSe substrates, no physical or electrochemical cleaning was done to prevent unwanted oxidation of the deposits.

Solution bottles were cleaned with Nochromix (Godax Labratories) for at least an hour and then rinsed multiple times with nanopure water. Cadmium precursor solution contained 10 mM $CdSO_4$ (Sigma-Aldrich), 0.1 M $HClO_4$ (GFS Chemicals, Inc.), 0.45 M H_2SO_4 (Fisher Chemical), and was adjusted to pH=2.0 with NaOH pellets (Fisher Chemical). Copper precursor solution contained 0.1 mM $CuSO4 \cdot 5H_2O$ (Sigma-Aldrich), 0.45 M H_2SO_4, and was adjusted to pH=2.0 with NaOH. Gold precursor solution contained 0.1 mM $AuCl_3$ (Aldrich, 99.99%) and 0.1 M $HclO_4$, and was adjusted to pH=2.0 with NaOH. Cadmium Telluride precursor solution contained 10 mM $CdSO_4$, 0.2 mM TeO_2 (Johnson Matthey Materials Company 99.9995% pure), 0.1 M $HclO_4$, 0.45 M H_2SO_4, and was adjusted to pH=2.0 with NaOH. Before the solutions were introduced to the cell, they were purged in N_2 gas (Airgas) for at least an hour to limit O_2 exposure. Solutions were quite stable, and able to survive for months before any precipitation occurred. Gold precursor solution had to be wrapped in Al foil to avoid photo-degradation but was stable as long as it was wrapped.

SEM (FE-SEM Thermo Fisher Teneo) was used to observe the morphology and elemental structure of the deposits using 5 keV and 10 keV accelerating voltages. The attached EDS detector (150mm Oxford Xmax^N) was used for stoichiometry.

4.4 RESULTS AND DISCUSSION

4.4.1 PRECURSOR VOLTAMMETRY ON CDSE

Previous work by Zhang et al left a blueprint for how to identify the amount of Cd and Cu deposited on CdTe samples by electrochemical anodic stripping. It relied on scanning the potential positively in a blank solution until the stripping features of the Cd or Cu were observed. Cd UPD is known to strip at -50 mV and bulk Cu strips at 0 mV with UPD Cu stripping at 200 mV as shown in the voltammetry of Figures 4.1 and 4.2. The coulometry of the curves could be used to determine the number of ML present of each. Previously, the samples were epitaxial CdTe on an Au substrate with the voltammetry of the constituents very well known. In the case of this experiment, the films are CdSe on a relatively rough stainless-steel substrate. Swapping the chalcogenide from Te to Se in the semiconductor leads to a change in the stripping potential of the compound. The roughness of the substrate and deposited films for CdSe also likely leads to easier stripping due to the greater surface area exposed. This same roughness also leads to an increased affinity for HER as seen by the change in onset potentials in Figure 4.3.

Figure 4.3 shows that in a blank solution at pH=2.0, the CdSe strips oxidatively starting at -50 mV. This is drastically different than the 400 mV stripping for CdTe that was observed by Zhang et al., and makes stripping coulometry difficult for determining if the process is working for Cu exchange. In Figure 4.4 the Cd CV on CdSe shows that the Cd UPD feature is still evident at -100 mV on the positive going scan. This is important because if Cd UPD could not be deposited using E-ALD, the process would

not be able to work for the later exchanges of Cu and Au. Instead, the Cu exchange would happen with the Cd from the CdSe film, which is undesirable because these new layers would be pitted instead of smooth and uniform.

The Cd UPD process begins at -500 mV with HER occurring after -600 mV. A change in the surface as the UPD Cd is deposited can be observed in the potential for the onset of the HER. When Cd UPD is present on the surface, the HER is pushed 100 mV more negative suggesting the Cd covered surface is more stable at negative potentials than the CdSe. In Figure 4.5 for Cu deposition on CdSe, however, the voltammetry greatly resembles that of the blank, meaning that no Cu can electrodeposit. It is also challenging for seeing if Cu can exchange with the Cd because Cu stripping can't be seen in the anodic stripping curve because CdSe strips at -50mV and even bulk Cu doesn't strip before 0 mV. Because there is no in-situ stripping way of qualitatively or quantitively determining if Cu SLRR works, all samples were characterized via SEM/EDS.

4.4.2 SELECTION OF CU SLRR PARAMETERS

In previous Au SLRR processes on CdTe, a significant layer of Cu was deposited by the Cu SLRR process before exchange with Au was done. This was due to the oxidizing power of Au extending down into the film, leading to degradation if Cd was the sacrificial layer. As such, a deposition sequence for a repeatable Cu SLRR on CdSe was created. As no bulk Cd features are evident in the Cd CV scan on CdSe, choosing a suitable Cd potential is slightly less volatile than on CdTe films. Since only the UPD Cd can form, the only consideration is that the deposition potential must be positive of -600 mV to avoid bubbles on the surface due to the HER interference. A potential of -500 mV for 20 s was chosen for the Cd deposition. The exchange with the Cu was found to happen relatively quickly with complete exchange done within 15 s. In Figure 4.6, a sample Cu SLRR deposition cycle is shown where 10 cycles

were deposited. After the first exchange, a UPD amount of Cu is exchanged which is indicated by the OCP reached in the Cu solution. Because the potential goes to 200 mV, it indicates that only UPD Cu is there. As the number of cycles increases, eventually a steady state of 0 mV is reached by cycle 5. This suggests that the Cu UPD feature has been fully deposited and the beginning of Cu bulk is starting to appear. Therefore 5 layers of Cu SLRR was determined as optimal to provide the best surface completely covered by a fine layer of Cu to perform exchange with Au.

4.4.3 SELECTION OF PARAMETERS FOR AU SLRR

When Au is exchanged for the Cu, it was found that not all the Cu was exchanged, and that some of the Cu was buried. This is likely due to some bulk Cu nucleating on the surface due to 5 Cu SLRR cycles being performed. The deformed ball-like structures such as are shown in Figure 4.7 were found to be Cu rich, further suggesting that Cu nucleation was occurring. Instead of allowing excess Cu to grow, a single Cu SLRR cycle was used as the base for the Au SLRR. These new deposition parameters still buried a little bit of Cu as seen in Figure 4.8, however, the amount did not grow with subsequent cycles. The Au percentage increased with each cycle linearly suggesting that the process was successful at growing Au layers, seen in Figure 4.9. The morphology shown in Figure 4.8 is much smoother suggesting epitaxial growth.

The excitation power of the laser used in SEM/EDS characterization is important as a lesser power will yield more information about the surface, and a higher power will penetrate further into the film. While lesser powers yield more and more surface information, the power must be sufficient to excite the correct Ka and La lines that allow EDS to detect composition. 5 keV excitation was used throughout this experiment so that an understanding of the composition of the surface could be obtained. For these thicker samples, 10 keV was also used to get an idea whether Cu or Au had

penetrated the CdSe film or stainless-steel substrate. The ratios for Cu and Au do not change despite the larger energy source suggesting that they are mainly on the surface as seen in figure 4.10. The deeper excitation into the film reveals the underlying stainless-steel underlayer without any other doping.

4.5 CONCLUSION

E-ALD was used to create a sacrificial UPD Cd layer on CdSe films. These films were on a rough stainless-steel substrate. The Cd layer was then exchanged at OCP in the presence of Cu2+ ions where the Cd layer was oxidized while the Cu reduced onto the surface. These Cu layers were then subsequently oxidized and exchanged with Au3+ ions to form an Au atomic layer on the CdSe film. This Cu/Au SLRR method differed from previous methods where multiple cycles of Cu were deposited before Au SLRR was performed, to make sure the film was sufficiently covered. Instead, only one Cu SLRR cycle was done, yielding only the smallest amount of UPD Cu possible. While this method still buried a little bit of Cu, it was less than when a steady state amount of Cu seed layer was used. The resulting Au deposits were found to grow linearly with number of cycles without increasing the amount of Cu buried. This suggests that the Cu is buried in the initial cycle of Au SLRR but doesn't form subsequently.

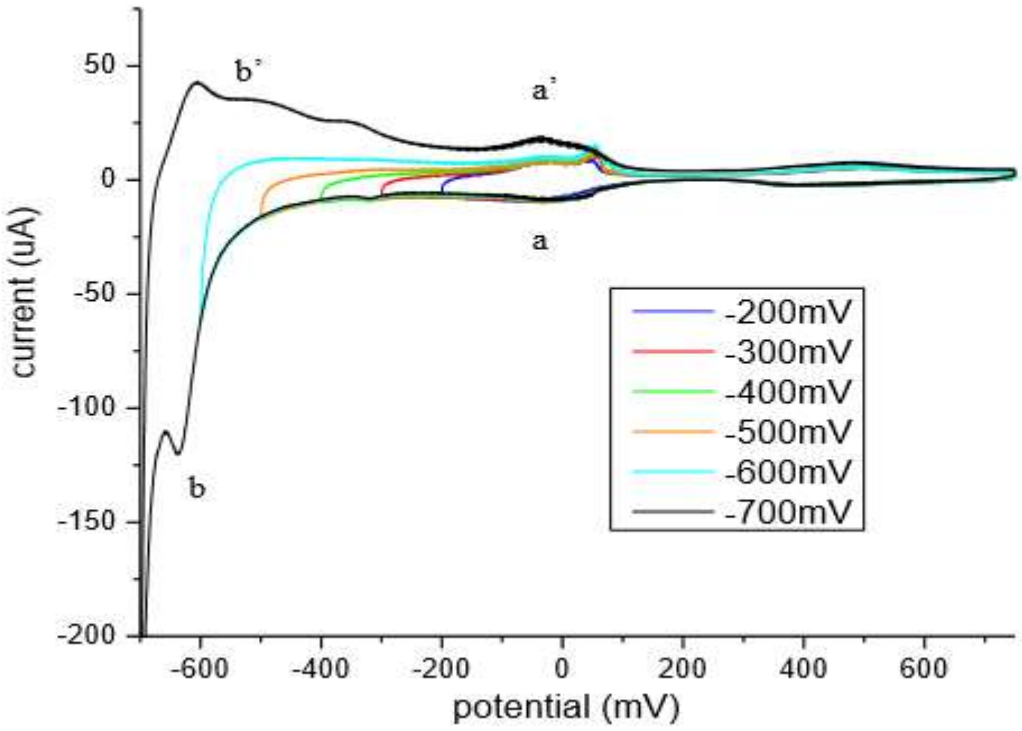

Figure 4.1- Voltammetry of Cd deposition on Au substrate.

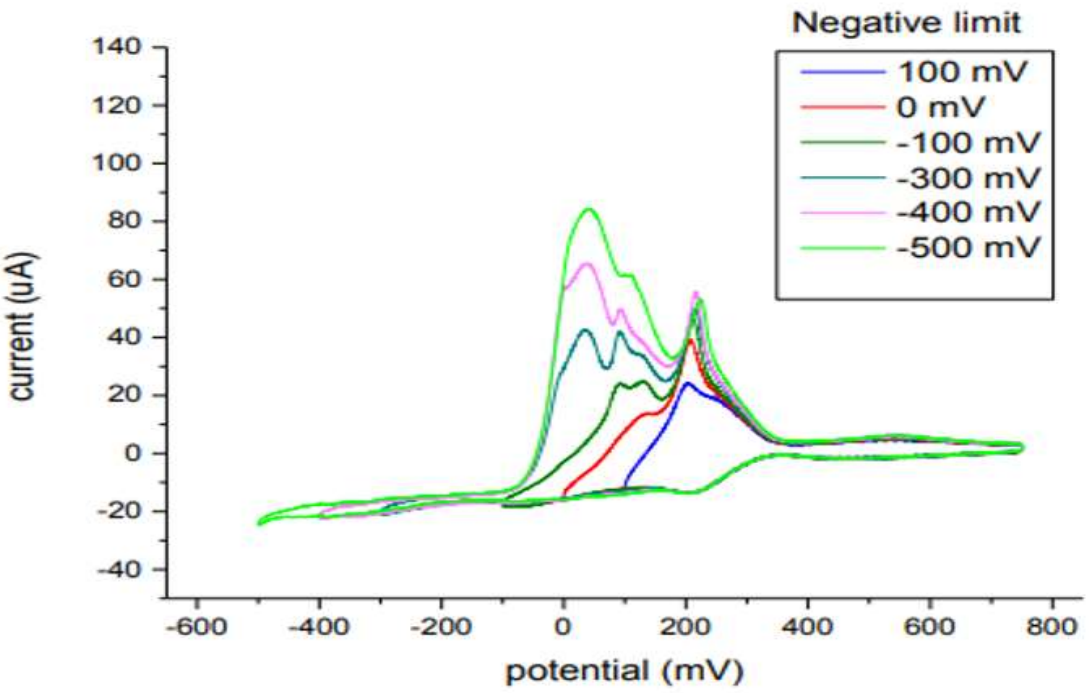

Figure 4.2- Voltammetry of Cu deposition on Au substrate.

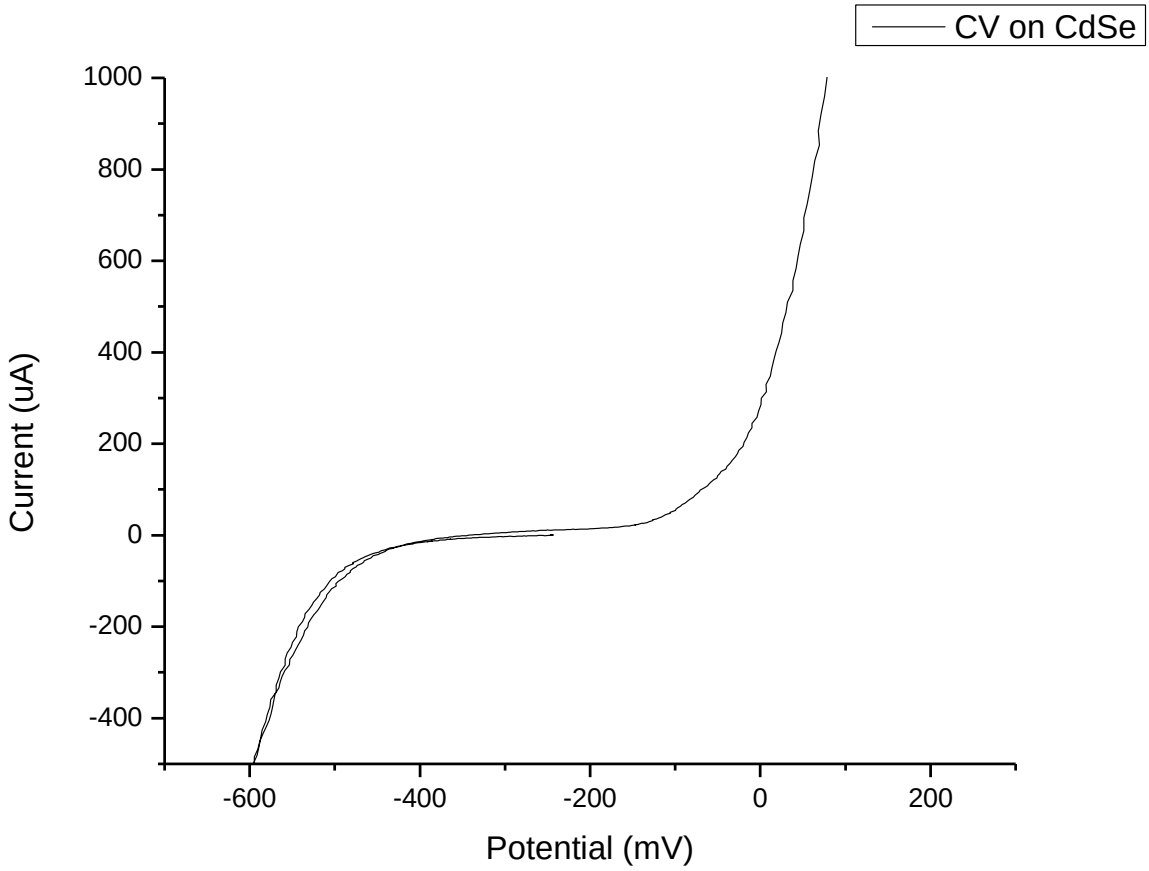

Figure 4.3- CV in blank solution on a CdSe thin film. Oxidative stripping is seen to occur starting at -50 mV while reductive stripping of the Se occurs negative of -500 mV.

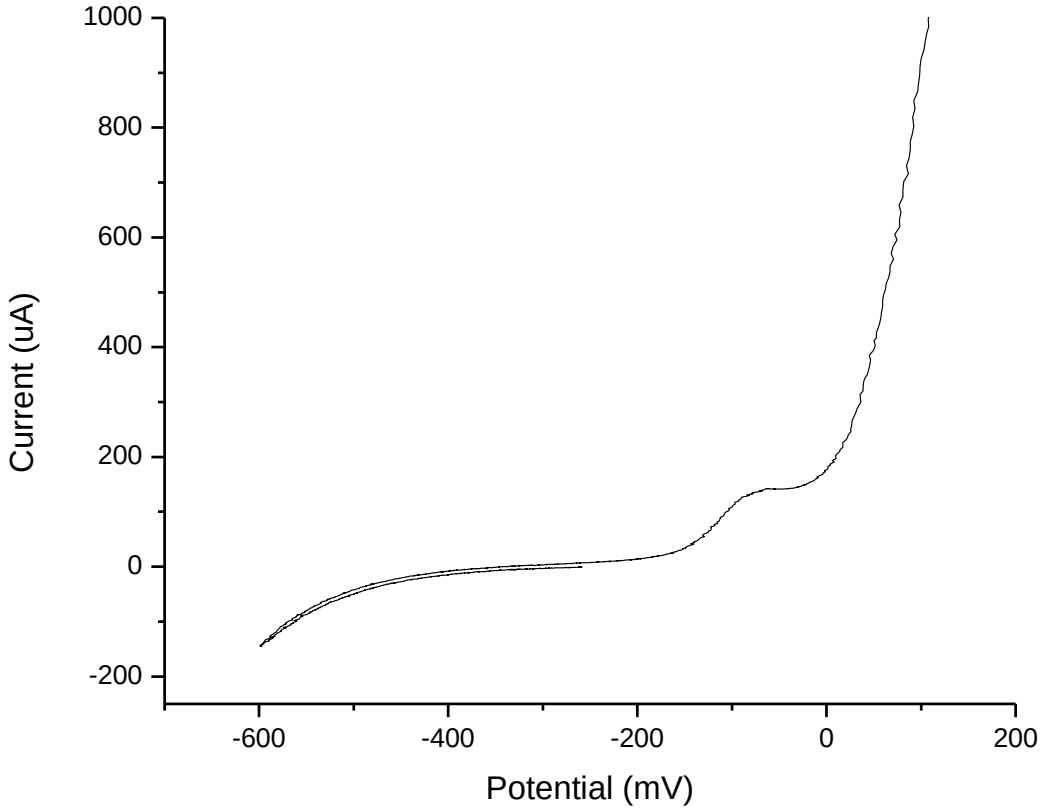

Figure 4.4- When a CV of Cd solution is performed on CdSe film, there is Cd UPD deposition evident on the positive going scan at -100 mV. This suggests that Cd UPD can deposit on CdSe film, meaning that the SLRR process can be performed.

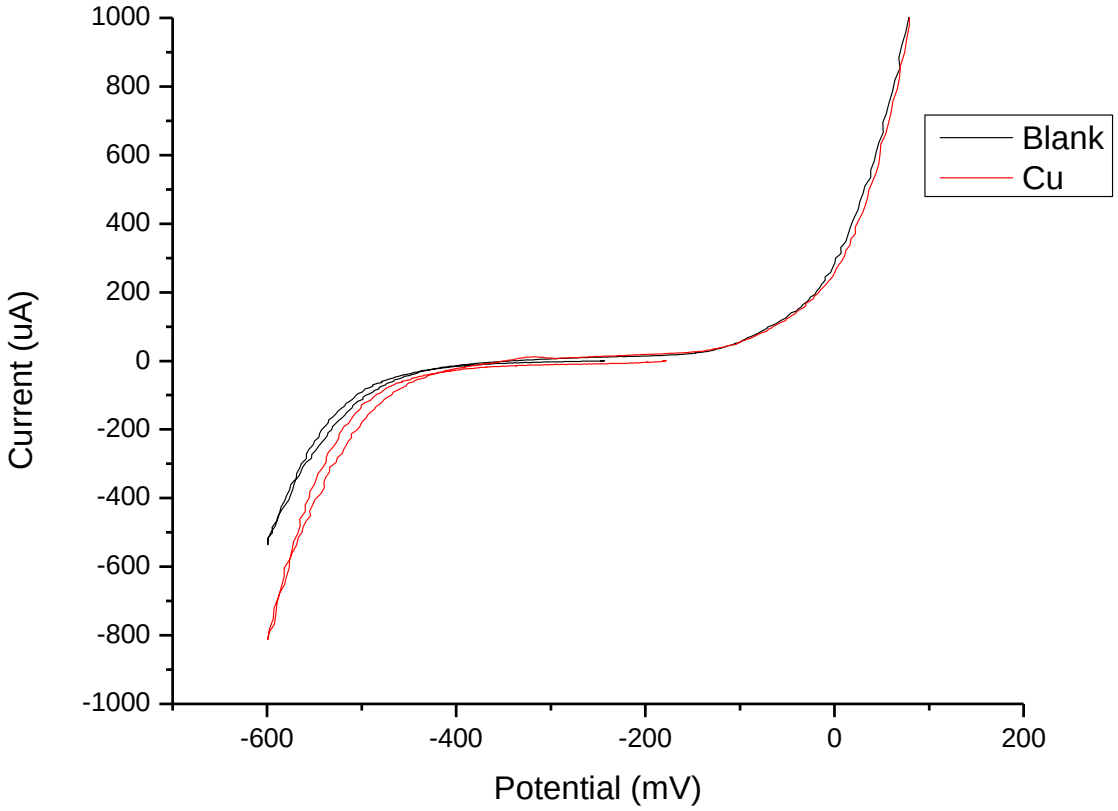

Figure 4.5- Cu voltammetry on CdSe film resembles that of blank voltammetry. This suggests that Cu does not electrodeposit on CdSe at this pH.

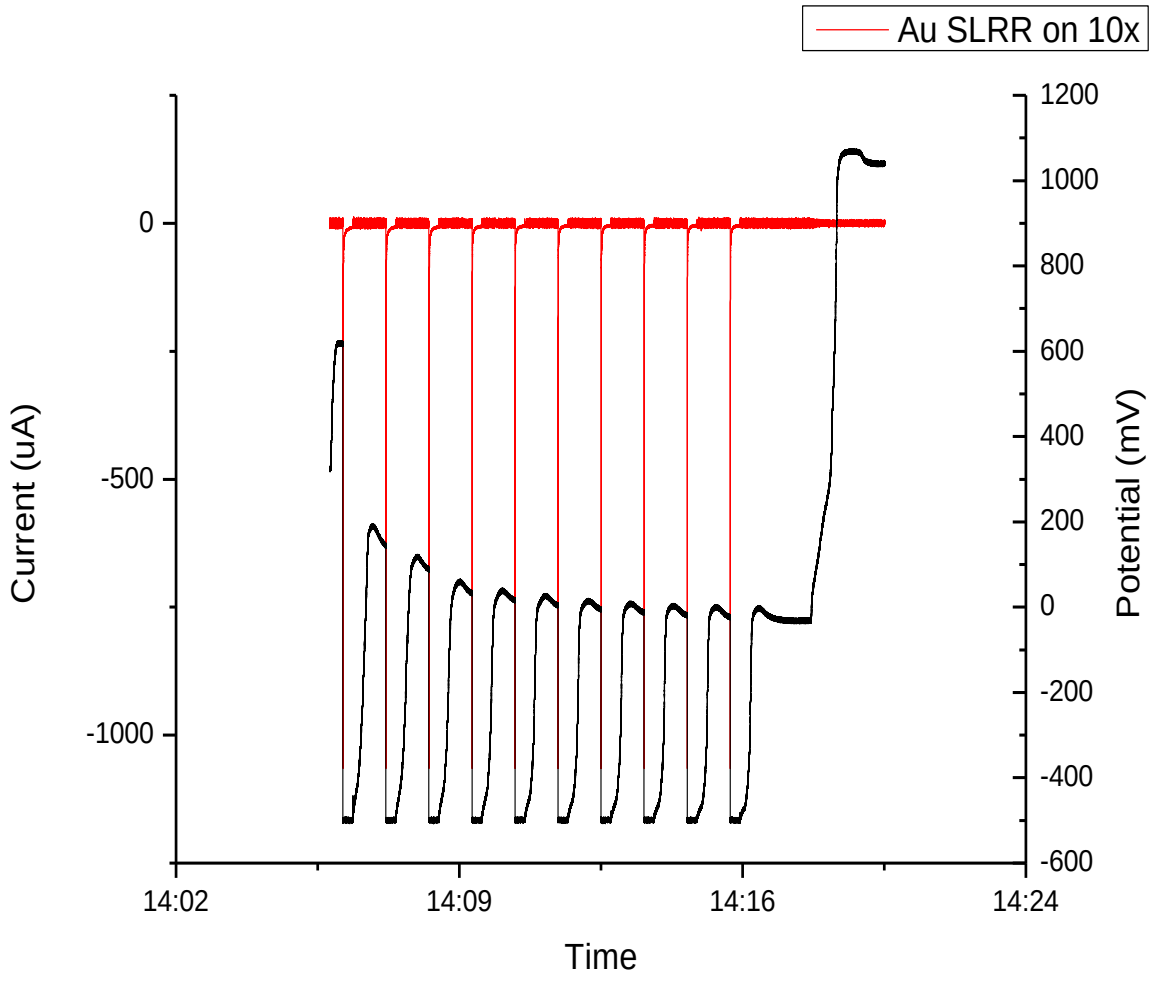

Figure 4.6- A typical Cu/Au SLRR deposition sequence is shown where 10 cycles of Cu SLRR were performed before an exchange with Au occurred. After 5 cycles of Cu SLRR the OCP for Cu is seen to settle at a steady state potential of 0 mV suggesting that the full UPD Cu layer had been put down and the beginning of bulk Cu was starting.

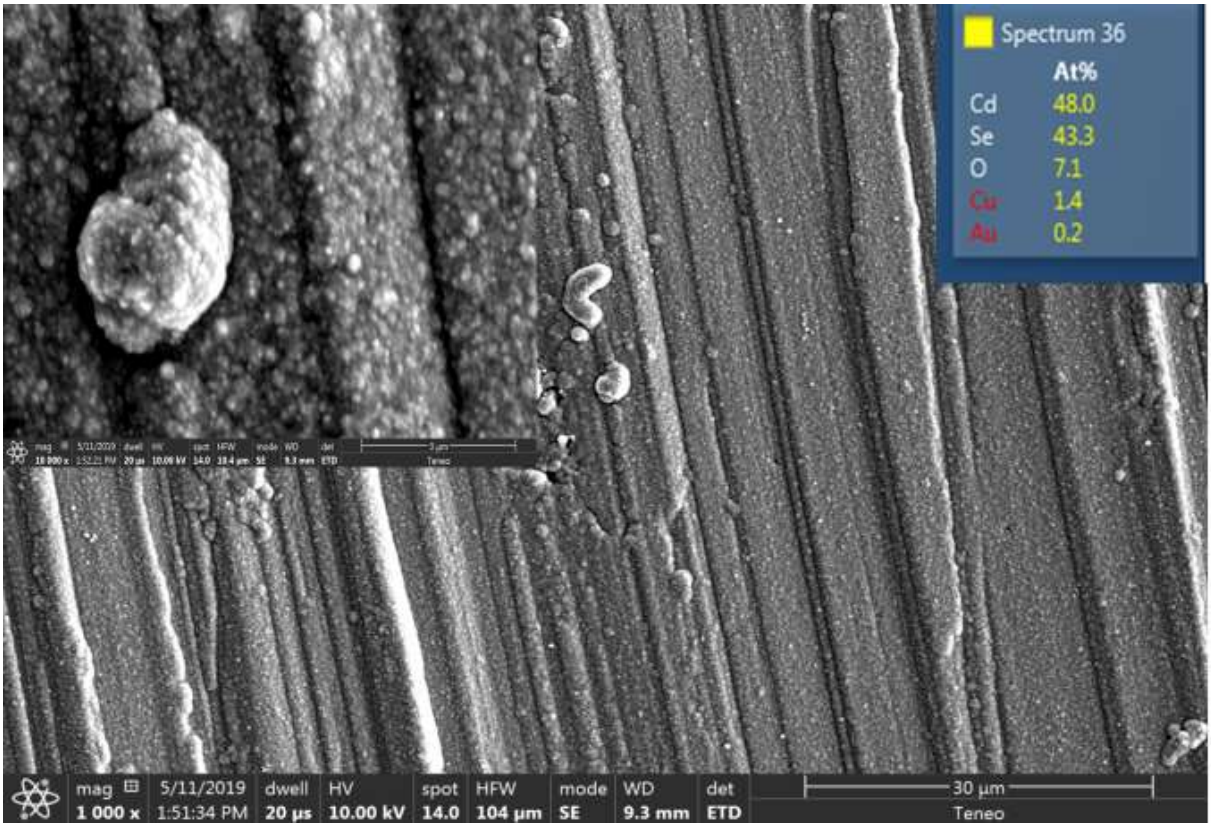

Figure 4.7- The SEM shows the morphology of the films where 5 cycles of Cu SLRR were performed before Au exchange. The surface had irregularly shaped balls on the surface that were Cu rich suggesting that Cu nucleation was occurring.

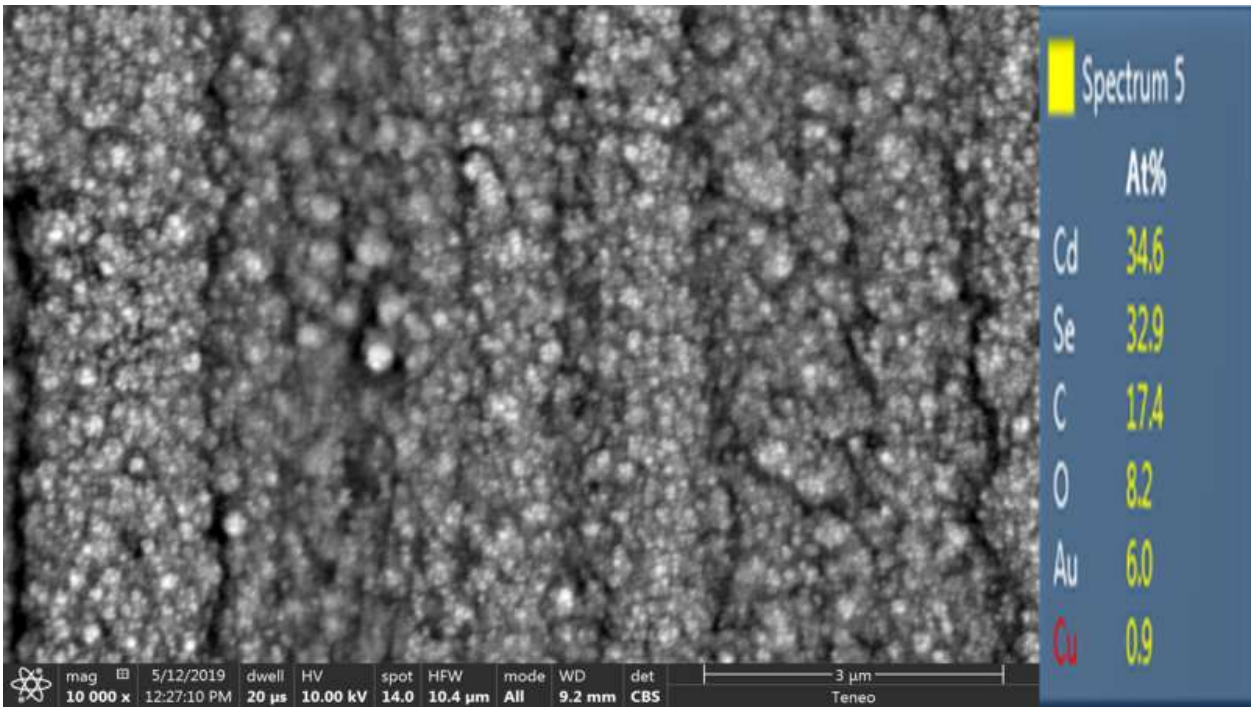

Figure 4.8- The morphology for having 1 Cu SLRR per Au exchange was much smoother and more uniform. The EDS confirmed that Au concentration can be grown.

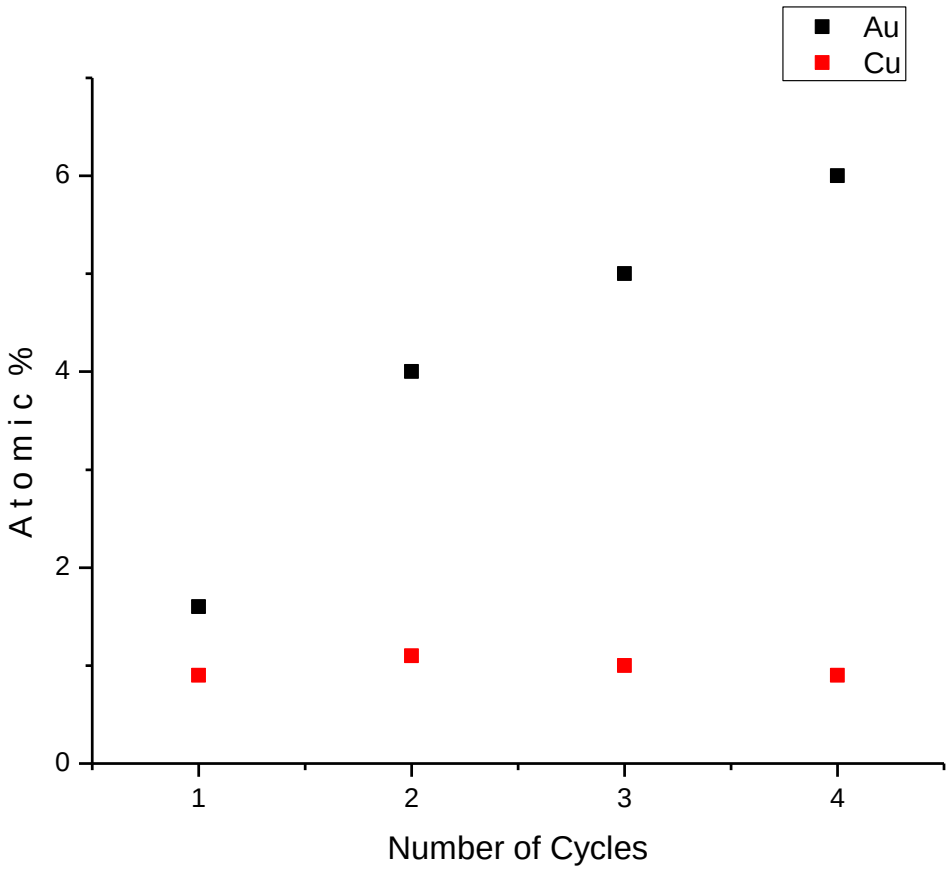

Figure 4.9- As the number of cycles of Cu/Au SLRR are increased the Au concentration increases linearly. However, the Cu, while present, doesn't increase suggesting that it is buried initially and not added to.

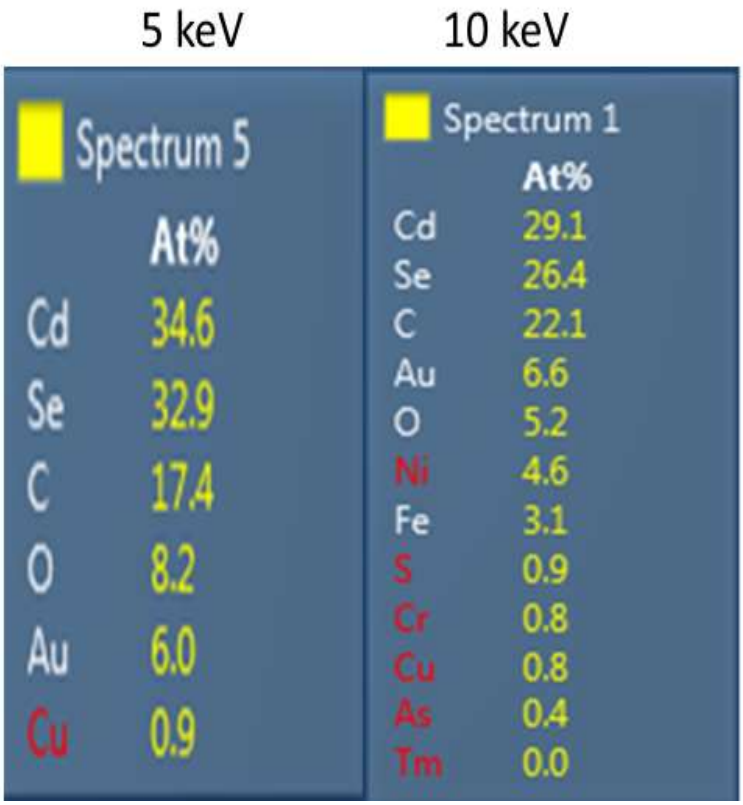

Figure 4.9- A comparison of the Au capped films when irradiated with a 5 keV vs. a 10 keV electron source. 10 keV irradiation penetrates deeper into the films and gives more information about the substrate.

REFERENCES

1. Timalsina, Y.; Horning, A.; Spivey, R.F.; Lewis, K.M.; Kuan, T.S.; Wang, G.C.; Lu, T.M. Effects of nanoscale surface roughness on the resistivity of ultrathin epitaxial copper films. *Nanotechnology* **2015**, 26, 1-10.

2. Lee, H.; Lopatin, S.D. The influence of barrier type on the microstructure and electromigration characteristics of electroplated copper. *Thin Solid Films* **2005**, 492, 279-284.

3. Liu, C.M.; Lin, H.W.; Lu, C.L.; Chen, C. Effect of grain orientations of Cu seed layers on the growth of <111>-oriented nanotwinned Cu. *Scientific Reports* **2014**, 4:6123, 1-4.

4.Kroger, R.; Eizenberg, M.; Cong, D.; Yoshida, N.; Chen, L.Y.; Ramaswami, S.; Carl, D. Influence of diffusion barriers on the nucleation and growth of CVD Cu for interconnect applications. *Microelectronic Engineering* **2000**, 50, 375-381.

5. Timalsina, Y.P.; Washington, M.; Wang, G.C.; Lu, T.M. Slow oxidation kinetics in an epitaxial copper (100) film. *Applied Surface Science* **2016**, 363, 209-216.

6. Bhandari, H.B.; Yang, J.; Kim, H.; Lin, Y.; Gordon, R.G.; Wang, Q.M.; Lehn, J.S.M.; Li, H.; Shenai, D. Chemical Vapor Deposition of Cobalt Nitride and its Applications as an Adhesion-Enhancing Layer for Advanced Copper Interconnects. *ECS J. Solid State Sci. Technol.* **2012**, 1:5, 79-84.

7. Fung, D.D.S.; Qiao, L.; Choy, W.C.H.; Wang, C.; Sha, W.E.I.; Xie, F.; He, Sailing. Optical and electrical properties of efficiency enhanced polymer solar cells with Au nanoparticles in a PEDOT-PSS layer. *J. Mater. Chem.* **2011**, 21, 16349-16356.

8. Topp, K.; Borchert, H.; Johnen, F.; Tunc, A.V.; Knipper, M.; Hauff, E.V.; Parisi, J.; Al-Shamery, K. Impact of the Incorporation of Au Nanoparticles into Polymer/Fullerene Solar Cells. *J. Phys. Chem. A.* **2010**, 114, 3981-3989.

9. Kirkeminde, A.; Retsch, M.; Wang, Q.; Xu, G.; Hui, R.; Wu, J.; Ren, S. Surface-passivated plasmonic nano-pyramids for bulk heterojunction solar cell photocurrent enhancement. *Nanoscale* **2012**, 4, 4421-4425.

10. Gregory, B.W.; Stickney, J.L. Electrochemical Atomic Layer Epitaxy (Ecale). *Journal of Electroanalytical Chemistry* **1991**, 300, 543-561.

11. Suggs, D.W.; Stickney, J.L. Studies of the Surface-Structures Formed by the Alternated Electrodeposition of Cd and Te on the Low-Index Planes of Au Stm Studies. *Surface Science* **1993** 290, 375-387.

12. Lister, T.E.; Huang, B.M.; Herrick, R.D.; Stickney, J.L. Electrochemical Formation of Se Atomic Layers on Au (100). *Journal of Vacuum Science and Technology B* **1995**, 13, 1268-1273.

13. Lister, T.E.; Stickney, J.L. Atomic level studies of selenium electrodeposition on gold (111) and gold (110). *Journal of Physical Chemistry* **1996**, 100, 19568-19576.

14. Lister, T.E.; Stickney, J.L. Formation of the first monolayer of CdSe on Au (111) by electrochemical ALE. *Applied Surface Science* **1996**, 107, 153-160.

15. Stickney, J.L. Electrochemical atomic layer epitaxy. *Electroanalytical Chemistry* **1999** 21, 75-209.

16. Sorenson, T.A.; Lister, T.E.; Huang, B.M.; Stickney, J.L. A comparison of atomic layers formed by electrodeposition of selenium and tellurium- Scanning tunnel microscopy studies on Au (100) and Au (111). *Journal of the Electrochemical Society* **1999**, 146, 1019-1027.

17. Sorenson, T.A.; Suggs, D.W.; Nandhakumar, I.; Stickney, J.L. Phase transitions in the electrodeposition of tellurium atomic layers on Au (100). *Journal of Electroanalytical Chemistry* **1999**, 467, 270-281.

18. Vaidyanathan, R.; Stickney, J.L.; Cox, S.M.; Compton, S.P.; Happek, U. Formation of In2Se3 thin films and nanostructures using electrochemical atomic layer epitaxy. *Journal of Electroanalytical Chemistry* **2003**, 559, 55-61.

19. Venkatasamy, V.; Shao, I.; Huang, Q.; Stickney, J.L. ALD approach toward electrodeposition of Sb2Te3 for phase-change memory applications. *Journal of the Electrochemical Society* **2008**, 155, 693-698.

20. Liang, X.H.; Kim, Y.G.; Gebergziabiher, D.K.; Stickney J.L. Aqueous Electrodeposition of Ge Monolayers. *Langmuir* **2010**, 26, 2877-2884.

21. Banga, D.; Perdue, B.; Stickney, J.L. Formation of CuIn(1-x)GaxSe2 (CIGS) by Electrochemical Atomic Layer Deposition (ALD). *Journal of the Electrochemical Society* **2014**, 161, 141-146.

22. Bui, N.N.; Ledina, M.; Reber, T.J.; Jung, J.; Stickney, J.L. Electrochemical Scanning Tunneling Microscopic Study of the Potential Dependence of Germanene Growth on Au (111) at pH 9.0. *ACS Nano* **2017**, 11, 9481-9489.

23. Jayaraju, N.; Vairavapandian, D.; Kim, Y.G.; Banga, D.; Stickney, J.L. Electrochemical Atomic Layer Depostiong (E-ALD) of Pt Nanofilms Using SLRR Cycles. *Journal of the Electrochemical Society* **2012**, 159, 616-622.

24. Sheridan, L.B.; Czerniawski, J.; Jayaraju, N.; Gebregziabiher, D.K.; Stickney, J.L.; Robinson, D.B.; Soriaga, M.P. Electrochemical Atomic Layer Deposition (E-ALD) of Palladium Nanofilms by Surface Limited Redox Replacement (SLRR), with EDTA Complexation. *Electrocatalysis* **2012**, 3, 96-107.

25. Dimitrov, N. Recent Advances in the Growth of Metals, Alloys, and Multilayers by Surface Limited Redox Replacement (SLRR) Based Approaches. *Electrochimica Acta* **2016**, 1-47.

26. Gokcen, D.; Yuan, Q.; Brankovic, S.R. Nucleation of Pt Monolayers Deposited via Surface Limited Redox Replacement Reaction. *Journal of the Electrochemical Society* **2014**, 161, 3051-3056.

27. Gokcen, D.; Bae, S.E.; Brankovic, S.R. Reaction kinetics of metal deposition via surface limited red-ox replacement of underpotentially deposited metal monolayers. *Electrochimica Acta* **2011**, 56, 5545-5553.

28. Gokcen, D.; Bae, S.E.; Brankovic, S.R. Kinetics of Metal Deposition via Surface-limited Redox Replacement Reaction. *ECS Transactions* **2011** 35, 11-22.

29. Zhang, X.; Shen, S.; Stickney, J.L. Metal Thin Film Epitaxial Deposition by SLRR on Semiconductor Substrate. To be submitted to *Journal of the Electrochemical Society.*

30. Zhang, X.; Shen, S.; Stickney, J.L. Cu and Au Films Epitaxially Deposition by Surface Limited Redox Replacement (SLRR) on Metal Substrate. To be submitted to *Journal of the Electrochemical Society*

CHAPTER 5

CONCLUSION AND FUTURE STUDIES

In the second chapter, GeTe films were deposited with a 1:1 ratio of Ge/Te. It was found that the growth of GeTe was dependent on both deposition potential as well as the length of the deposition. By carefully manipulating the deposition parameters, unwanted structures such as bulk Te or germanene could be avoided. For up to 30 cycles of deposition the stoichiometry could be monitored using electrochemical stripping of the samples and reading the resulting coulometry. The charge calculated could be converted into ML quantification of each constituent. It was shown that Ge and Te growth was linear as the number of cycles was increased. Once the films were sufficiently thick, SEM/EDS were used for GeTe quantification and thickness. Determination of the GeTe compound was done by looking at the stripping patterns of the deposited films. When GeTe compound was formed, the Ge stripping was at more negative potentials and resembled a gaussian peak. When only germanene is stripped there is a severe fronting to the peak, and it is stripped at more positive, stable potentials which makes sense given its tight lattice structure. There is also the noticeable lack of a stripping peak identifying Ge on Au when Ge is bound with Te. This suggests that even though Ge was deposited first, Te deposited under the Ge onto the Au substrate, causing that signature Ge on Au peak to disappear. This first GeTe layer was found to change the surface enough that future deposition parameters were significantly changed for future cycles. By treating the initial deposition cycle as its own entity, incremental 1:1 growth was achieved. The subsequent cycles required more negative Ge deposition potentials and more positive Te potentials. This helped to deposit enough Ge each cycle to help stabilize

the addition of more Te. While this greatly increased the amount of GeTe deposited each cycle, the process is still quite lengthy.

Future studies in this area would look to make thicker samples of GeTe. While the stoichiometry is ideal for the films, the deposition sequence is lengthy for such thin samples. It was an effective strategy to treat the first GeTe layer as its own entity and build a separate deposition sequence using different parameters afterwards. This was because it was found that Ge deposited at more negative potentials once the surface was changed to one resembling GeTe. By staggering the Ge deposition potential more and more negative as the sample gets thicker it is likely that more Ge can be deposited from each cycle. It has been shown that Te growth is directly tied to Ge growth. If Ge growth is increased, it is likely that Te would increase equally as they stabilize each other. It would be important to limit the rate of staggering as depositing too much Ge at one time may lead to germanene formation which could poison future deposition. It is also likely that it could become necessary to stagger the Te deposition potential more positive as Te reductive stripping becomes easier as well as the film gets thicker. Blank solution potential would also need to be monitored. Another possible way to grow thicker films would be if the precursors qualified to combine in one solution. This would allow for the use of PP-ALD deposition methods which would solve many of the issues with deposition sequence length that current methods have. Due to the thin nature of the current deposited films, Raman Spectroscopy detection could be greatly enhanced by using a SERS substrate. The SERS effect was shown to help detect germanene samples as thin as one ML so it should be able to apply in the case of the thin GeTe films.

In the third chapter, In_2Se_3 and InSe thin films are deposited using PP-ALD, a quicker one-solution variant of E-ALD. Prior In_2Se_3 films were deposited at pH=1.0 and were inhibited by the proximity of the deposition potential to the HER. The H_2 bubbles formed caused areas on the surface of the substrate where precursor ions could not reach. As a result, there were areas of varying amounts of

deposition across the surface. By changing the pH to 2.0, the deposition potential was shifted away from the HER and films were more conformal and smoother. This was expected due to manipulation of the Nernst equation, the equation governing electrodeposition parameters. With the shift in potential due to pH change, there emerged another deposition feature relating to Se reductive stripping to Se^{2-}. By depositing material in this regime, a second stoichiometry and different compound was formed. These two different In_xSe_y materials behaved differently when exposed to light. The In_2Se_3 films acted as N-type films while the InSe was P-type. Additionally, it was found that even the growth of the films was dictated by the light conditions during deposition. In regions of the flow cell that were more exposed to light there was a higher presence of Se, likely due to its ability to form 8-membered amorphous rings. These regions of amorphous Se were clearly viewable by Raman Spectroscopy. When the lights were turned out for deposition, the Se ratio decreased as expected. These deposits were found to be quite scalable as longer deposition sequences were used.

Future studies on InSe and In_2Se_3 films should be done in a dark environment. It was proved that smoother films were created in the dark, however they were not optimized. If the correct stoichiometries for dark grown samples were obtained it is likely that the results would be more single-crystalline than their light grown counterparts. Additionally, thermal annealing would probably help promote film crystallinity and give higher detection using Raman Spectroscopy and XRD methods. Further work to characterize the deposited films should be done to fully explore the photoelectric properties of the films. This would be done through a collaboration with the Mubeen Group at the University of Iowa. Possible improvements could be made as the solar cell viability was tested. It is likely that the P-type InSe could function as a photocathode in a PEC setting. This would allow for the splitting of H_2O at ambient conditions into H_2 gas, a good fuel source. Likewise, the N-type In_2Se_3 would be a candidate for O_2 formation as a photoanode. Early In_2Se_3 and InSe samples sent to the Mubeen Group suggested that while photoactivity was high, that stability of the films in electrolyte was very low. This

suggests that use of a capping layer would be beneficial. It is possible that the Cu/Au SLRR methods introduced in fourth chapter could be used for capping purposes.

The fourth chapter focuses on creating a capping, barrier layer of Au on top of CdSe films that were created by a collaborator. The process started by using E-ALD to form a sacrificial layer of Cd on the CdSe substrate surface. It is important that only a UPD amount of Cd is deposited because all future exchanges will resemble the smoothness of this initial sacrificial layer. The atomically thin Cd layer was then exchanged using SLRR to form a single atomic layer of Cu. This Cu layer was then used as a further sacrificial layer for the epitaxial growth of Au. By using a single layer of Cu SLRR before Au SLRR a linear growth of Au epitaxial film was achieved. This was confirmed morphologically using SEM and quantitatively by EDS.

Future work would seek to completely remove all the sacrificial Cu layer from the films. Currently 0.9% atomic percentage of Cu remained suggesting a partial layer of Cu was buried during the first Au SLRR exchange process. As the amount of Cu is not seen to grow between subsequent cycles, it is likely this only occurs at the beginning. It would be important to fine tune the Au solution exposure time to completely exchange with the Cu. If Au exchange is done for too long, it is likely to oxidize into the underlying CdSe film causing damage. Another possibility to consider is that too much Cd layer is being deposited in the initial Cd on CdSe step. If bulk Cd is being deposited it is possible that Cu exchanges with all of the Cd and there is a bit of bulk Cu formed. This could explain why Cu is buried in the films. This Cu wouldn't be able to be exchanged completely due to the short time period Au is introduced. In future scans, we know that only UPD Cd is being deposited as the Cu concentration in the films stays constant. Additionally, it would be interesting to see how effective the capping layer was in certain media. This could be tested in collaboration with the Mubeen Group. If it protected the films from oxidation it could be used for subsequent deposition. This could allow another semiconductor such as CdTe to be deposited on top leading to multijunction functionality and an improved cell.

REFERENCES

1. Gregory, B.W.; Stickney, J.L. Electrochemical Atomic Layer Epitaxy (ECALE). *Journal of Electroanalytical Chemistry* **1991**, 300, 543-561.

2. Suggs, D.W.; Stickney, J.L. Studies of the Surface-Structures Formed by the Alternated Electrodeposition of Cd and Te on the Low-Index Planes of Au Stm Studies. *Surface Science* **1993** 290, 375-387.

3. Lister, T.E.; Huang, B.M.; Herrick, R.D.; Stickney, J.L. Electrochemical Formation of Se Atomic Layers on Au (100). *Journal of Vacuum Science and Technology B* **1995**, 13, 1268-1273.

4. Lister, T.E.; Stickney, J.L. Atomic level studies of selenium electrodeposition on gold (111) and gold (110). *Journal of Physical Chemistry* **1996**, 100, 19568-19576.

5. Lister, T.E.; Stickney, J.L. Formation of the first monolayer of CdSe on Au (111) by electrochemical ALE. *Applied Surface Science* **1996**, 107, 153-160.

6. Stickney, J.L. Electrochemical atomic layer epitaxy. *Electroanalytical Chemistry* **1999** 21, 75-209.

7. Sorenson, T.A.; Lister, T.E.; Huang, B.M.; Stickney, J.L. A comparison of atomic layers formed by electrodeposition of selenium and tellurium- Scanning tunnel microscopy studies on Au (100) and Au (111). *Journal of the Electrochemical Society* **1999**, 146, 1019-1027.

8. Sorenson, T.A.; Suggs, D.W.; Nandhakumar, I.; Stickney, J.L. Phase transitions in the electrodeposition of tellurium atomic layers on Au (100). *Journal of Electroanalytical Chemistry* **1999**, 467, 270-281.

9. Vaidyanathan, R.; Stickney, J.L.; Cox, S.M.; Compton, S.P.; Happek, U. Formation of In_2Se_3 thin films and nanostructures using electrochemical atomic layer epitaxy. *Journal of Electroanalytical Chemistry* **2003**, 559, 55-61.

10. Venkatasamy, V.; Shao, I.; Huang, Q.; Stickney, J.L. ALD approach toward electrodeposition of Sb_2Te_3 for phase-change memory applications. *Journal of the Electrochemical Society* **2008**, 155, 693-698.

11. Liang, X.H.; Kim, Y.G.; Gebergziabiher, D.K.; Stickney J.L. Aqueous Electrodeposition of Ge Monolayers. *Langmuir* **2010**, 26, 2877-2884.

12. Banga, D.; Perdue, B.; Stickney, J.L. Formation of $CuIn_{(1-x)}Ga_xSe_2$ (CIGS) by Electrochemical Atomic Layer Deposition (ALD). *Journal of the Electrochemical Society* **2014**, 161, 141-146.

13. Bui, N.N.; Ledina, M.; Reber, T.J.; Jung, J.; Stickney, J.L. Electrochemical Scanning Tunneling Microscopic Study of the Potential Dependence of Germanene Growth on Au (111) at pH 9.0. *ACS Nano* **2017**, 11, 9481-9489.